Sedimentological Heterogeneity of the Late Ordovician Glacio-Fluvial Sarah Formation, Al-Qaseem Area, Saudi Arabia: Impact on Petrophysical Properties and Reservoir Quality

BY

Islam Mahmoud El-Deek

A Thesis Presented to the
DEANSHIP OF GRADUATE STUDIES

KING FAHD UNIVERSITY OF PETROLEUM & MINERALS
DHAHRAN, SAUDI ARABIA

In Partial Fulfillment of the
Requirements for the Degree of

MASTER OF SCIENCE

In

GEOLOGY

April, 2014

KING FAHD UNIVERSITY OF PETROLEUM & MINERALS
DHAHRAN- 31261, SAUDI ARABIA
DEANSHIP OF GRADUATE STUDIES

This thesis, written by **ISLAM MAHMOUD EL-DEEK** under the direction of his thesis advisor and approved by his thesis committee, has been presented and accepted by the Dean of Graduate Studies, in partial fulfillment of the requirements for the degree of **MASTER OF SCIENCE IN GEOLOGY.**

Dr. Osman M. Abdullatif
(Advisor)

Dr. Abdulaziz Al-Shaibani
Department Chairman

Dr. Khalid Al-Ramadan
(Member)

Dr. Salam A. Zummo
Dean of Graduate Studies

Dr. Gabor Korvin
(Member)

28/4/14

Date

Dedication

This thesis is dedicated to the soul of my beloved *father* as a great source of inspiration to me; to my wonderful *mother* for her love and encouragement; and to my future *wife*, who contributed to this thesis in ways she will never know

ACKNOWLEDGMENTS

First and foremost, I thank Allah for endowing me with health, patience, and knowledge to complete this work. Acknowledgments are due to King Fahd University of Petroleum & Minerals for granting me this scholarship and supporting my research. I would like to express my deep and sincere appreciation to my Committee Chairman, Dr. Osman Abdullatif. I am very grateful to him for his contribution to the success of this work through his kind guidance and assistance. Thanks are also due to the other Committee members, Professor Gabor Korvin and Dr. Khalid Al-Ramadan. I'd like to acknowledge the support and help provided by the Deanship of Scientific Research "*Reservoir Characterization Research Group*" – Project RCRG 1114.

Thanks and appreciation to Dr. Abdulaziz Al-Shaibani, the chairman of Earth Sciences Department. He has been very kind and cooperative and facilitated all the administrative needs during the course of my scholarship. I am also grateful to all the department's faculty members for teaching, support and guidance.

Acknowledgements are extended to all my colleagues in the department; students, technicians and staff for helping me in the field and laboratory work. Furthermore, my sincerest acknowledgments are due to my family for their moral support.

TABLE OF CONTENTS

LIST OF TABLES

LIST OF FIGURES

ABSTRACT

Full Name	: Islam Mahmoud El-Deek
Thesis Title	: Sedimentological Heterogeneity of the Late Ordovician Glacio-Fluvial Sarah Formation, Al-Qaseem Area, Saudi Arabia: Impact on Petrophysical Properties and Reservoir Quality.
Major Field	: Geology
Date of Degree	: April, 2014

The Late Ordovician Sarah Formation represents the first glacio-fluvial event in the Arabian Peninsula. Sarah Formation is outcropping in areas of central and northern Arabia bordering the Arabian Shield, while it occupies several sub-basinal areas in the subsurface. The glacio-fluvial Sarah Formation is considered as an important reservoir target, especially as tight gas reservoir. This study was conducted to characterize and compare different scales of depositional and post-depositional heterogeneity of the late Ordovician glacio-fluvial paleochannels. This might help to reveal and understand reservoir quality at outcrop scale and its prediction in the subsurface. Several glacio-fluvial channels of the Sarah Formation were studied from a number of outcrops in central Arabia. Five paleovalleys were the target of this study, namely Bukayriyah, Rawd Al-Jawa, Hanadir, Sarah and Khanasir Sarah paleovalleys. The approach followed in this study included sedimentological field investigations and laboratory petrological analysis. Variability is noted within paleochannels in terms of vertical and lateral distribution and their stacking pattern and architecture. Proximal to distal variability was also noted on facies types, geometries and their abundances. Outcrop relationships also showed vertical and lateral facies change with other Paleozoic formations. Variability in texture, composition, sandstone type, facies, geometry and architecture at outcrop scale were also noted. Geologic controls in terms of periods of ice advance and retreat, tectonic, sea level, and sediment supplies seem to have played important role on facies types, paleoenvironments, stratigraphic hierarchies and their distribution within the Paleozoic strata. Reservoir architecture varies within and among paleochannels of the Sarah Formation. Understanding various geologic controls at outcrop scale might help better understanding of facies and environmental setting, reveal complexity and determine meso- and macro-scale sedimentological and stratigraphical heterogeneities. This consequently might help to determine their impact on reservoir quality and architecture and enhances the prediction of reservoir properties in the subsurface. Properties examined included facies, facies geometry or architecture, sediment texture and composition and diagenetic overprint which all tend to influence the internal make-up and reservoir properties. Laboratory studies included thin section petrography, XRD, SEM and MICP investigations. The porosity and permeability measurements were carried out for the core plugs to detect the micro-heterogeneity within the five paleovalleys. The Sarah galcio-fluvial paleovalleys show variation from micro- to macro-scales. Porosity and permeability also show variation among the investigated paleovalleys. The lithofacies analysis indicates that these sediments were deposited during periods of ice advance and retreat. The facies ranges from brownish to reddish, silty, fine to coarse grained quartz arenites with clay cement not exceeding 5%. The coating of quartz grains by authigenic kaolinites prevented quartz overgrowth; and thus preserved the initial porosity and permeability. Thin section petrography showed good correlation between the textural variability and porosity and permeability measurements. Both depositional and diagenetic controls have impacted porosity and permeability patterns in Sarah Formation. These factors include grain size, sorting, cement and matrix content, pore size distribution and their connectivity. Evaluation of these different scales of heterogeneity might help to understand and predict reservoir quality in the subsurface. The reservoir heterogeneity analysis conducted using three static measures (coefficient of variation, Dykstra-parsons coefficient and Lorenz coefficient) indicates that the Sarah Formation can be considered to represent heterogeneous to very heterogeneous reservoir.

ملخص الرسالة

الاسم الكامل: إسلام محمود الديك

عنوان الرسالة: دراسة التنوع الترسيبي لمتكون صارة الجليدي (أوردوفيشي متأخر) بمنطقة القصيم بالمملكة العربية السعودية مع التركيز على الخواص البتروفيزيقية وجودة المكمن النفطي.

التخصص: جيولوجيا

تاريخ الدرجة العلمية: أبريل 2014

يمثل متكون صارة ذو العصر الأردوفيشي المتأخر أول حدوث لظاهرة الجليد النهري في شبه الجزيرة العربية. ينكشف متكون صارة في وسط وشمال شبه الجزيرة العربية حيث يحد الدرع العربي، بينما يشغل عدة مناطق تحت سطحية. ويعد متكون صارة مكمن نفطي مهم خاصة للغاز المحكم. تم القيام بهذه الدراسة لتوصيف والمقارنة بين التنوع الترسيبي وبعد الترسيبي للقنوات الترسيبية من عصر الأردوفيشي المتأخر على عدة مستويات والذي قد يساعد على كشف وفهم جودة المكمن النفطي على مستوى المكشف والتنبؤ بها على المستوى تحت السطحي. تم دراسة عدة قنوات ترسيبية لمتكون صارة من خلال عدد من المكاشف الجيدة بوسط المملكة العربية السعودية مع استهداف خمسة وديان قديمة للمتكون هم: البكيرية، روض الجواء، الحنادر، صارة، وخناصر صارة. تضمن النهج المتبع في هذا البحث دراسات ترسيبية حقلية وتحاليل صخرية معملية. لوحظ التنوع في القنوات القديمة من خلال التوزيع الأفقي والرأسي ونمط التكدس والزخرفة. كما لوحظ التنوع في السحن الصخرية وأشكالها الهندسية تبعا لاختلاف موضعها من المصدر، بالإضافة إلى التنوع في النسيج الصخري والتركيب وأنواع الحجر الرملي على مستوى المكشف. ولعبت العوامل الجيولوجية - متمثلة في فترات تقدم وتراجع الجليد وتكتونية الألواح ومستوى سطح البحر والإمداد الرسوبي - دورا هاما في التأثير على أنواع السحن الصخرية المتكونة واختلاف البيئات الترسيبية القديمة وتركيب الطبقات وتوزيعها بين رواسب العصر الباليوزوي. فهم ودراسة كل تلك التأثيرات من الممكن أن يساعد في تحديد خواص المكمن النفطي وجودته. شملت الدراسات المعملية فحص بتروجرافي لقطاعات رقيقة من الصخور واستخدام تقنية حيود الأشعة السينية والمجهر الالكتروني الماسح وفحوصات الضغط الشعيري بطريقة حقن الزئبق. وتم قياس المسامية والنفاذية للعينات الصخرية لتحديد ماهية عدم التجانس على المستوى المجهري بين الوديان الترسيبية القديمة لمتكون صارة والتي أظهرت تنوعا واضحا على جميع المستويات – من مستوى المكشف إلى المستوى المجهري. كما أشار تحليل السحن الصخرية إلى أن تلك الرواسب قد تم ترسيبها خلال فترات مختلفة من تقدم وتراجع الجليد. حيث تتراوح السحن بين الكوارتز أرينيت البني والبني المحمر، الغريني، ناعم إلى خشن الحبيبات، ويحتوي على نسبة لا تتجاوز 5 % من معادن الطين التي يغلب عليها معدن الكاولينيت. وساعد هذا المعدن بدوره في تغليف حبيبات الكوارتز مما منع زيادة نموها؛ وبالتالي ساعد على الحفاظ على المسامية والنفاذية الأصليتين للصخر. أثرت كل من العوامل الترسيبية وما بعد الترسيبية على خواص المسامية والنفاذية لمتكون صارة، وشملت تلك العوامل: حجم الحبيبات، توزيعها، نوع ومحتوى راسب الأرضية والمواد اللاحمة، وتوزيع المسام ودرجة نفاذها. وأشارت معاملات عدم التجانس إلى أن متكون صارة يمثل مكمنا نفطيا غير متجانس إلى غير متجانس عالي.

CHAPTER ONE

INTRODUCTION

The Late Ordovician (Hirnantian) glaciation covered West Gondwana continent (Hambrey, 1985) which mainly included Africa, South America and Arabia (Paris and Robardet, 1990). The Middle East and North Africa region was affected by the Hirnantian glaciation, e.g., Mauritania, Morocco, Algeria, Libya, Egypt and Saudi Arabia (Le Heron et al., 2009), and the Ashgilian glaciation, e.g., Jordan (Abed et al., 1993; Amireh et al., 2001; Turner et al., 2005) . The Late Ordovician glaciogenic deposits were recorded in both the proximal areas (Mauritania, Algeria, Libya, Niger, Saudi Arabia) and the ice distal zone in Morocco, Spain and Turkey (Ghienne, 2011). In Saudi Arabia, outcropping equivalents for Paleozoic glacial and fluvial strata are excellently exposed. Equivalent outcrops are also recorded in northern Saudi Arabia, southwestern Saudi Arabia at Wajid Formation, and limited subsurface penetration in Rub al Khali Basin.

Sarah Formation is exposed in the center of the Arabian Plate between the southeastern Great Nafud and Wadi Al-Rimah with thickness ranging from 90 to 300 m of fine to medium grained sandstone, accompanied by a tillite facies of glacial to marine origin. These sediments provide a good opportunity to examine different scales of sedimentary heterogeneity and their impact on reservoir quality. Nairn and Alsharhan (2003) described the lower part of Sarah Formation as glacial paleovalley deposits, associated with fluvial and marine sediments.

The Sarah paleochannels have sheet to lenticular geometry and unconformably cut through Zarqa, Qaseem and Saq Formations (Figure 1-2). The facies in outcrop varies from diamectite and massive, horizontal to trough cross-bedded sandstones. Lithologically, the facies ranges from brownish to reddish, silty, fine to coarse grained sandstone. Both depositional and diagenetic controls have impacted porosity and permeability patterns in Sarah Formation. These factors include grain size, sorting, cement and matrix content, pore size distribution and their connectivity. Understanding these controls might help to assess and predict the quality of Sarah reservoir in the subsurface.

Sarah Formation is considered to be a potential reservoir with the mostly unexplored areas of the Paleozoic petroleum system in the Arabian Peninsula (Millson et al., 1996; Schenk and Pollastro, 2000). It is also considered as a primary reservoir target for tight gas in the subsurface in Saudi Arabia (Al-Mahmoud and Al-Ghamdi, 2010).

1.1 Problem Statement

Recently, demand to get the maximum recovery from oil and gas fields has been increasing in Saudi Arabia, especially for natural gas. The Sarah Formation is studied here because it represents an important tight gas reservoir target in the subsurface (Al-Mahmoud and Al-Ghamdi, 2010) of the Arabian Peninsula, especially in Rub' Al-Khali Basin (Briner et al., 2010; Bukhamseen et al., 2010)

Khalil (2012) defined three types of tight gas sweet spots in the subsurface, namely the depositional, diagenetic and tectonic types. The complexity of facies, environments and paleogeography of the Late Ordovician Sarah Formation in the subsurface makes the prediction of reservoir quality difficult (Al-Mahmoud and Al-Ghamdi, 2010; Briner et al., 2010). Therefore, this study intends to use the outcrop analog of Sarah Formation to investigate some of the complexity indicated by the above mentioned authors.

The limitation of techniques and difficulties to determine detailed reservoir heterogeneity in the subsurface encouraged the use of surface outcrop analog. The outcrop analog can provide information about rock body dimension, size, and orientation, at a resolution which is unavailable from the subsurface (Abdullatif and Makkawi, 2004; Abdullatif and Makkawi, 2010; Al-Ajmi et al., 2011; Grammer et al., 2004; Thurmond et al., 2005). Consequently, this provides insight for geological modeling, understanding and predicting the behavior of hydrocarbon reservoirs and water aquifers.

Understanding the geologic controls on the variation of reservoir quality is a key factor for predicting reservoir properties in the subsurface. This will increase the understanding of reservoir heterogeneity in the subsurface and can help predicting the distribution of the potential reservoir facies, and their petrophysical properties. The study may also provide reference and input that may allow refinement of reservoir characterization models based on subsurface data. The direct benefit of such input is to improve reservoir characterization and fluid simulation model(s) that will allow taking sound and concrete decisions related to development and management of oil and gas in glacial and fluvial reservoirs.

1.2 Objectives

The aim of the study is to describe, understand, and determine the depositional and post-depositional heterogeneity, and investigate its impact on reservoir quality and petrophysical parameters (e.g. porosity and permeability patterns) in Sarah Formation. The study is based on sedimentological field investigations and laboratory petrological analysis of selected outcrop sections from the Late Ordovician Sarah Formation.

1.3 Location of the Study Area

The study area is located in Al-Qaseem area, central Saudi Arabia where Sarah Formation is well exposed. Figure 1-1 shows the locations of the studied outcrops and their distribution within the paleovalleys of Sarah Formation. Table 3-1 shows the coordinates of the studied outcrops.

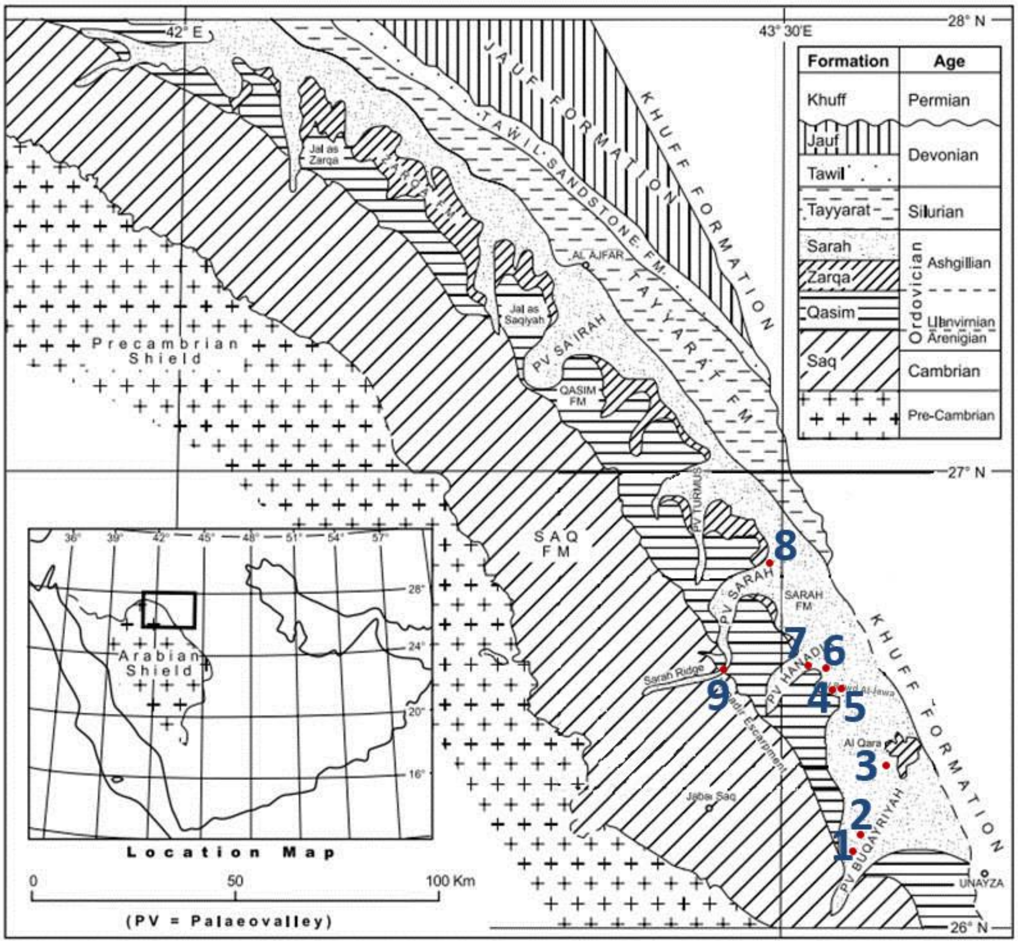

Figure 1-1: Regional distribution of Sarah paleovalleys within the Paleozoic strata of Al-Qaseem district, Saudi Arabia, (after Clark-Lowes, 2005). The numbers represent the locations of the studied Sarah outcrops as listed in Table 3-1.

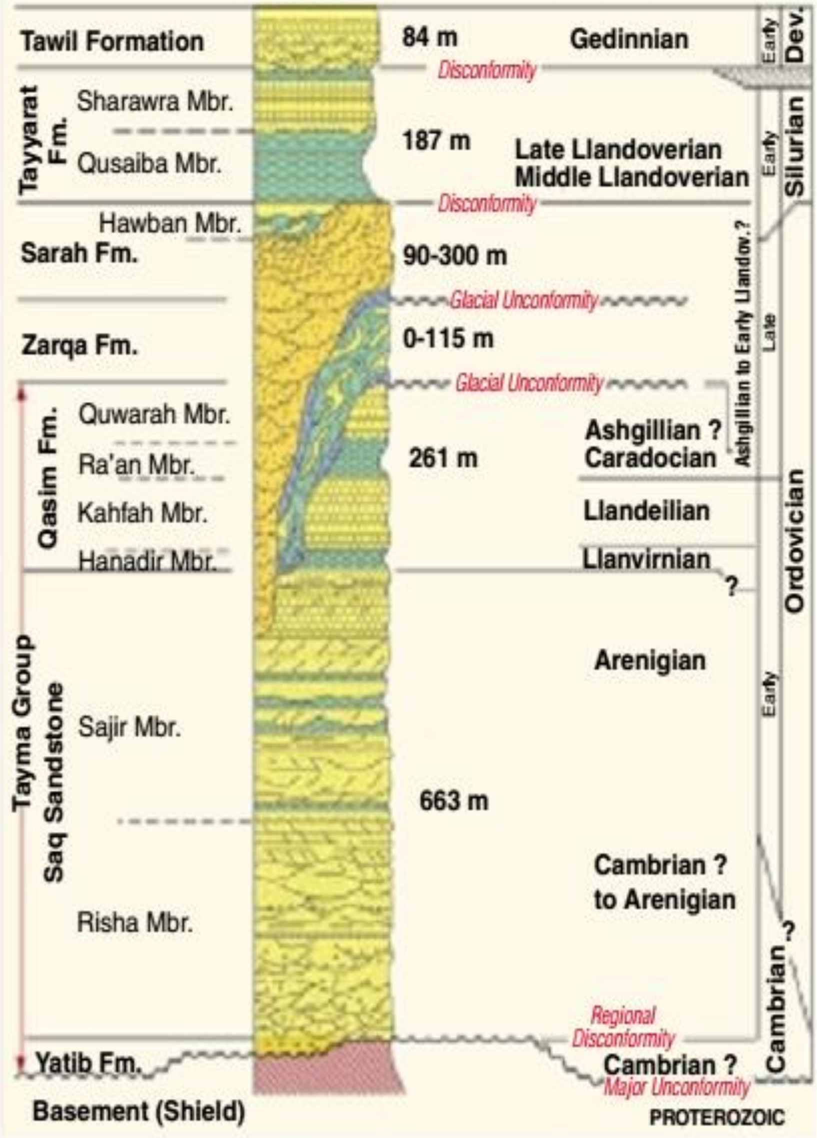

Figure 1-2: Sarah Formation within the Paleozoic stratigraphy of Central Saudi Arabia (Senalp and Al-Laboun, 2000; after Vaslet, 1989).

1.4 Previous Studies

McClure (1978) was the first to identify and provide evidence to the Late Ordovician Glaciation in Saudi Arabia. Mapping of Sarah paleovalleys was carried out by Vaslet (1987, 1989 and 1990). In 1992, Saudi Aramco started to conduct field trips to study the Late Ordovician Glaciation of Sarah Formation and its sedimentologic significance (Senalp and Al-Laboun, 2000). The first detailed sedimentologic studies of both the Zarqa and Sarah formations in the Qaseem and Hayil regions were carried out by Senalp and Al-Laboun (2000). They located the glacial boulders, tillite and striations within the Late Ordovician paleovalleys, Sarah and Zarqa Formations, in central Saudi Arabia (Figure 1-3). Moscariello et al. (2009) studied the paleogeography of Sarah Formation based on well data, outcrop analogs, and glacial equivalents in Mauritania, Algeria, South Turkey and Jordan.

The concept of tight gas sands was introduced in the 1978 *U.S. Gas Policy Act* as those reservoirs of permeability less than or equal to 0.1 md (Kazemi, 1982). Since then, several other definitions have been introduced, but, so far, this is the most commonly accepted one. Tight gas sands are one type of unconventional gas sources, side by side to shale gas, coal bed methane, and natural gas hydrates (Aguilera et al., 2008).

According to the important workflow suggested by Aguilera et al. (2008) for studying tight gas reservoirs, the first step should be inspecting the outcrop analog. When the outcrop proves a good quality, then 3D models should be established based on structural, stratigraphical, petrophysical and sedimentological analyses. After constructing the 3D virtual outcrop models, comes the integration with subsurface data such as cores, well logs, and considering porosity and permeability under reservoir conditions.

Le Heron et al. (2006) studied the Late Ordovician glaciogenic reservoir heterogeneity in the Murzuq Basin, Libya. Bukhamseen et al. (2010) developed a strategy for fracture stimulation that gave birth to the first discovery from Sarah Formation tight gas reservoirs in the Rub Al-Khali, Saudi Arabia. Laboun (2010) studied the glaciation events within the Paleozoic tectono-stratigraphic framework of the Arabian Peninsula. He pointed out that Zarqa and Sarah Formations represent the syn-glaciation cycle. Ghienne (2011) studied the distribution of the glacial features in both the proximal areas (Mauritania, Algeria, Libya, Niger, Saudi Arabia) and the ice distal zone (Morocco, Spain, Turkey).

Al-Harbi and Khan (2011) studied the petrography, geochemistry and diagenesis for samples of Sarah Formation in Central Saudi Arabia. They concluded that cementation was the main diagenetic event occurring as grain coats and pore fillings. They assigned the probable parent area of paleovalley-fill sediments to a complex of granite, metasedimentary and pre-existing sedimentary rocks.

Dogan et al. (2012) presented an overview of Sarah Formation as an example for unconventional tight gas sandstones in Saudi Arabia. They accounted the increased exploration potential of Sarah Formation due to the close relationship between Sarah Sandstones and the “hot shale” facies of the Qusaiba Member of Qaliba Formation.

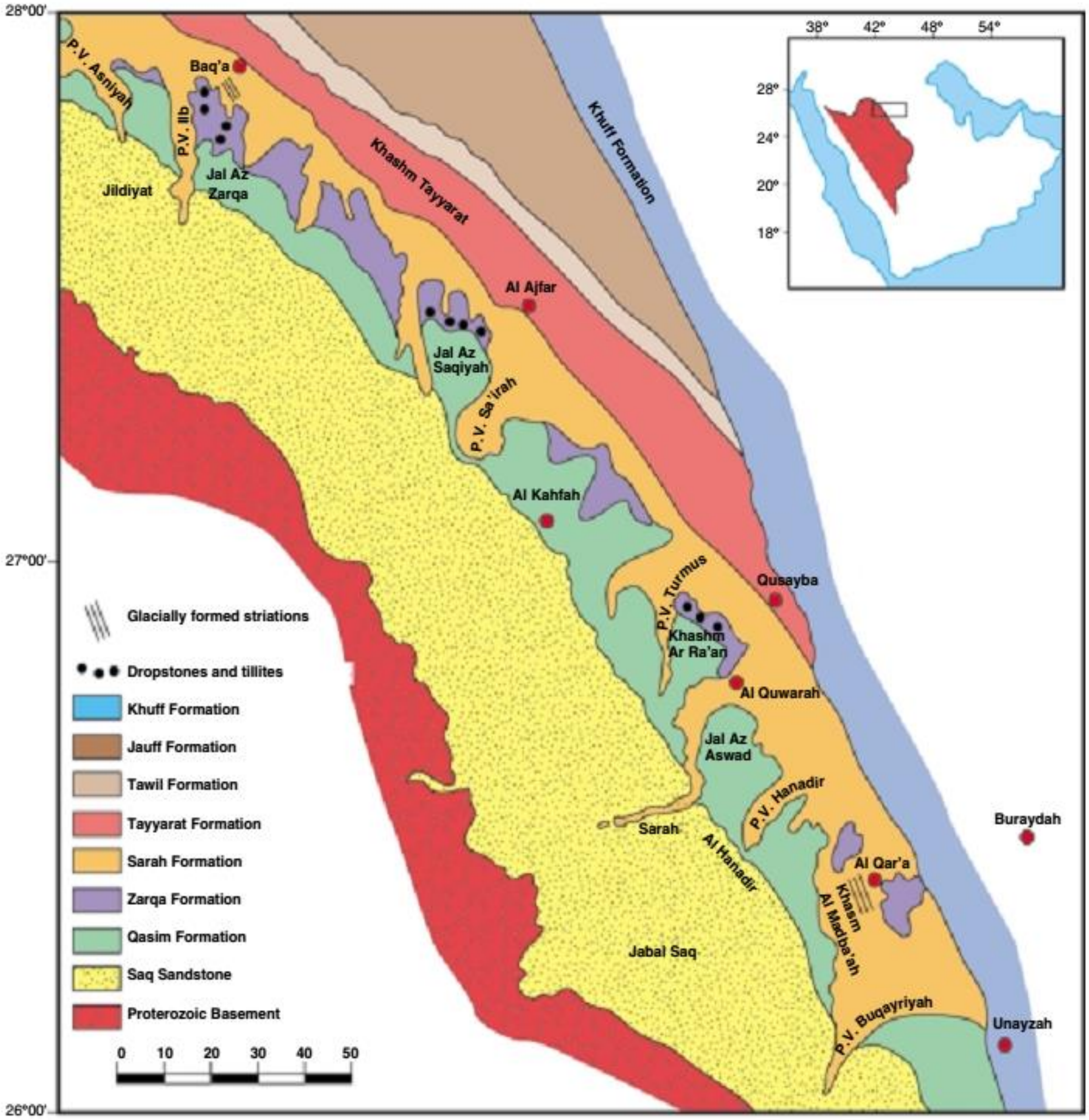

Figure 1-3: The locations of the glacial boulders, tillite and striations within the Late Ordovician paleovalleys in central Saudi Arabia (Senalp and Al-Laboun, 2000).

CHAPTER TWO

METHODOLOGY

2.1 Introduction

The study comprised of field sedimentological investigations, followed by various laboratory analyses of samples and data interpretation. An outline of the methods used in the study is shown in the flow chart (Figure 2-1) and discussed briefly in this chapter.

2.2 Field Investigation

Field data were obtained through studying ten outcrop sections representing five paleovalleys of Sarah Formation (Figure 1-1), namely Bukayriyah, Hanadir, Sarah and Sarah Ridge (Khanasir Sarah). Facies were described on the basis of grain sizes, sedimentary structures, color, fossils, etc. The architectural elements were recorded for the facies analysis using the facies code of (Miall, 1996) as described in Table 3-2. Throughout the course of field study, a total of about 100 samples representing different paleovalleys from different localities were collected for laboratory examinations and petrophysical measurements.

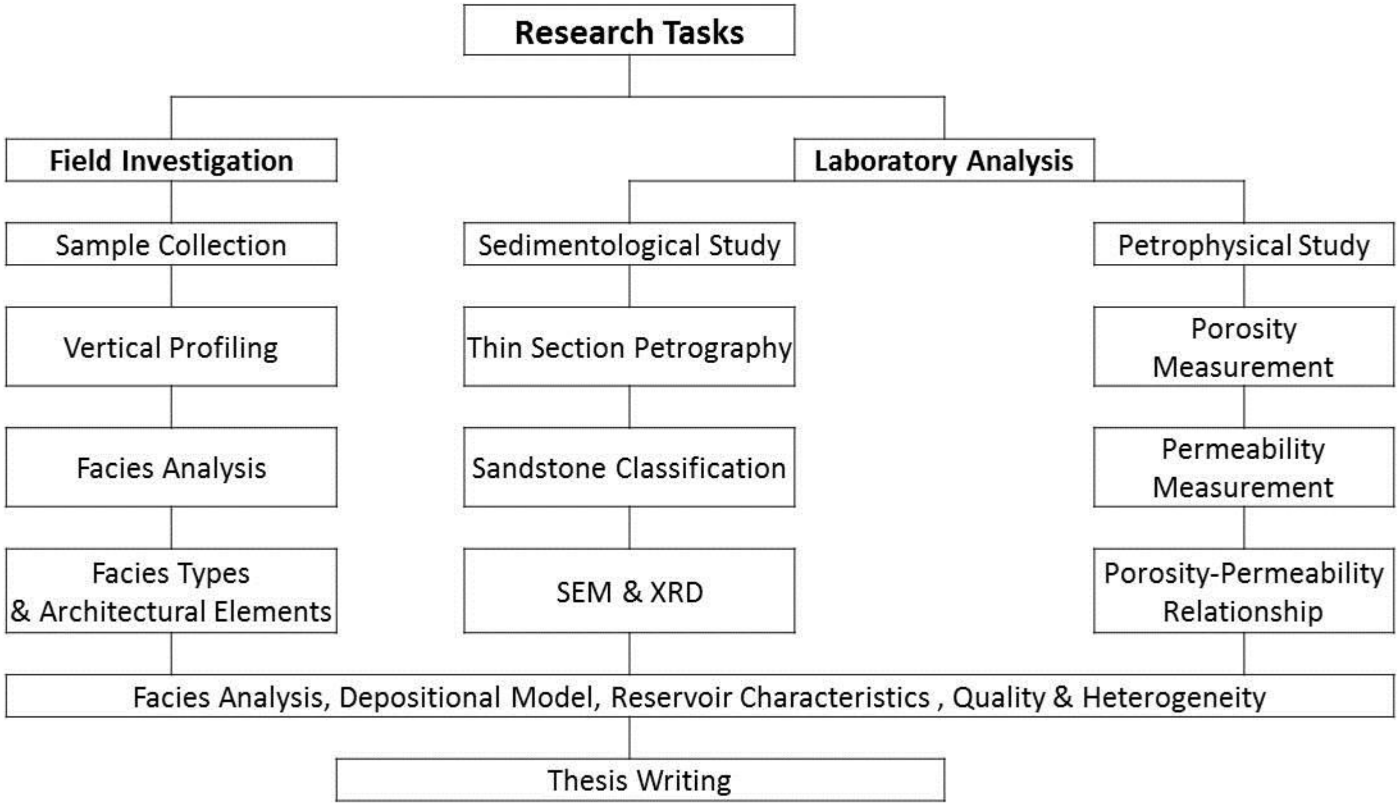

Figure 2-1: Flow chart showing basic steps and methods of study.

2.3 Laboratory Analysis

Out of the samples collected from different paleovalleys during the field investigation, 290 core plugs were prepared and processed for petrophysical analysis (porosity and permeability measurements). A total of 90 plugs were processed for petrographic analysis. From those 90 samples, thin sections were prepared. Also, 15 samples were analyzed using scanning electron microscopy (SEM), and 20 others by X-ray powder diffraction technique.

2.3.1. Thin Section Petrography

Thin sections were required to get information on sandstone composition, texture, sorting, mineralogical composition and porosity. The effects of depositional facies and diagenetic processes on the sediment heterogeneity were also taken into consideration. 78 thin sections were prepared from the selected samples. The samples were impregnated with blue epoxy under vacuum pump to reveal the distribution of pores. Then, the impregnation was allowed to cure overnight. The slabs were smoothly polished with calcium carbide on plane glass and mounted on glass slide. The glass-mounted slabs were subsequently polished for thin section microscopy after curing. The petrographic analysis of thin sections was conducted based on Tucker (2001).

2.3.2. Scanning Electron Microscopy (SEM)

Better observation of features was achieved through the application of SEM analysis on 15 samples. SEM was useful in getting a clearer idea of grain boundaries, microstructures and elemental analysis. It also helped in the identification of the clay types based on morphology and its effects on porosity. The samples for SEM study were placed in holders (platinum disc) held with carbon paint, dried and gold-coated in vacuum with sputter coater. The coated samples were subsequently scanned with SEM**,** Model *JEOL JSM-5900LV* (Figure 2-2); under electron beam not stronger than 20 keV. Having an Oxford Energy Dispersive Spectrometer (EDS) attached to the SEM helped in analyzing the elemental composition of the examined rock samples.

2.3.3. X-Ray Powder Diffraction (XRD)

The aim of using XRD was to identify the mineralogical composition of the rock samples of Sarah Formation, recognize the clay minerals present in the samples and identify them. 20 samples of Sarah Formation, from different paleovalleys, were subjected to XRD analysis. The samples were ground to fine powders. In this powdered form, grains tend to arrange themselves in some preferred orientations that produce distinct diffraction patterns. The device *JEOL JDX-3530* (Figure 2-3) has been used for the analysis.

Figure 2-2: The SEM device, JEOL *JSM-5900LV*.

Figure 2-3: The XRD device, JEOL *JDX-3530*.

2.3.4. Porosity and Permeability

Thorough porosity and permeability measurements were carried out on about 290 core plugs to detect the micro-heterogeneity within the studied paleovalleys. The core plugs have 1" diameter and various lengths, but mainly 2". The selected samples were analyzed using the *TPI-219* helium-porosimeter and the *TKA-209* gas-permeameter (*Coretest Systems, Inc.*) devices (Figure 2-4). The standard procedures for porosity and permeability measurements have been followed as stated in the User’s Manuals of both devices.

The helium-porosimeter requires sample core plugs. The weight, length and diameter of these plugs are input parameters to be loaded to the system to calculate the grain volume, pore volume and bulk volume. These calculations were used to calculate the grain density and hence to get the porosity percentage.

The same core plugs were used in the gas-permeameter. The gas injected into the rock samples was helium. For each plug, five gas permeability measurements, at different pressures, are plotted versus the inverse of mean pressure (Figure 2-5). Liquid permeability is equivalent to the value at the intercept of the average straight line with the gas permeability axis, so-called “Klinkenberg correction”.

(a)

(b)

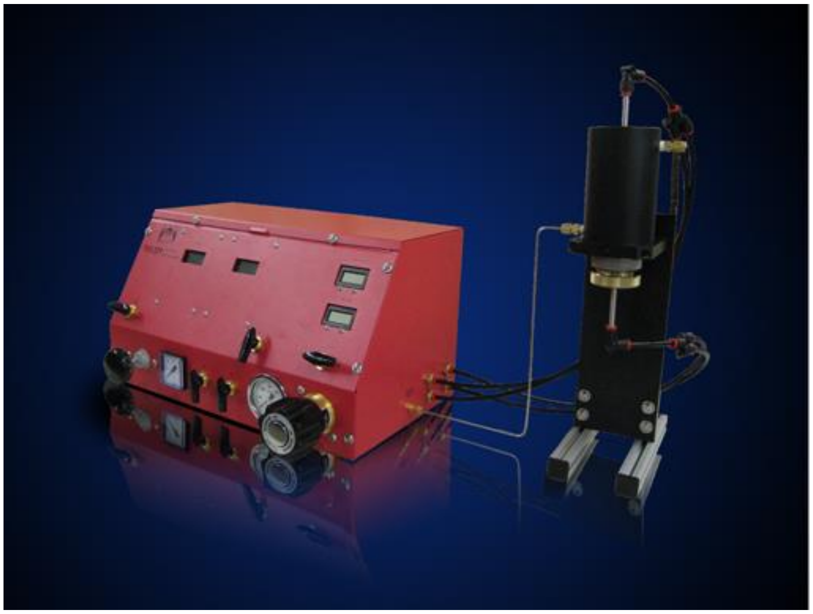

Figure 2-4: (a) *TPI-219* helium-porosimeter, and (b) *TKA-209* gas-permeameter (*Coretest Systems*, *Inc*., California, U.S.A.). http://www.coretest.com/

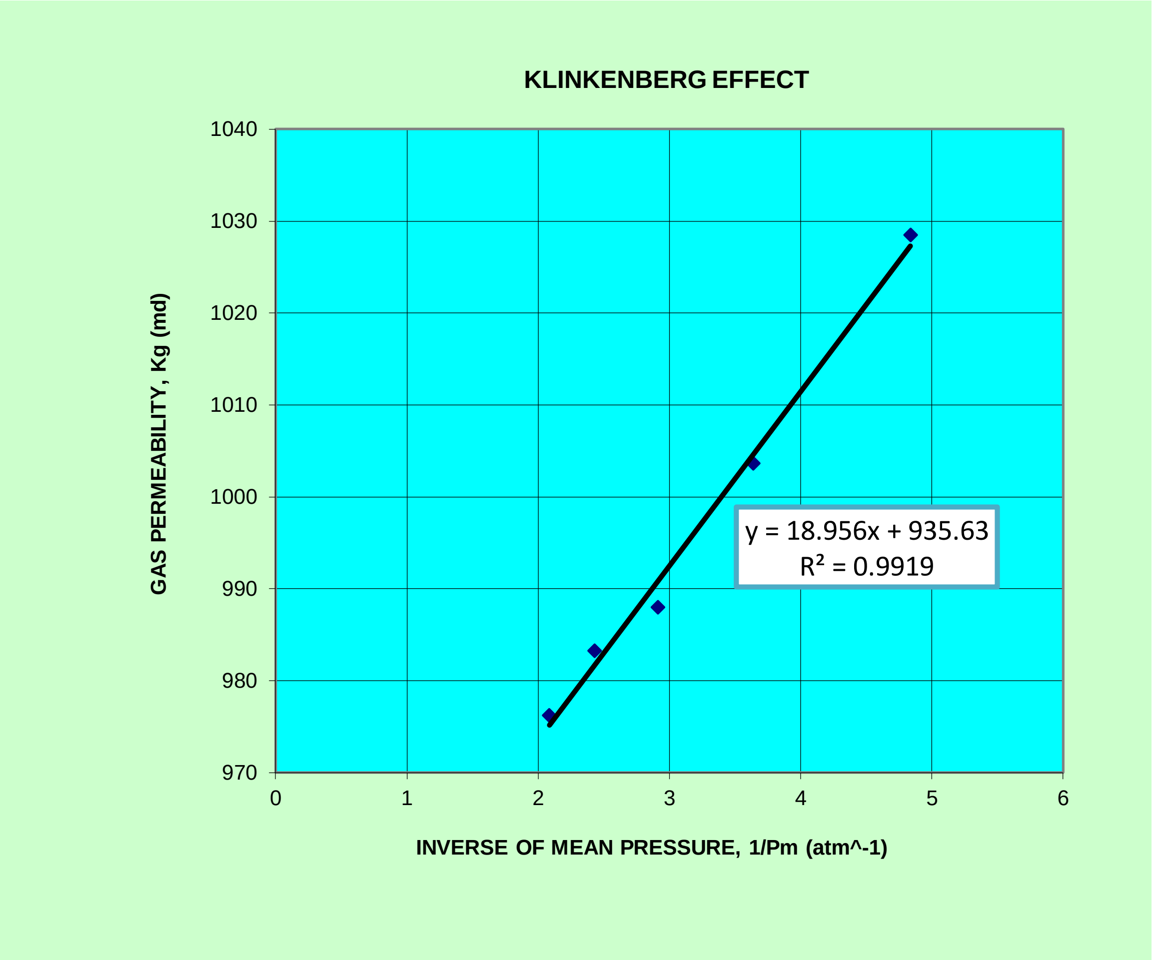

Figure 2-5: An example from sample # S1V1 for calculating liquid permeability from gas permeability using the Klinkenberg correction (five pressure steps). The y-intercept is the Klinkenberg-corrected permeability.

2.3.5. Mercury Injection Capillary Pressure (MICP)

Washburn (1921) was the first to use mercury injection to determine the pore aperture size distribution. The MICP method was further developed by Purcell (1949) and many others. Mercury injection is used to determine the interconnected porosity and the size distribution of pore apertures, both influencing permeability and non-wetting phase (e.g., hydrocarbon) saturations (Shafer and Neasham, 2000).

Pore-throat aperture size analysis was conducted for 10 selected samples representing the different studied paleovalleys. The analysis was conducted using the *Micromeritics AutoPore IV 9500* high-pressure (up to 60,000 psia) mercury porosimeter (Figure 2-6). It can measure pore diameter range from approximately 360 to 0.003 µm. The cleaned and dried core plugs were injected by mercury, as a non-wetting phase, in customized pressure increments. Being non-wetting to most substances and having high surface tension, mercury intrudes into the pores, and hence the pore volume can be calculated. The instrument automatically records the volume of mercury injected at each pressure increment up to 100 % pore-volume Hg saturation (see Chapter Five).

Figure 2-6: the *Micromeritics AutoPore IV 9500* high-pressure porosimeter.

http://www.micromeritics.com/product-showcase/AutoPore-IV.aspx

CHAPTER THREE

FIELD INVESTIGATION

3.1. Introduction

A detailed field work was conducted to provide the basic data required for sedimentology, petrophysics and heterogeneity description in the studied paleovalleys of Sarah Formation. Nine selected outcrop sections representing various paleovalleys of Sarah Formation were studied and described as shown in Figure 1-1. Representative samples were collected from these sections to be subjected to further laboratory analysis.

Table 3-1 shows the locations of the studied outcrops within Sarah Paleovalleys, and their geographic coordinates. This chapter includes description of each outcrop and facies based on the study of the vertical and lateral outcrop profiles. Facies were analyzed and architectural elements identified based on the facies code after Miall (1996). Facies assemblages and architectural elements encountered in Sarah Formation are described briefly in Table 3-2. This provided information about depositional processes and spatial configuration of deposits. The depositional model of Sarah Formation has been proposed based on the facies analysis.

Sarah Formation appears as deeply incised glacial paleovalleys in outcrops, as described by McGillivray and Husseini (1992) and Vaslet (1987, 1989 and 1990). The concept of Sarah paleovalleys was investigated thoroughly by Clark-Lowes (2005) with extensive photogeological and sedimentological work. He concluded that Sarah Formation is deeply incised into the lower Ordovician sediments, and it was deposited onto an erosional surface that has a geometry similar to that of a valley. Later regional marine transgression occurred during the Early Silurian, which flooded these valleys resulting in the deposition of the Qusaiba shale (Senalp and Al-Laboun, 2000).

In most of the outcrops, Sarah Formation is highly affected by erosion and the remaining section is the most resistive preserved part of Sarah Formation, as in Bukayriyah, Rawd Al-Jawa and Sarah paleovalleys. In other outcrops, Sarah Formation unconformably cuts through Hanadir, Kahfa, Ra’an and Quwarah members of Qasim Formation, As in Hanadir and Khanasir Sarah paleovalleys. In these outcrops, the sharp contacts with the underlying beds of Qasim Formation indicate erosion or lack of deposition prior to the deposition of Sarah sandstones. The thickness of Sarah formation varies according to many factors including: paleotopography, size of the paleovalley, the resistance of erosion, the amount of preserved sedimentary infill and the position of the outcrop within the paleovalley (Manivit et al., 1986; Senalp and Allaboun, 2000).

Table 3-1: Locations of the studied outcrops of Sarah Formation in Central Saudi Arabia

Outcrop No.	Paleovalley	Locality	Longitude	Latitude	Sample code
1	Bukairiyah	Al-Bukairiyah	E 43° 38' 52.6"	N 26° 08' 58"	S1-
2	Bukairiyah	Al-Bukairiyah	E 43° 39' 6.3''	N 26° 09' 25.1''	S2-
3	Bukairiyah	Al-Qar’a	E 43° 45' 19''	N 26° 23' 08''	--
4	Rawd Al-Uyun	Uyun Al-Jawa	E 43° 35.836'	N 26° 31.656'	--
5	Rawd Al-Uyun	Uyun Al-Jawa	E 43° 35.861'	N 26° 31.600'	--
6	Hanadir	Uyun Al-Jawa	E 43° 35.784'	N 26° 33.133'	RC-
7	Hanadir	Uyun Al-Jawa	E 43° 34' 40.2''	N 26° 34' 14.6''	SR-
8	Sarah	Al-Quwarah	E 43° 28' 5.2''	N 26° 47' 22.8''	S3-
9	Khanasir Sarah	Jabal Al-Khanasir			KS-

3.2. Bukayriyah Paleovalley

Al-Bukayriyah paleovalley is the largest of the five studied paleovalleys. It extends from Al-Bukyriyah to Al-Qar’a towns over more than 50 km distance with a north-northeast orientation. Three outcrop sections were studied in this paleovalley. The first outcrop in Al-Bukayriyah (43° 38' 52.6" E; 26° 08' 58" N) lies near the entrance of Al-Bukayriyah city (Figure 1-1). The original section is no longer existent as it was removed completely. The remaining are some blocks and boulders of Sarah Formation. The sandstones are fine to medium-grained and horizontally laminated. Samples were collected from this outcrop for subsequent laboratory analysis.

The outcrop section No. 2 (Figure 3-2) is approximately three meters thick, located behind the main square at the entrance of Al-Bukayriyah town (43° 39' 6.3'' E; 26° 09' 25.1'' N). The vertical profile of this section demonstrates stacked channels of fine to medium-grained sandstone. These channels are separated by a scoured surface. Scour hollows were observed filled with finer sandstone.

The outcrop No. 3 in Bukayriyah paleovalley is located approximately two kilometers west of Al-Qar’a town (43° 45' 19'' N; 43° 45' 19'' E). It was previously referred to by Senalp and Al-Laboun (2000) and Senalp and Al Duaiji (1996) as “Sarah channel at Khashm Al-Madba’ah cuesta”. The base of the Sarah channel cuts deeply into the tide-dominated shallow marine sequence of Ra’an and Quwarah members of Qasim Formation (Figure 3-6, Figure 3-7).

The section begins at the bottom with about nine meters of the dark grey laminated Ra’an shale. The sequence is coarsening upward with 1-1.5 meters of fine-grained well sorted siltstone followed by the horizontally stratified, well sorted, off-white, bioturbated sandstone of Quwarah Member. Then, the incised Sarah channel cuts the underlying Quwarah Member then cuts deeply into the Ra’an Member with an angle of about 30 degrees (Figure 3-5, Figure 3-7).

The base of the channel is characterized by a continuous bed of diamictite. The Sarah Formation at the top of the section contains coarse to very coarse-grained, brownish and yellowish white, poorly sorted, massive sandstone. At the very top lies a bed of approximately 30 cm of crudely trough cross-bedded sandstone. At some parts, the diamictite is horizontally imbricated at the base of Sarah Formation. The sandstones are affected by syn- and post-sedimentation faults and soft-sediment deformation structures which outfaced the primary sedimentary structures. These are probably due to liquefecation, clay de-watering or differential compaction of partially lithified sediments (Clark-Lowes, 2005).

3.3. Rawd Al-Jawa Paleovalley

Moving north from Al-Bukayriyah paleovalley, lies the Rawd Al-Jawa paleovalley which has a north-east direction. Two sections were studied at this paleovalley. Outcrop profile No. 4 is located at Uyun Al-Jawa (26° 31.656' N, 43° 35.836' E). The vertical profile of this section (11 m) shows a coarsening and thickening upward sequence (Figure 3-10). It starts at the base with reddish color, fine-grained, well-sorted, laminated siltstone. The siltstone is rooted, bioturbated, contains vertical burrows (7-15 cm) filled with green mud, as well as muddy dropstones and diamictite.

The next interval is composed of medium to coarse-grained sandstone, cut by scoured surface of channel with intraformational conglomerate at the base, trough cross-bedding and diamictite. Diamictites usually indicate a glacial origin. The last interval (7m) at the top comprises medium-grained, trough cross-bedded sandstone, containing green pebbles and mud clasts.

Outcrop section No.5 is also located at Uyun Al-Jawa next to outcrop No. 4, (26° 31.600' N, 43° 35.861' E). The vertical profile (Figure 3-13) is composed of 11 m of vertically stacked channels with clear scoured channel bases. The lower interval is medium-grained sandstone, very well-sorted, horizontally and thinly laminated, containing iron concretion, overlying very fine-grained, *Scolithos*-rich and oxidized sandstone (Sb). The next interval is composed of medium-grained sandstone, thinly bedded, that contains vertical burrowing, commonly *Scolithos*-rich, bioturbation, iron concretions, interbedded with very fine-grained, well sorted siltstone.

3.4. Hanadir Paleovalley

Sarah Formation is well exposed in Hanadir paleovalley near Jabal Al-Hanadir. The paleovalley has a NE orientation. Outcrop No. 6 is a road-cut section on the highway to Uyun Al-Jawa town (26° 33.133' N, 43° 35.784' E). This section is composed of four intervals of sandstones with coarsening upward pattern (Figure 3-16). The first interval at the base is composed of very fine-grained, horizontally laminated, bioturbated reddish color sandstone. The overlying interval is mainly fine-grained, whitish grey, fractured sandstone. The third interval comprises fine to medium-grained horizontally laminated sandstone with local small-scale trough cross-bedding and limonite pebbles. The sandstone becomes very coarse-grained and trough cross-bedded at the upper interval.

Outcrop No.7 at Uyun Al-Jawa, Hanadir paleovalley (26° 34' 14.6'' N, 43° 34' 40.2'' E) is where Sarah Formation lies directly unconformably over the Ra’an Member of Qasim Formation (Figure 3-19, Figure 3-20). The Sarah channel cuts sharply and abruptly through the Ra’an shale. The Sarah sandstone is fine to medium-grained, yellowish brown, mostly massive, with local faint lamination, horizontally laminated in the upper part. The sandstone beds are affected with vertical fractures that caused general deformation structures. The channel base is marked by 1-2 m siltstone bed.

Figure 3-21 Shows correlation of vertical sections through the lateral profile of the outcrop that show the cutting of Sarah Formation into the underlying Ra’an shale.

3.5. Sarah Paleovalley

The outcrop No. 8 is located at Al-Quwarah (26° 47' 22.8'' N, 43° 28' 5.2'' E). It represents the thickest section of Sarah Formation of all the measured sections in the study area. It comprises 26 m of reddish color, fine-grained sandstone (Figure 3-22). The sandstones are mainly horizontally laminated. The thickness of the beds ranges from less than 1 cm to a few cm. the upper part of the section is sheared and fractured and contains local trough cross-bedding. Iron cementation appears clearly at the top of the section where hematite and limonite pebbles are common. The whole section is a group of stacked channels in which sandstone beds truncate each other.

3.6. Khanasir Sarah (Sarah Ridge) Paleovalley

Outcrop No. 9 at Sarah Ridge (Khanasir Sarah) reveals the lateral heterogeneity of Sarah Formation with relation to other Paleozoic formations. The Sarah channel cuts deeply through Kahfah sandstone and deeper into the Hanadir shale, both of Qasim Formation (Figure 3-27).

Sarah Formation, in the central part, consists of medium to coarse-grained sandstone, horizontally to low angle laminated, trough cross-bedded in some parts. The change in grain size or sedimentary structures is related to deposition of a new channel marked by a scoured base (Figure 3-25, and Figure 3-26).

Figure 3-1: Photographs from the first outcrop of Sarah Formation in Al-Bukayriyah (43° 38' 52.6" E; 26° 08' 58" N) showing (a) scattered blocks of Sarah Formation sandstones, (b) glacial grooves within the fine-grained sandstones, (c) a tillite block of horizontally stratified fine to medium-grained sandstone.

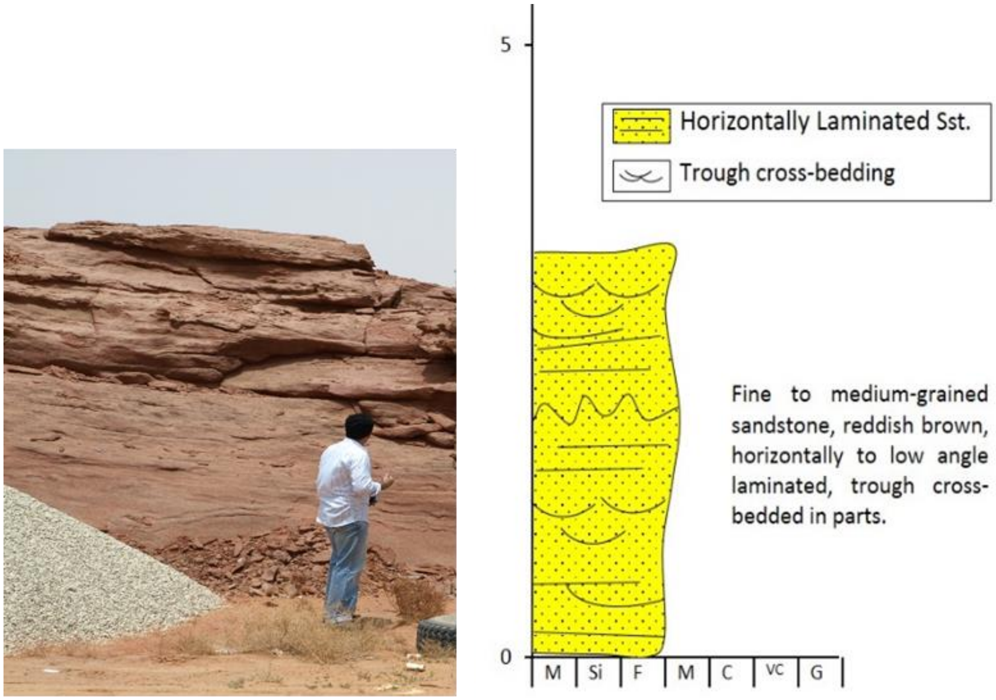

Figure 3-2: Vertical profile of outcrop No. 2 of Sarah Formation at Al-Bukayriyah (43° 39' 6.3'' E; 26° 09' 25.1'' N) consists of two stacked channels dominated by fine to medium-grained sandstone, trough cross-bedded, well sorted sandstone.

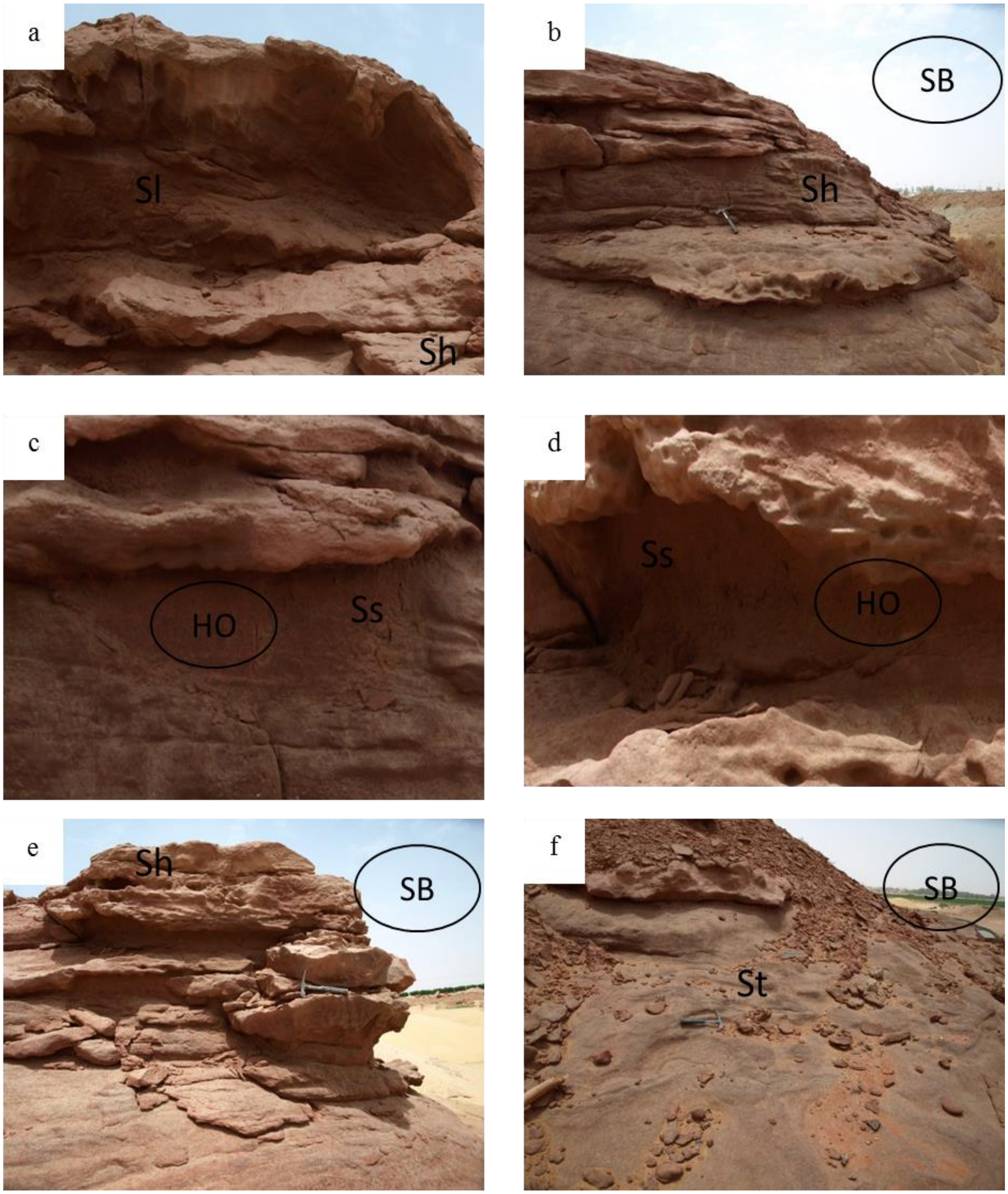

Figure 3-3: Photographs from outcrop section No. 2 of Sarah Formation at Al-Bukayriyah (43° 39' 6.3'' E; 26° 09' 25.1'' N) showing (a) horizontally bedded to low angle bedded sandstone, (b) sandy bedforms (SB) containing horizontally stratified sandstone, (c) and (d) scoop-shaped Scour hollows (HO) filled with fine sand, (e) SB architectural element with horizontally stratified sandstone, (f) trough cross-bedded sandstone at the base of SB.

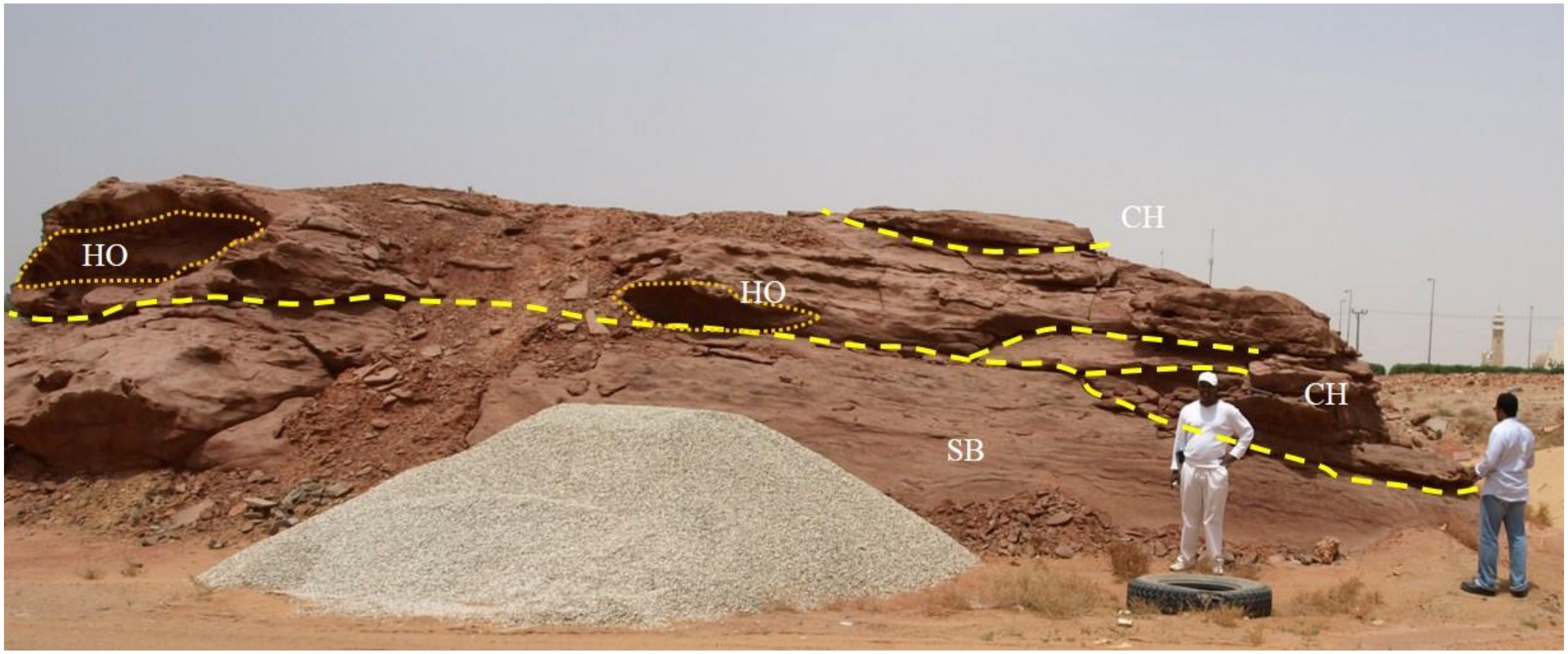

Figure 3-4: Lateral profile of outcrop No. 2 of Sarah Formation at Al-Bukayriyah (43° 39' 6.3'' E; 26° 09' 25.1'' N) showing sandstone body geometry and architectural elements classification. CH: channel, SB: sand bedforms, HO: scour hollows.

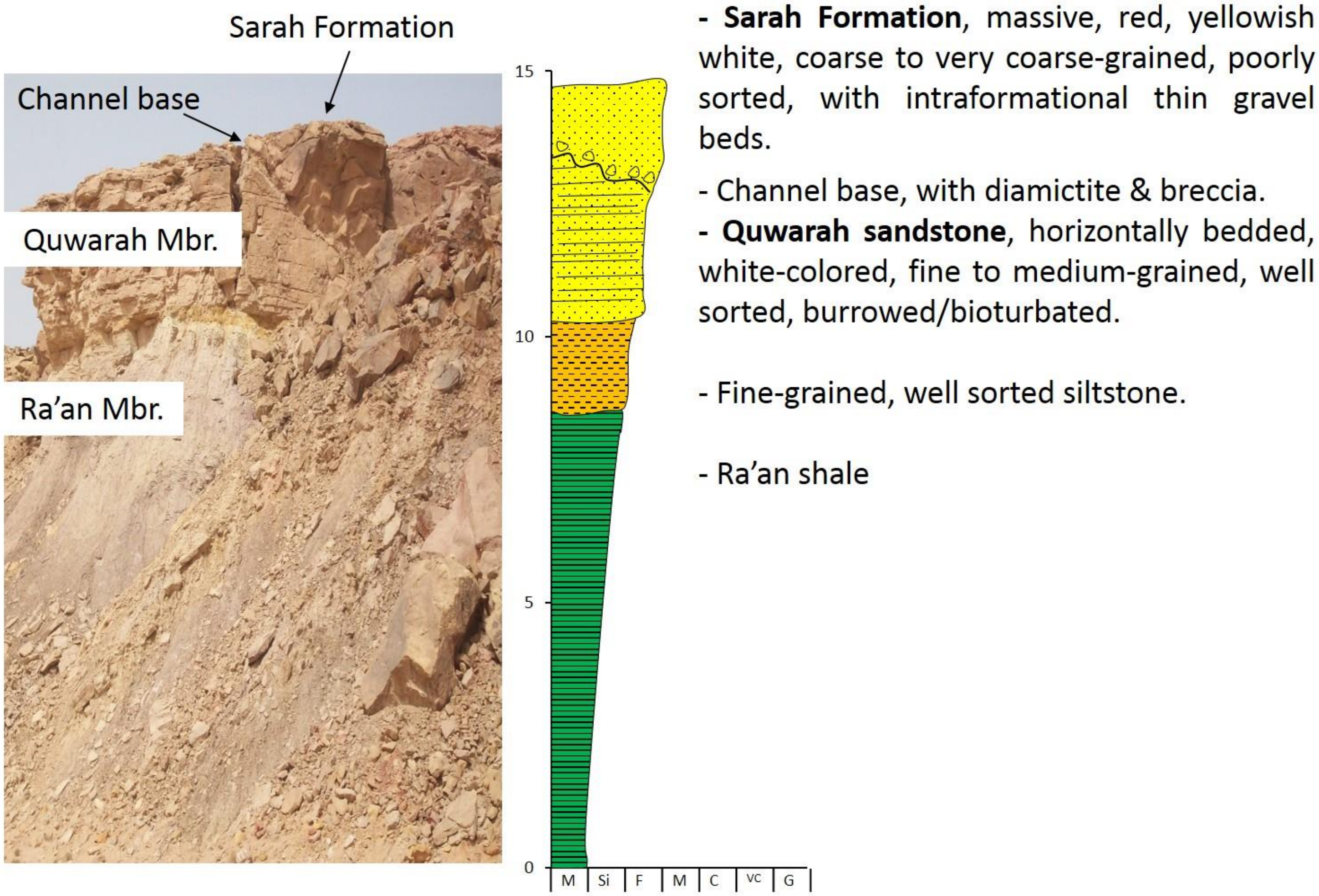

- **Sarah Formation**, massive, red, yellowish white, coarse to very coarse-grained, poorly sorted, with intraformational thin gravel beds.
- Channel base, with diamictite & breccia.
- **Quwarah sandstone**, horizontally bedded, white-colored, fine to medium-grained, well sorted, burrowed/bioturbated.
- Fine-grained, well sorted siltstone.
- Ra’an shale

Figure 3-5: Vertical profile of outcrop No. 3 of Sarah Formation at Al-Qar’a (43° 45' 19'' N; 43° 45' 19'' E) showing Sarah channel cutting through the Quwarah and Ra’an members of Qasim Formation.

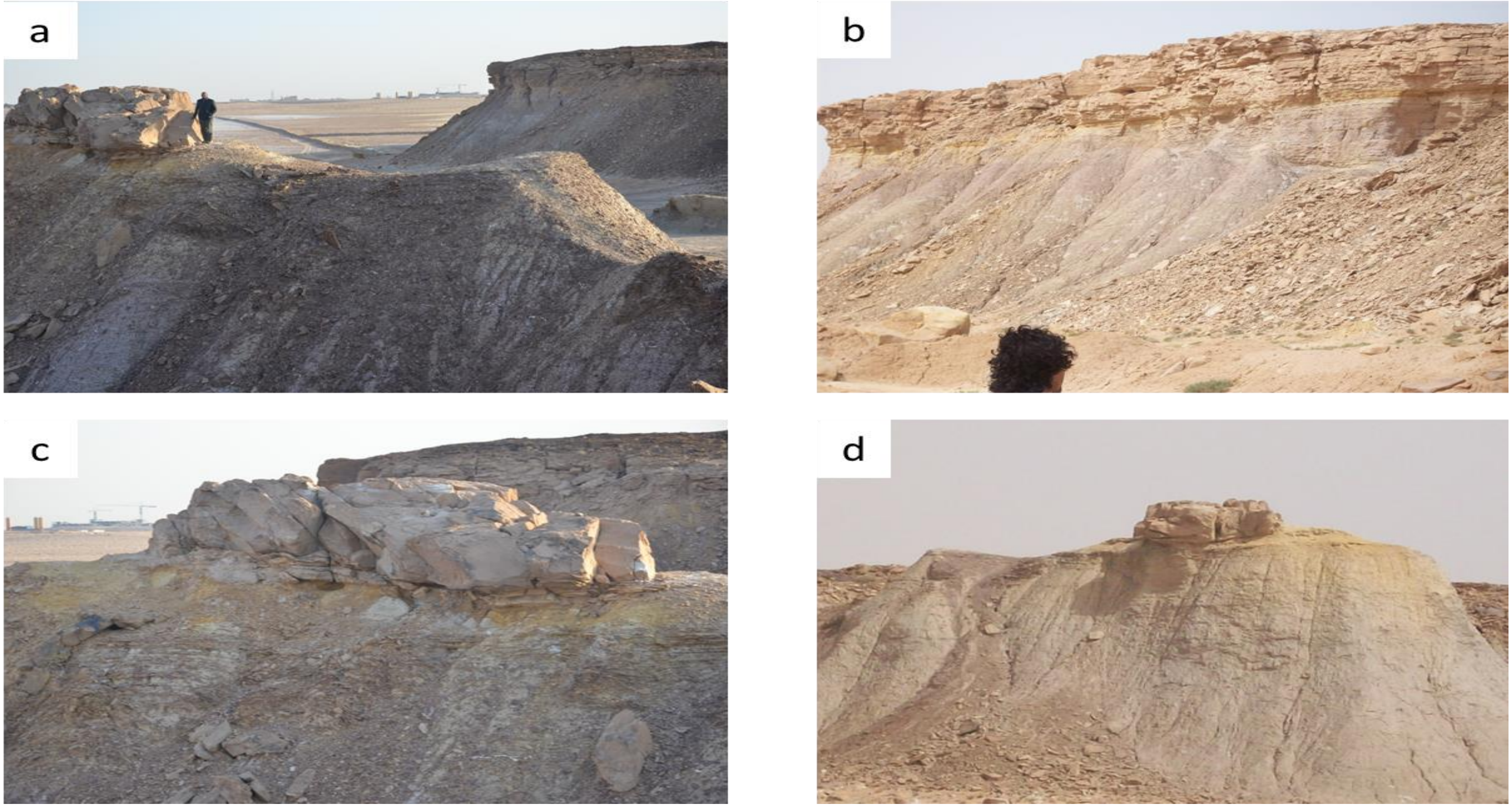

Figure 3-6: Photographs of outcrop No. 3 of Sarah Formation at Al-Qar’a showing (a) the northern end of the outcrop where at the right side of the photo Sarah Formation is completely eroded, while at the left side of the photo, Quwarah Member is eroded and Sarah Formation lies above Ra’an Member, (b) the progradational shallow marine sequence of Ra’an and Quwarah members of Qasim Formation while Sarah Formation is completely eroded, (c) close-up view of (a), (d) the other side of (a).

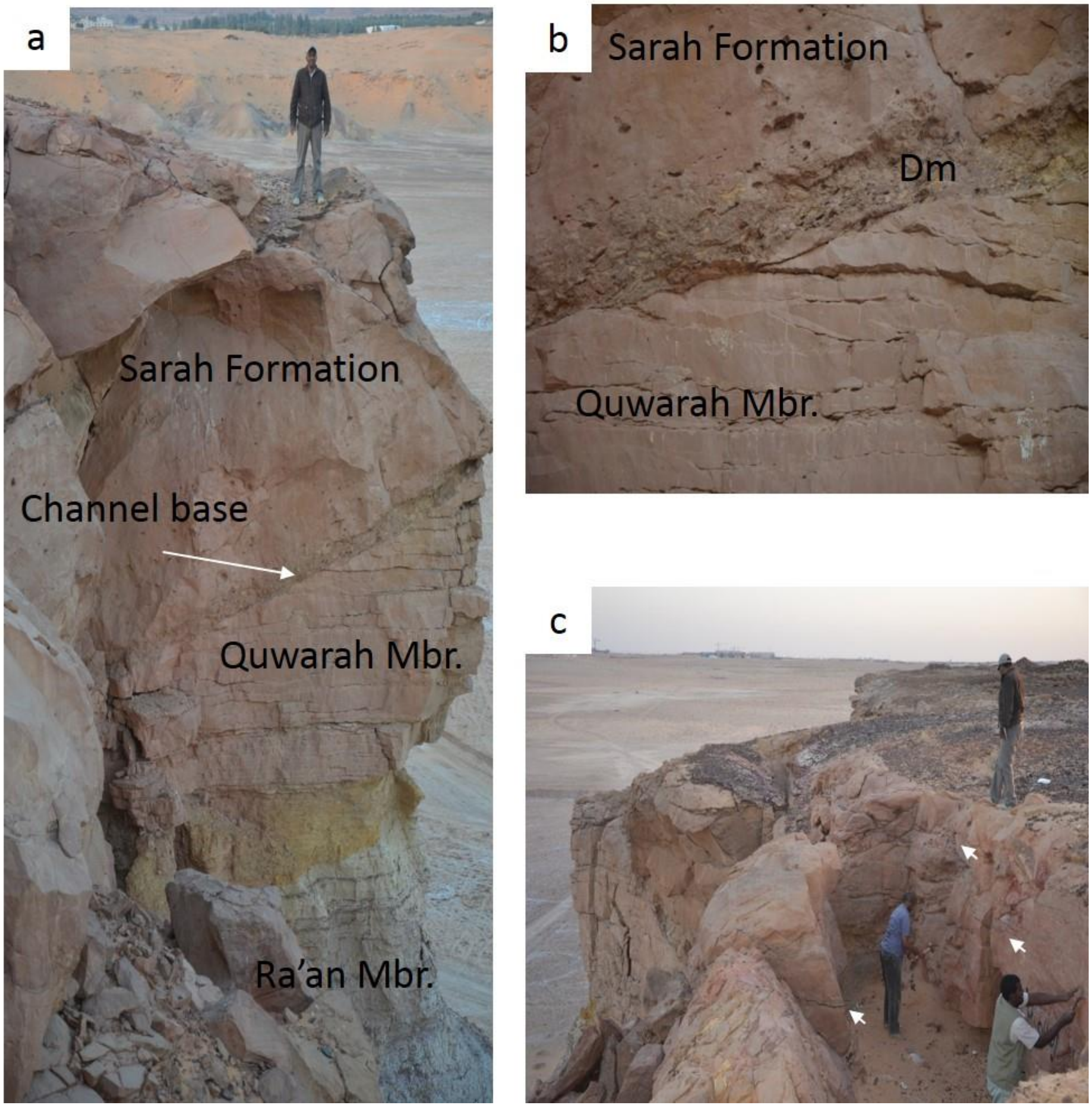

Figure 3-7: Photographs of outcrop No. 3 of Sarah Formation at Al-Qar’a showing (a) the opposite side of Sarah channel appearing in Figure 3-5 where Sarah Formation cuts into Quwarah and Ra’an members of Qasim Formation, (b) close-up view of the contact between Sarah Formation and Quwarah Member where the base of the channel is characterized by a diamectite (Dm) thin bed, (c) a cavity within Sarah Formation in which the arrows show the intraformational diamictite occurring as very thin beds within the trough cross-bedded sandstone.

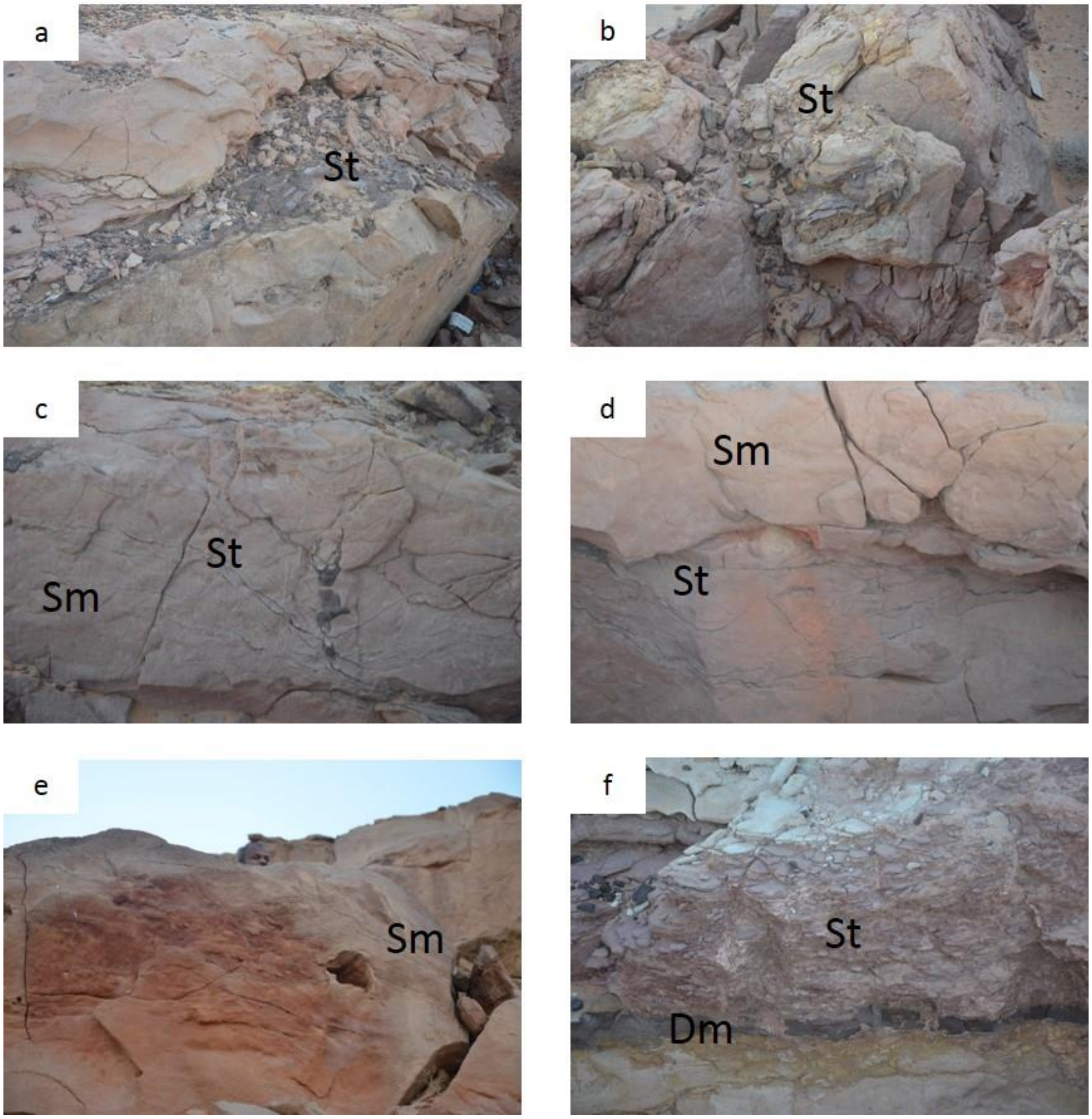

Figure 3-8: Photographs of outcrop No. 3 of Sarah Formation at Al-Qar'a showing the main lithofacies of Sarah Formation in this section: (a) trough cross-stratified sand bed at top of Sarah Fm., (b) trough cross-bedded sandstone imbricated within the deformed sand blocks of Sarah Fm., (c) and (d) trough cross-bedded sandstone interbedded with massive sandstone, (e) massive or faint-laminated coarse-grained sandstone, (f) glacial diamectie facies with mud clasts overlain by approximately 30 cm of trough cross-bedded sandstone.

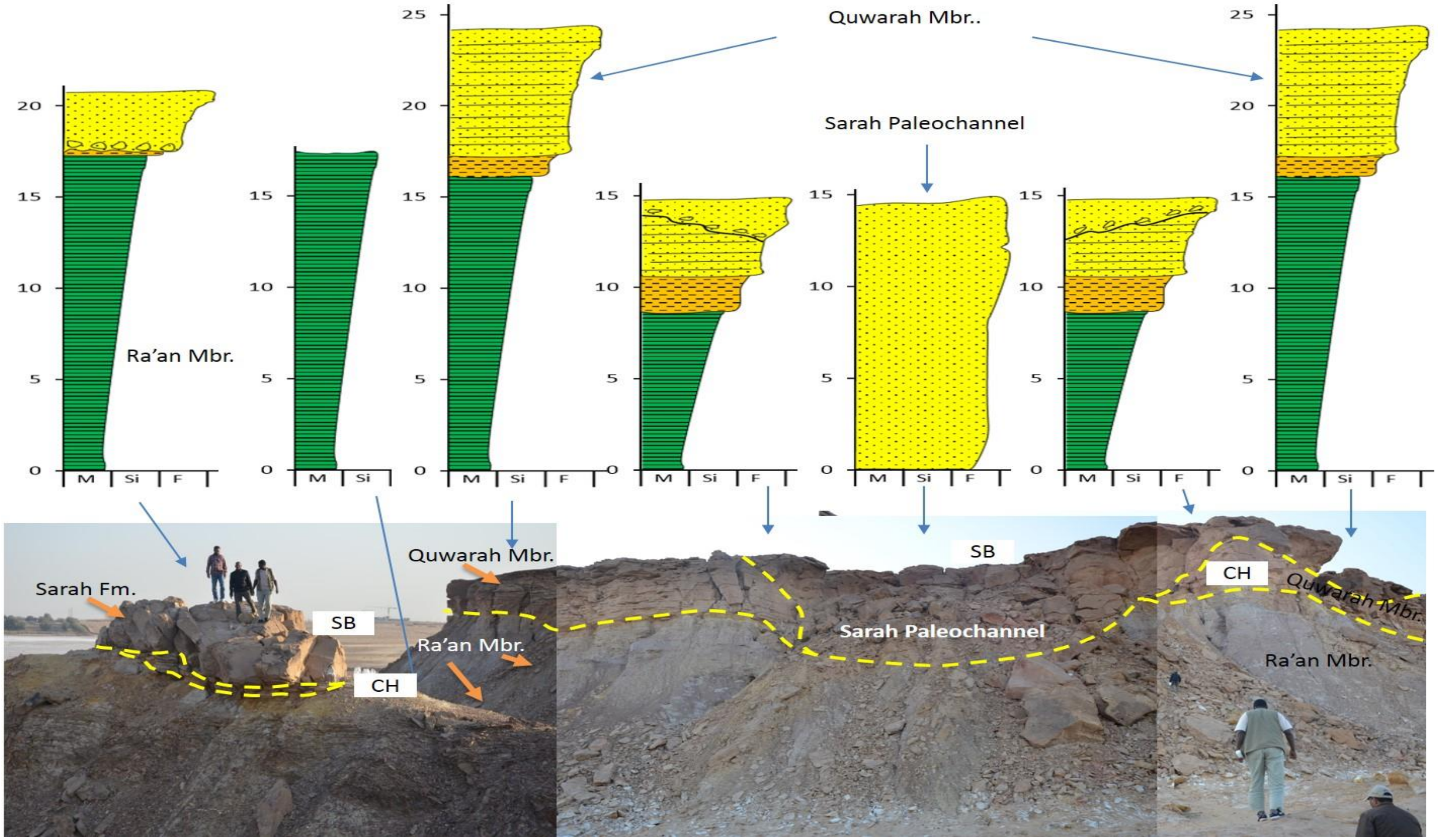

Figure 3-9: Annotated photomosaic for the lateral profile of outcrop No. 3 of Sarah Formation at Al-Qar’a showing the main architectural elements, with correlation of sedimentologic logs at different positions of the outcrop to illustrate the relationship with other Paleozoic formations. CH: channel, SB: sand bedforms.

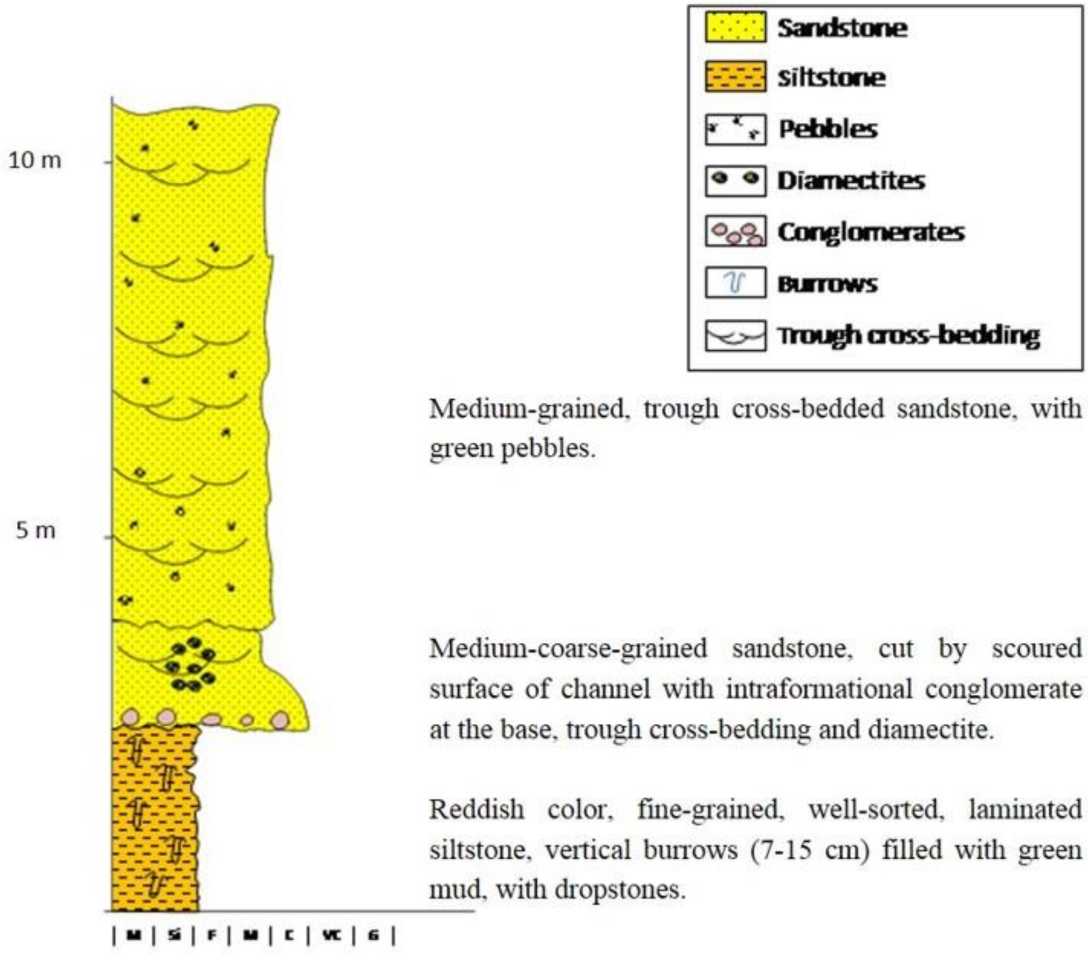

Medium-grained, trough cross-bedded sandstone, with green pebbles.

Medium-coarse-grained sandstone, cut by scoured surface of channel with intraformational conglomerate at the base, trough cross-bedding and diamectite.

Reddish color, fine-grained, well-sorted, laminated siltstone, vertical burrows (7-15 cm) filled with green mud, with dropstones.

Figure 3-10: The vertical profile of outcrop section No.4 of Sarah Formation at Uyun Al-Jawa, Rawd Al-Jawa paleovalley (26° 31.656' N, 43° 35.836' E).

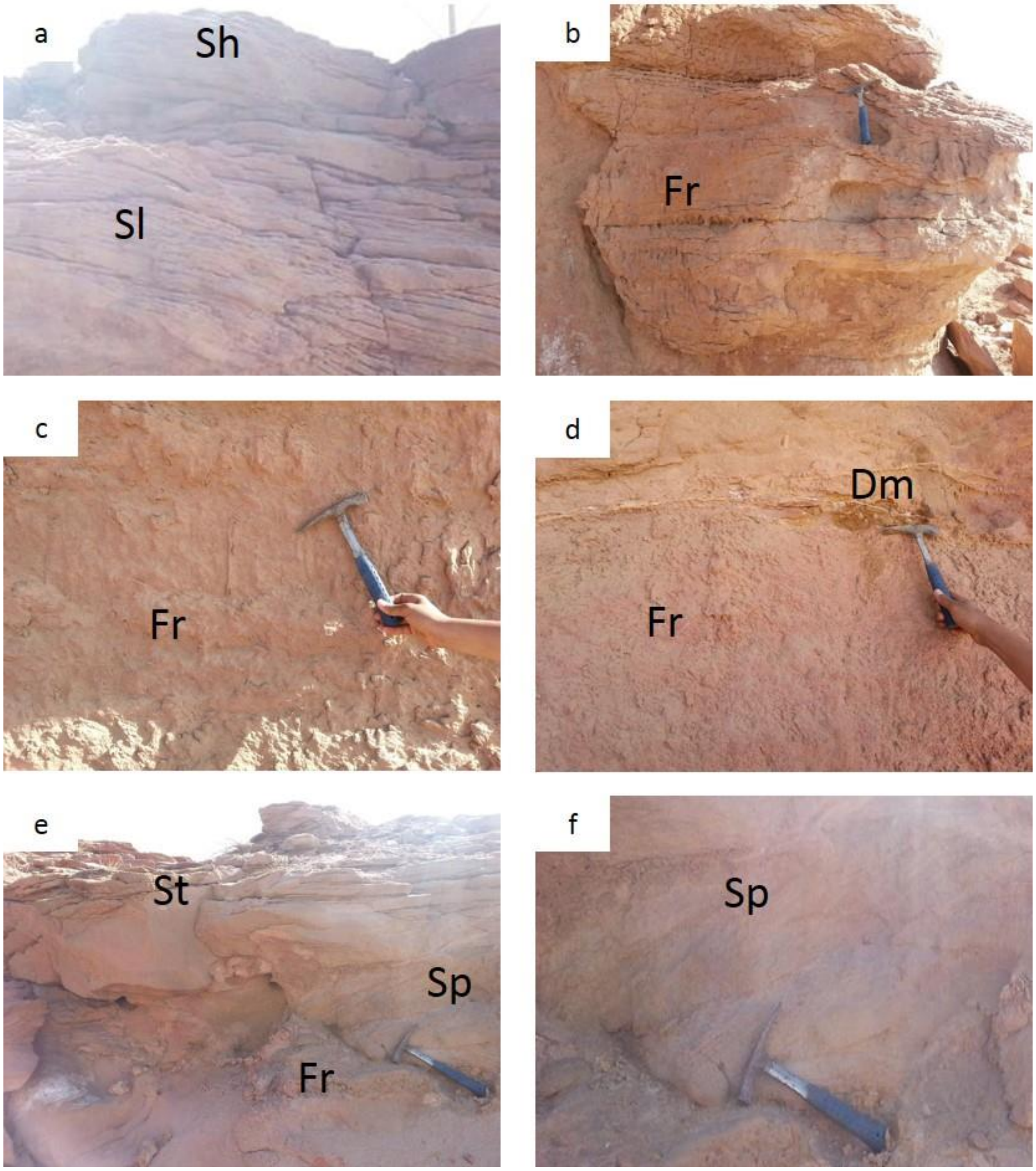

Figure 3-11: Photographs of outcrop No.4 of Sarah Formation at Uyun Al-Jawa, Rawd Al-Jawa paleovalley (26° 31.656' N, 43° 35.836' E) showing the dominant lithofacies: (a) horizontally and low angle laminated medium-grained sandstone, (b, c, d) well sorted, fine-grained siltstone, roots, bioturbation, mud interclasts, and diamictite, (e) planar and trough cross-bedded medium to coarse-grained sandstone lies above the fine-grained rooted siltstone, (f) solitary planar cross-bedded medium-grained sandstone.

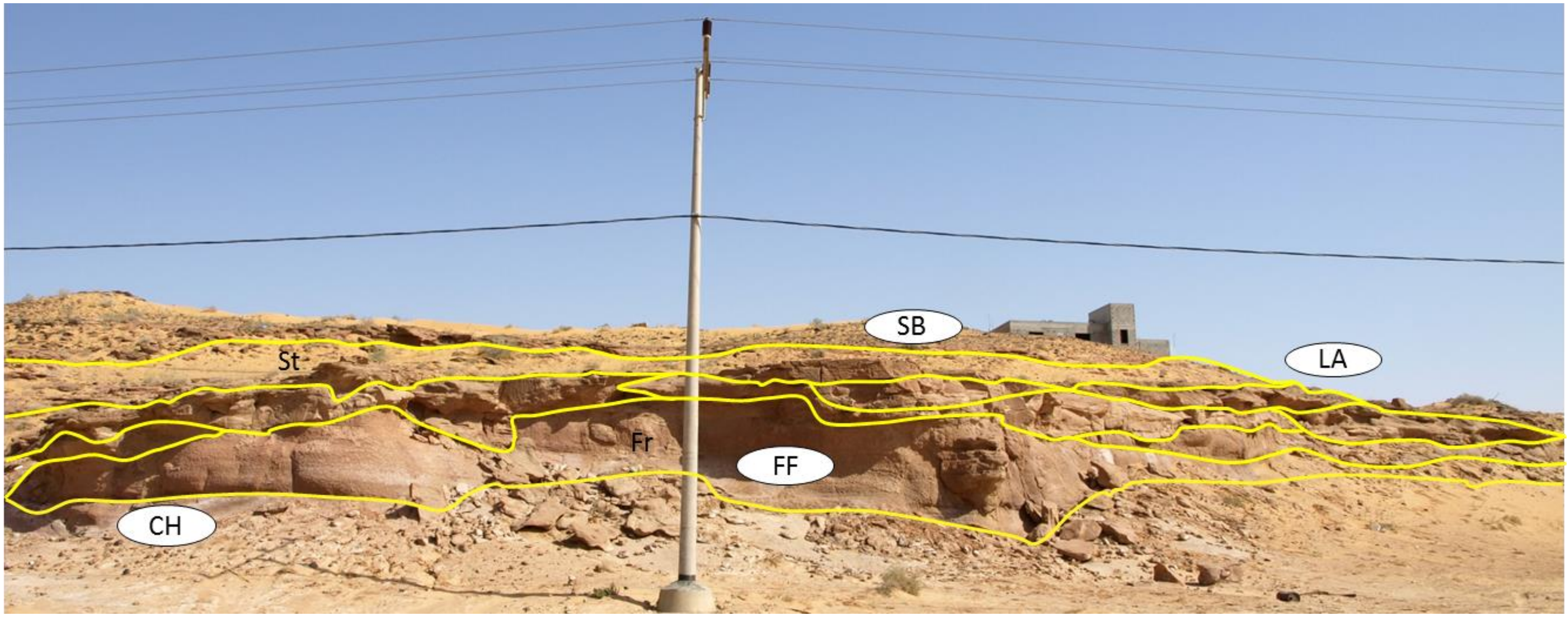

Figure 3-12: Annotated lateral profile of outcrop No.4 of Sarah Formation at Uyun Al-Jawa, Rawd Al-Jawa paleovalley (26° 31.656' N, 43° 35.836' E) showing the main facies assemblages and architectural elements. CH: channel, SB: sand bedforms, LA: lateral accretion, FF: overbank fines, St: medium-grained trough cross-bedded pebbly sandstone, Fr: well sorted, rooted and bioturbated siltstone.

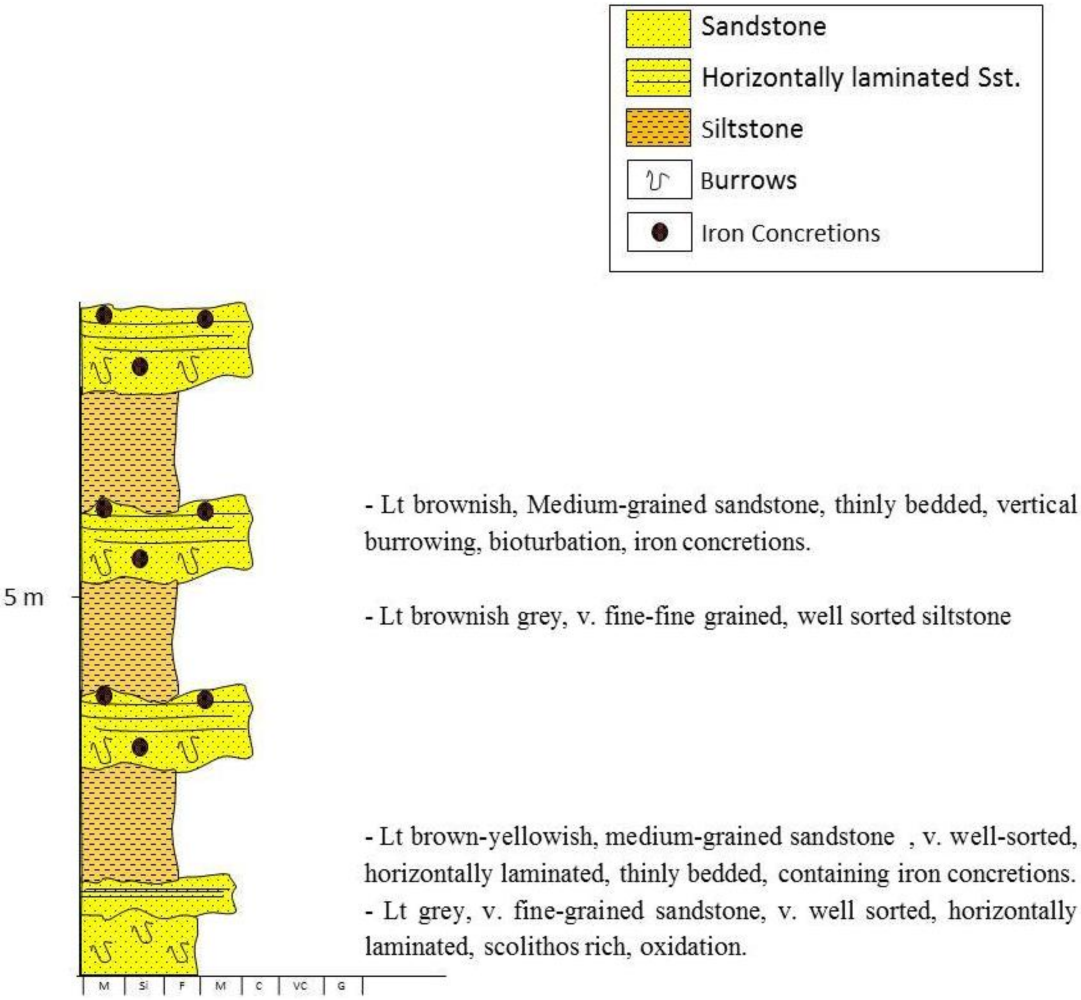

- Lt brownish, Medium-grained sandstone, thinly bedded, vertical burrowing, bioturbation, iron concretions.

- Lt brownish grey, v. fine-fine grained, well sorted siltstone

- Lt brown-yellowish, medium-grained sandstone , v. well-sorted, horizontally laminated, thinly bedded, containing iron concretions.
- Lt grey, v. fine-grained sandstone, v. well sorted, horizontally laminated, scolithos rich, oxidation.

Figure 3-13: The vertical profile of Outcrop section No.5 of Sarah Formation at Uyun Al-Jawa, Rawd Al-Jawa paleovalley (26° 31.600' N, 43° 35.861' E).

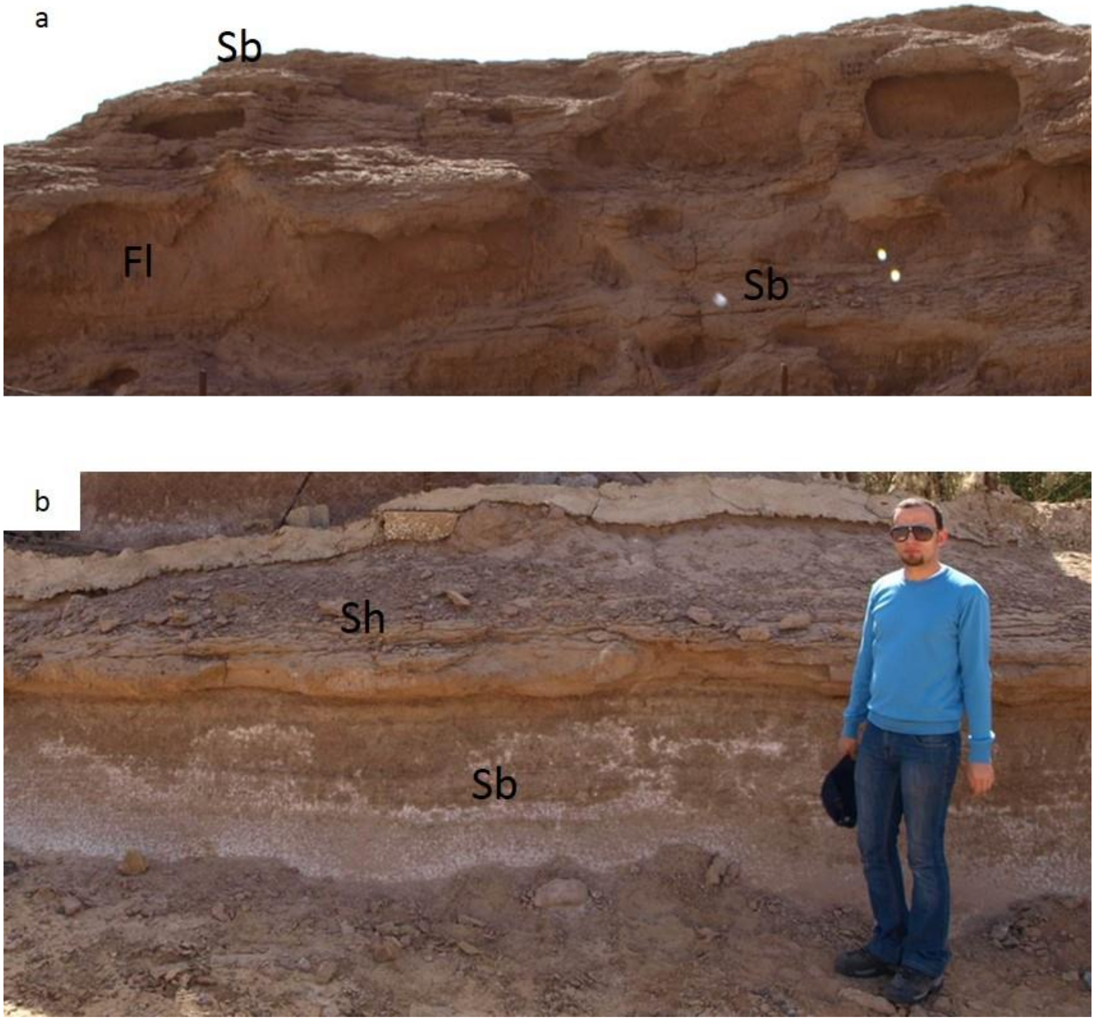

Figure 3-14: Photographs of Outcrop section No.5 of Sarah Formation at Uyun Al-Jawa, Rawd Al-Jawa paleovalley (26° 31.600' N, 43° 35.861' E) showing the main lithofacies:

a) Medium-grained sandstone, thinly bedded, vertical burrowing, bioturbation, iron concretions (Sb), and very fine-grained, well sorted siltstone (Fl).

b) Medium-grained sandstone, very well-sorted, horizontally laminated, thinly bedded, containing iron concretion (Sh), overlying very fine-grained, *Scolithos*-rich and oxidized sandstone (Sb).

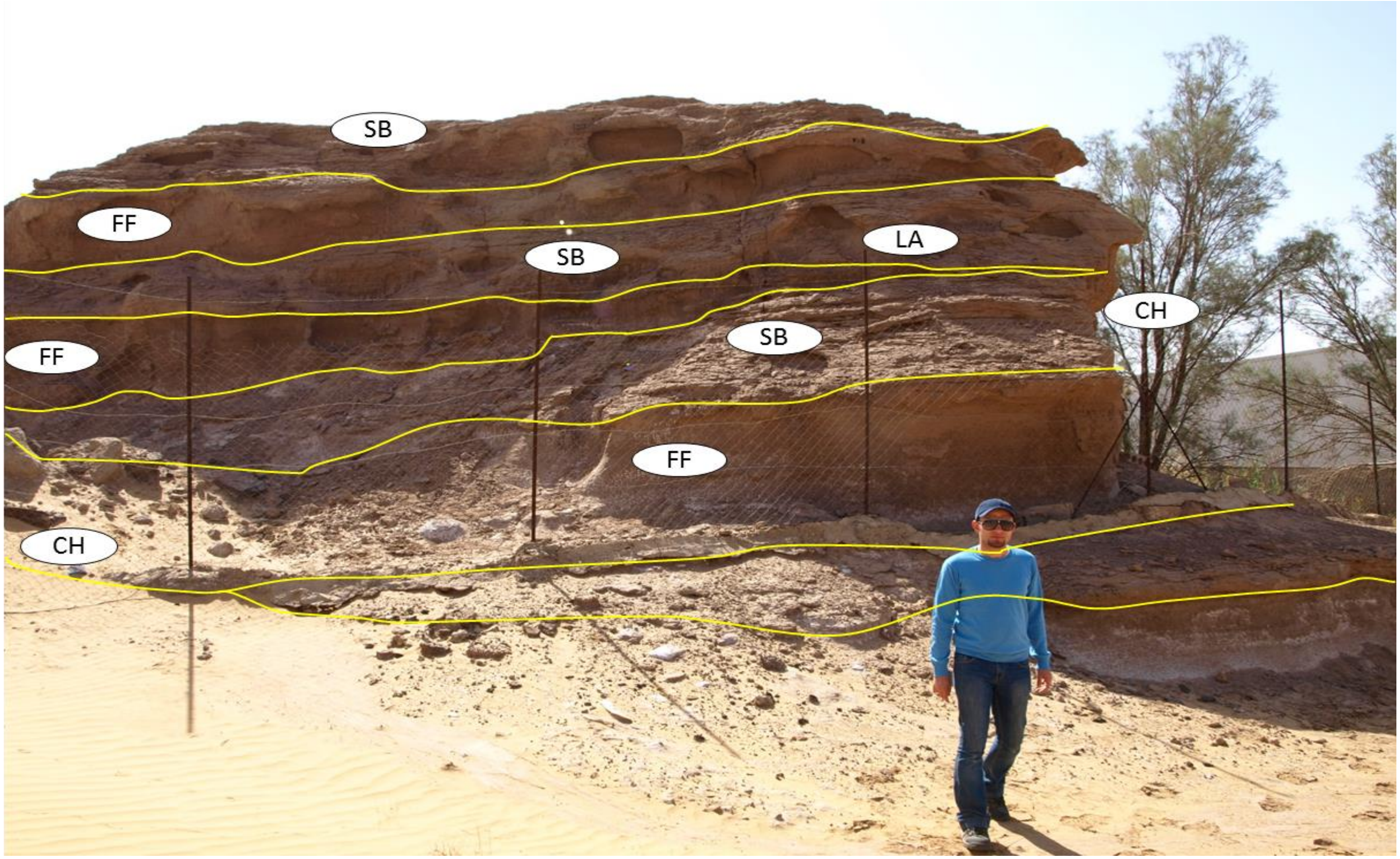

Figure 3-15: Lateral profile of Outcrop section No.5 of Sarah Formation at Uyun Al-Jawa, Rawd Al-Jawa paleovalley (26° 31.600' N, 43° 35.861' E) showing the main architectural elements. CH: channel, SB: sand bedforms, LA: lateral accretion, FF: overbank fines.

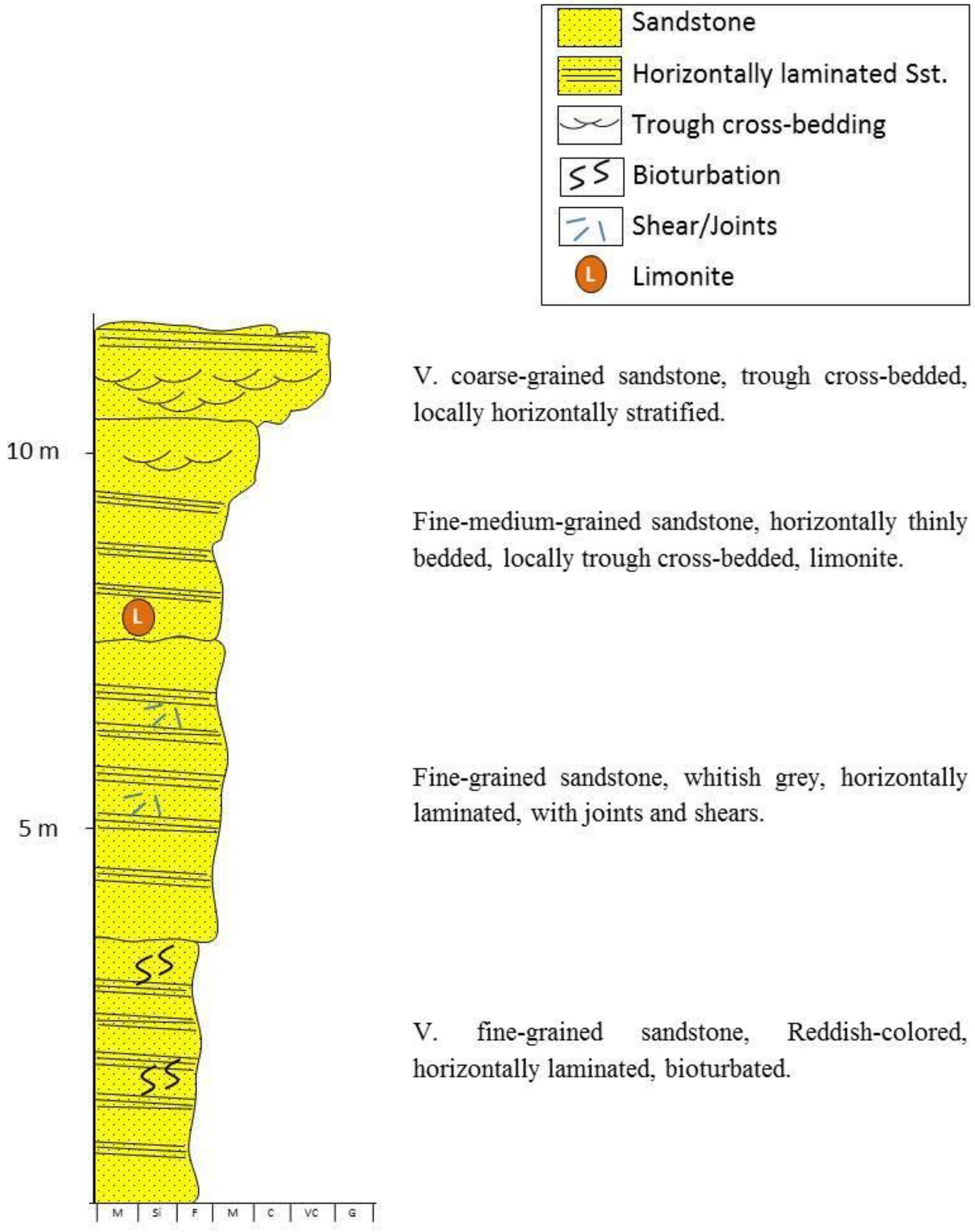

Figure 3-16: The vertical profile of outcrop No. 6 of Sarah Formation, road-cut section at Uyun Al-Jawa, Hanadir paleovalley (26° 33.133' N, 43° 35.784' E).

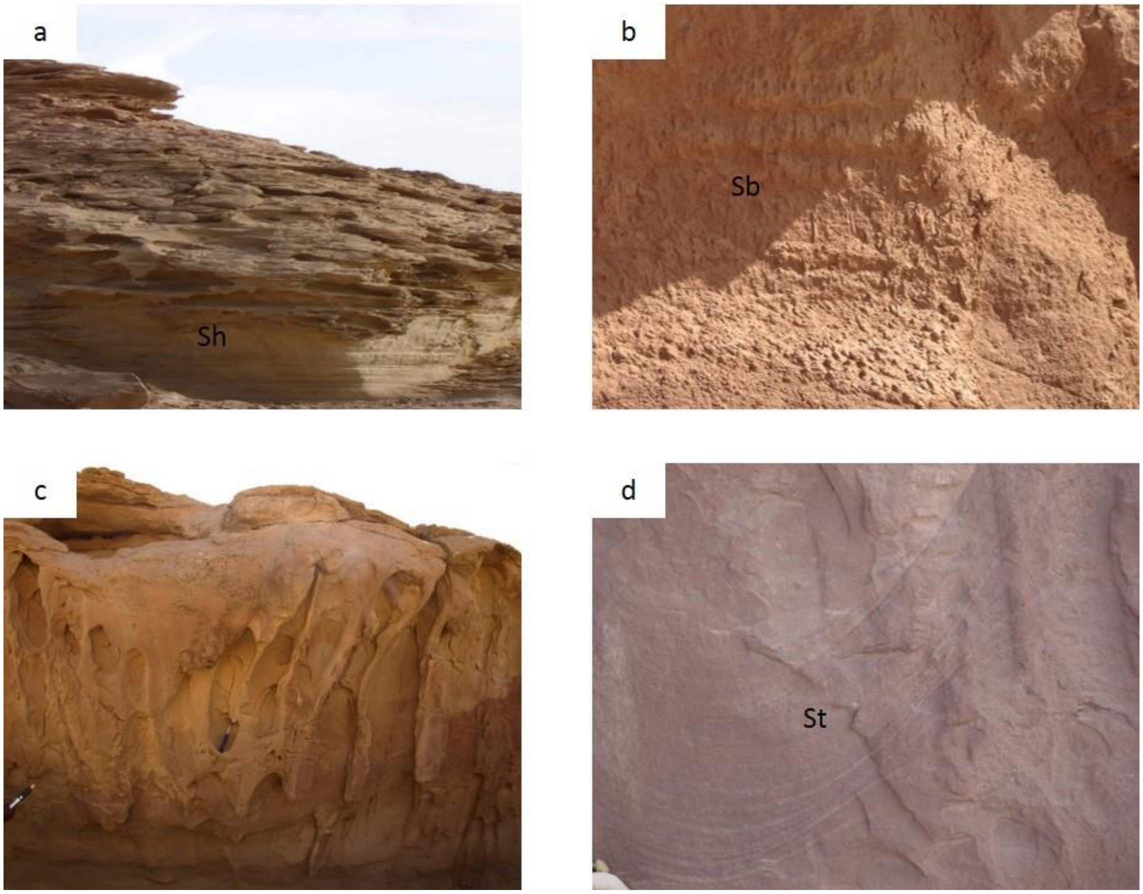

Figure 3-17: Photographs of outcrop No. 6 of Sarah Formation, road-cut section at Uyun Al-Jawa, Hanadir paleovalley (26° 33.133' N, 43° 35.784' E) showing the lithofacies (a) horizontally thinly-bedded fine to medium-grained sandstone, (b) rooted and bioturbated horizontally laminated very fine-grained sandstone at the base of the section, (c) the glacial outwash impact at the lower strata which covered the lamination, (d) coarse to very coarse-grained trough cross-bedded sandstone at the top of the section.

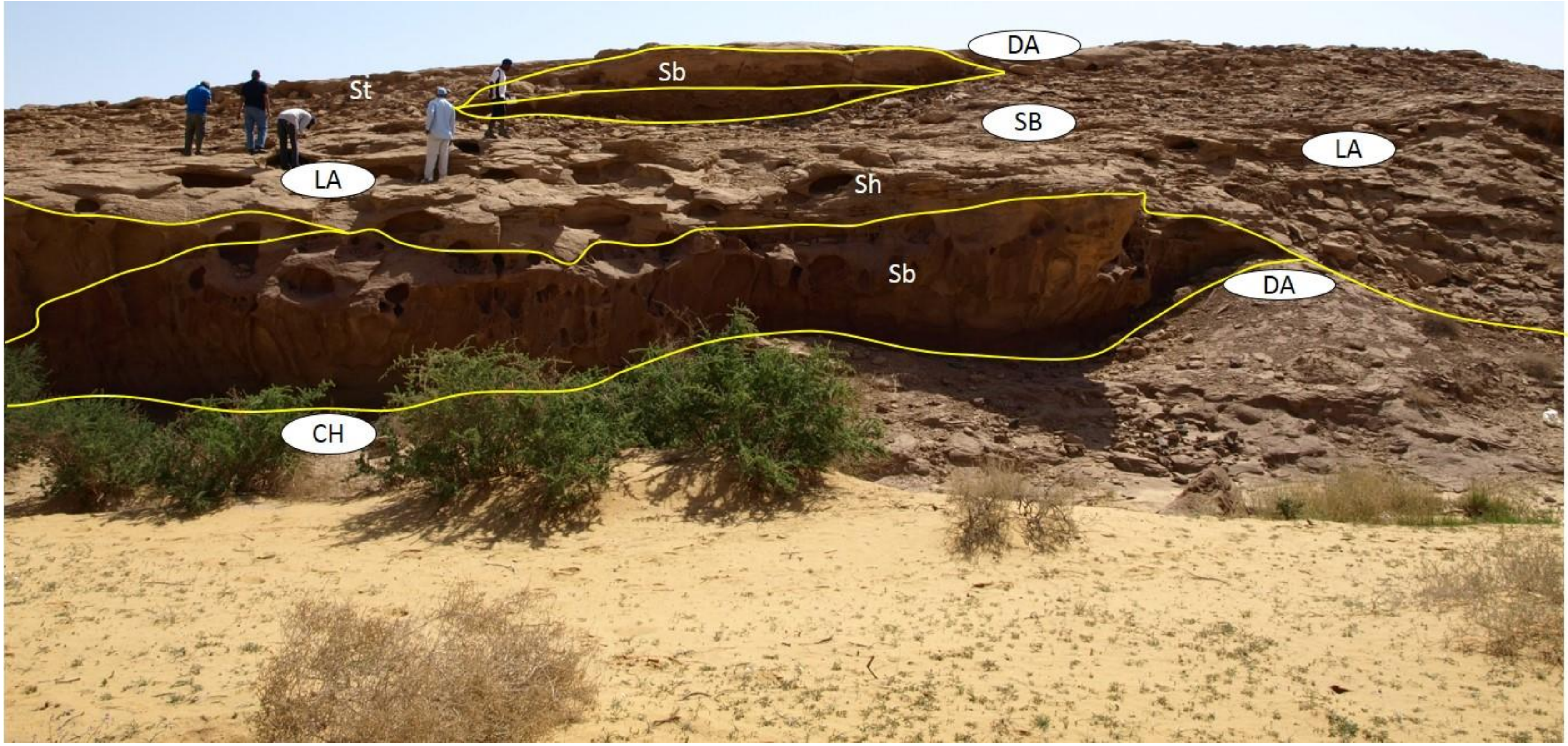

Figure 3-18: Lateral profile of outcrop No. 6 of Sarah Formation, road-cut section at Uyun Al-Jawa, Hanadir paleovalley (26° 33.133' N, 43° 35.784' E) showing the dominant facies and architectural elements in the vertically and horizontally stacked channels. CH: channel, SB: sand bedforms, LA: lateral accretion, DA: downstream accretion macroform, St: trough cross-laminated sandstone, Sh: horizontally laminated sandstone, Sb: horizontally laminated bioturbated sandstone.

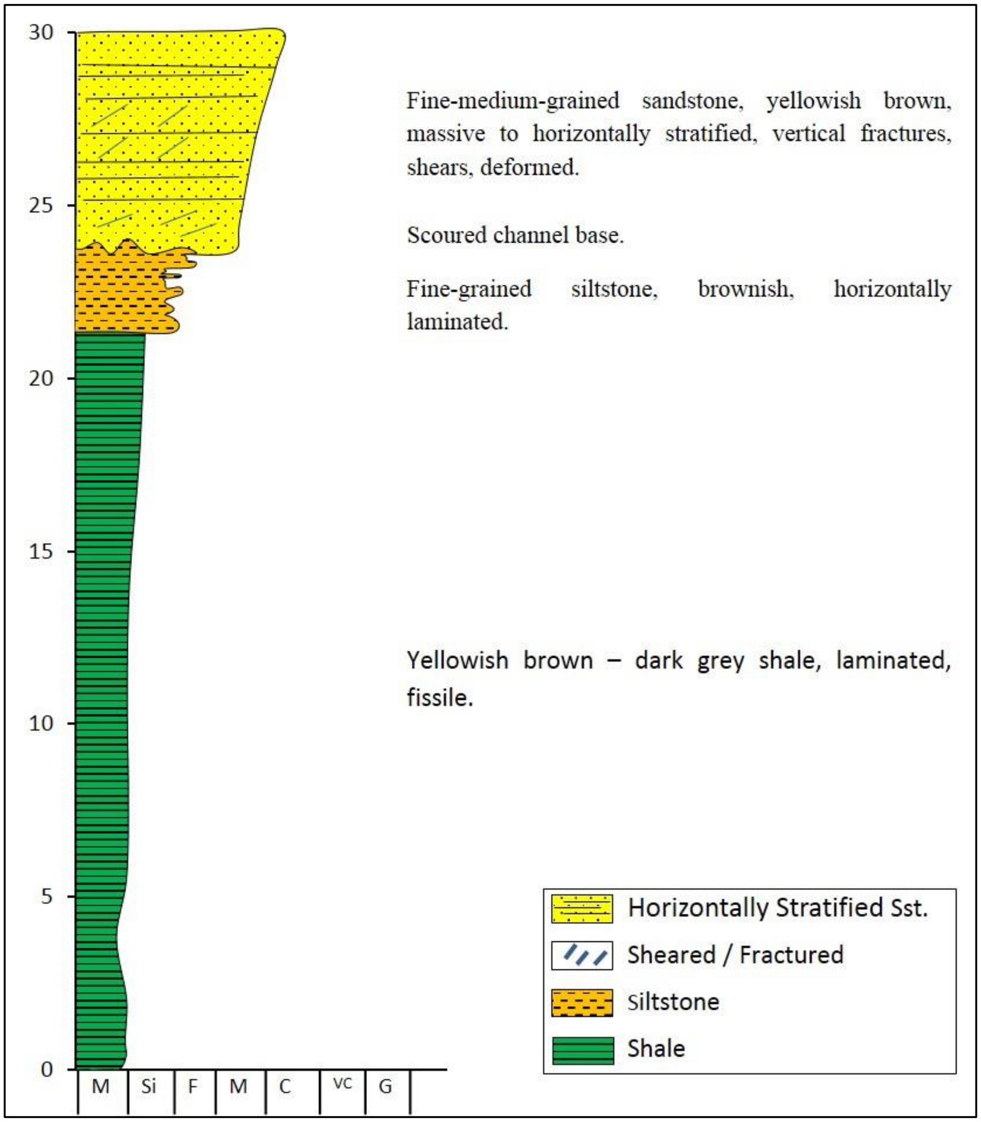

Figure 3-19: The vertical profile of Outcrop No.7 of Sarah Formation at Uyun Al-Jawa, Hanadir paleovalley (26° 34' 14.6'' N, 43° 34' 40.2'' E) showing Sarah sandstone overlying Ra’an s7hale.

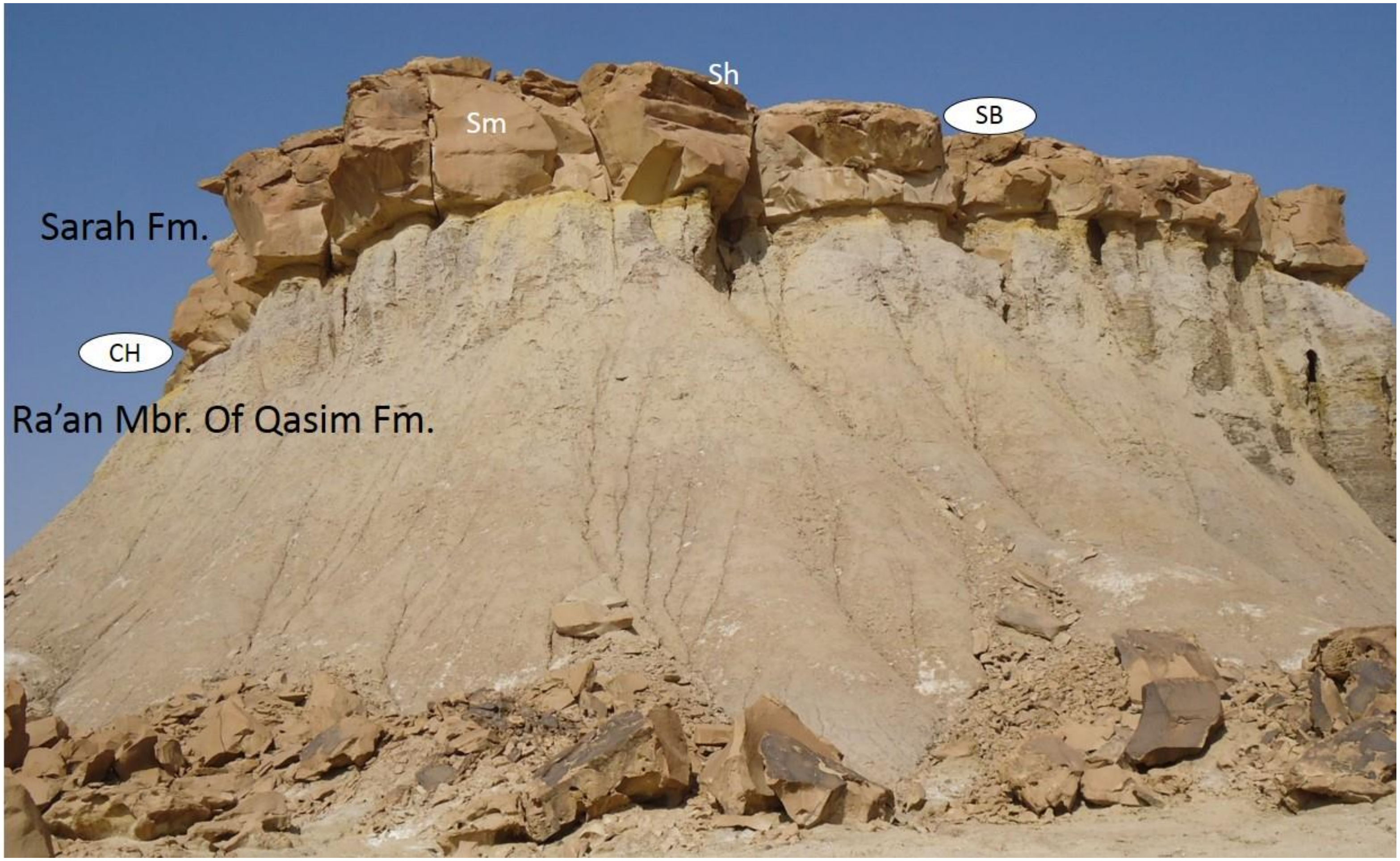

Figure 3-20: Photograph showing the vertical profile and main lithofacies and architectural elements of Outcrop No.7 of Sarah Formation at Oyoun Al-Jawa, Hanadir paleovalley (26° 34' 14.6'' N, 43° 34' 40.2'' E). Sh: horizontally laminated sandstone, Sm: massive sandstone.

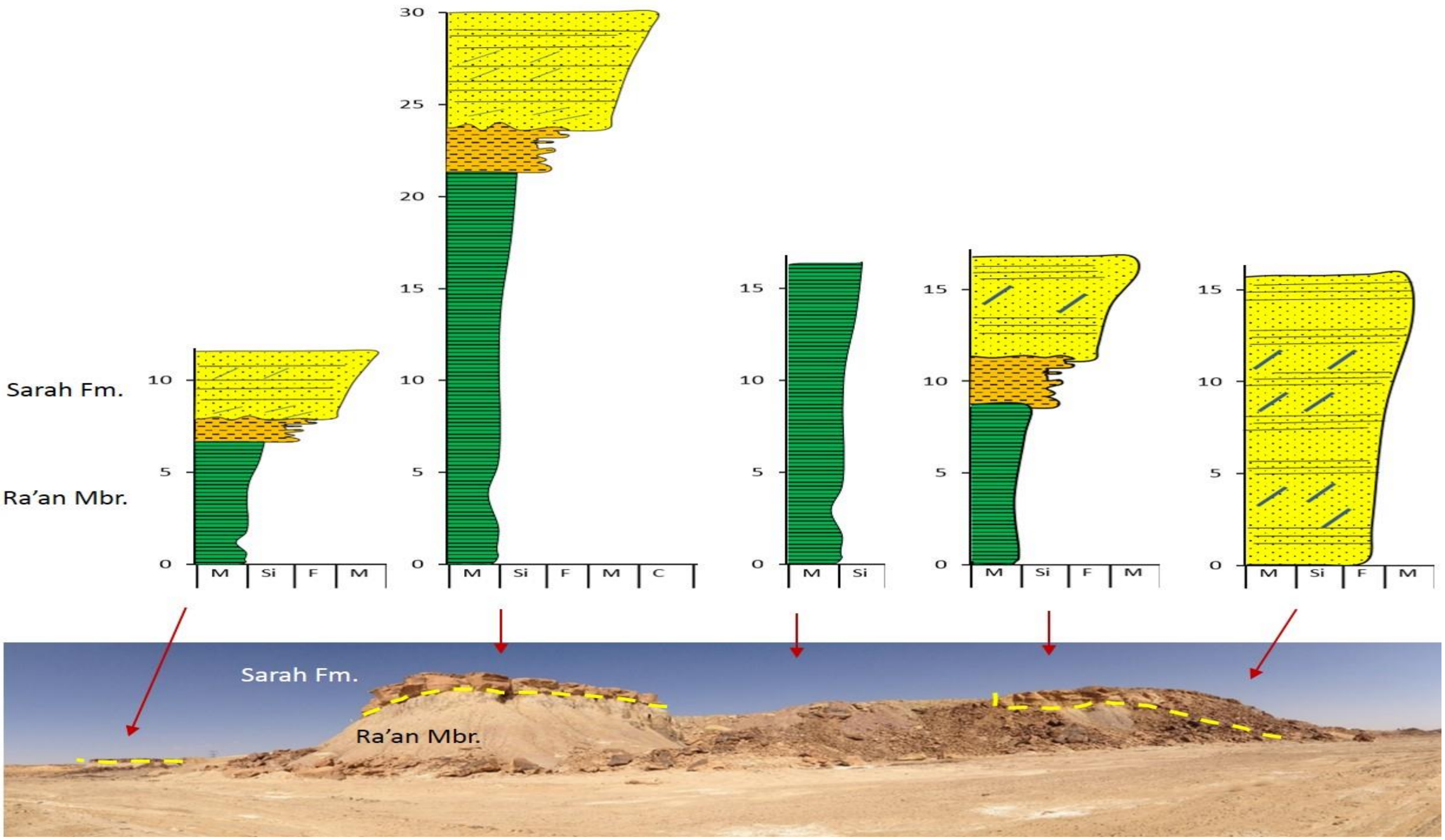

Figure 3-21: Lateral profile of Outcrop No.7 of Sarah Formation at Oyoun Al-Jawa, Hanadir paleovalley (26° 34' 14.6'' N, 43° 34' 40.2'' E) showing the contact between Sarah Formation and Ra’an Member of Qasim Formation.

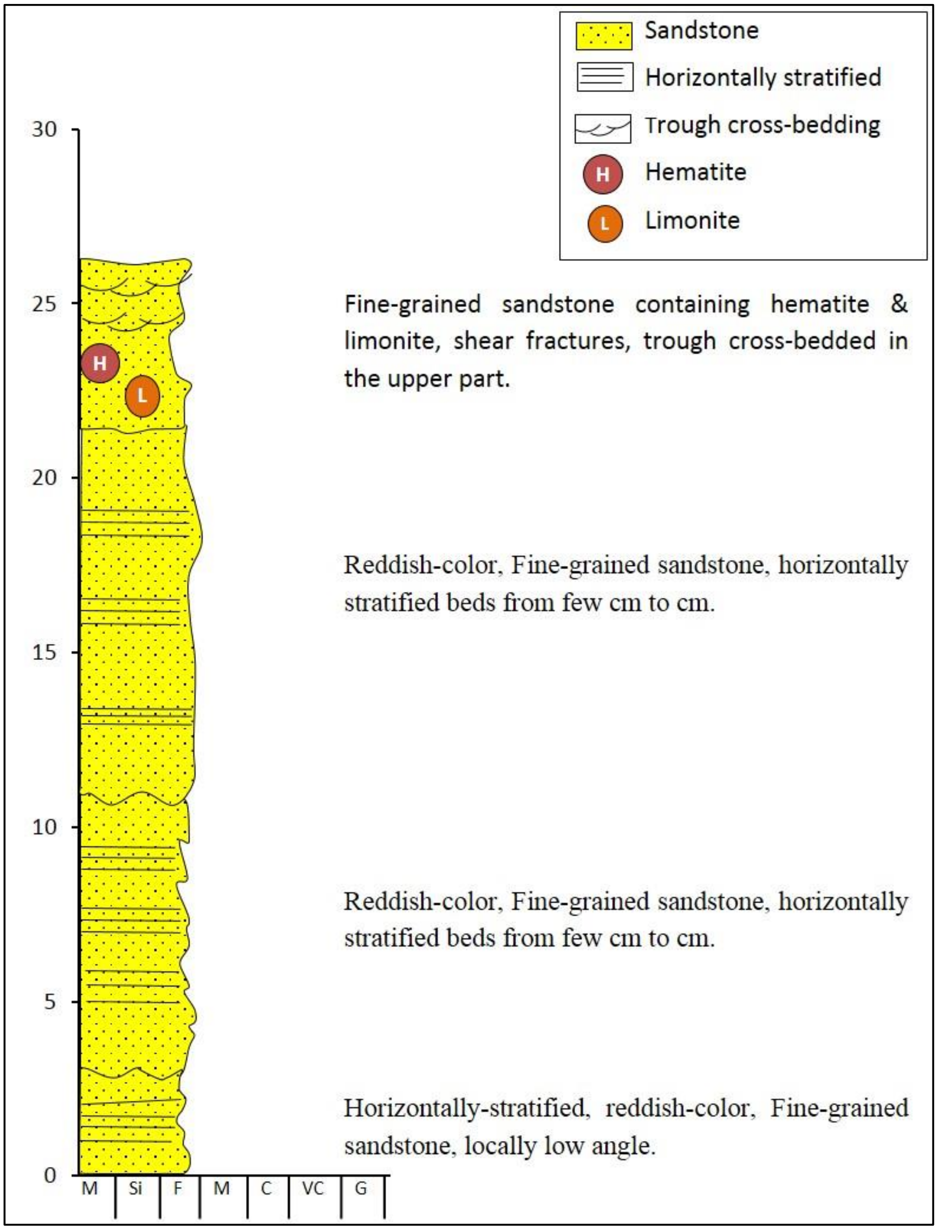

Figure 3-22: The vertical profile of outcrop No. 8 of Sarah Formation at Al-Quwarah, Sarah paleovalley showing stacked channels of fine-grained sandstone (26° 47' 22.8'' N, 43° 28' 5.2'' E).

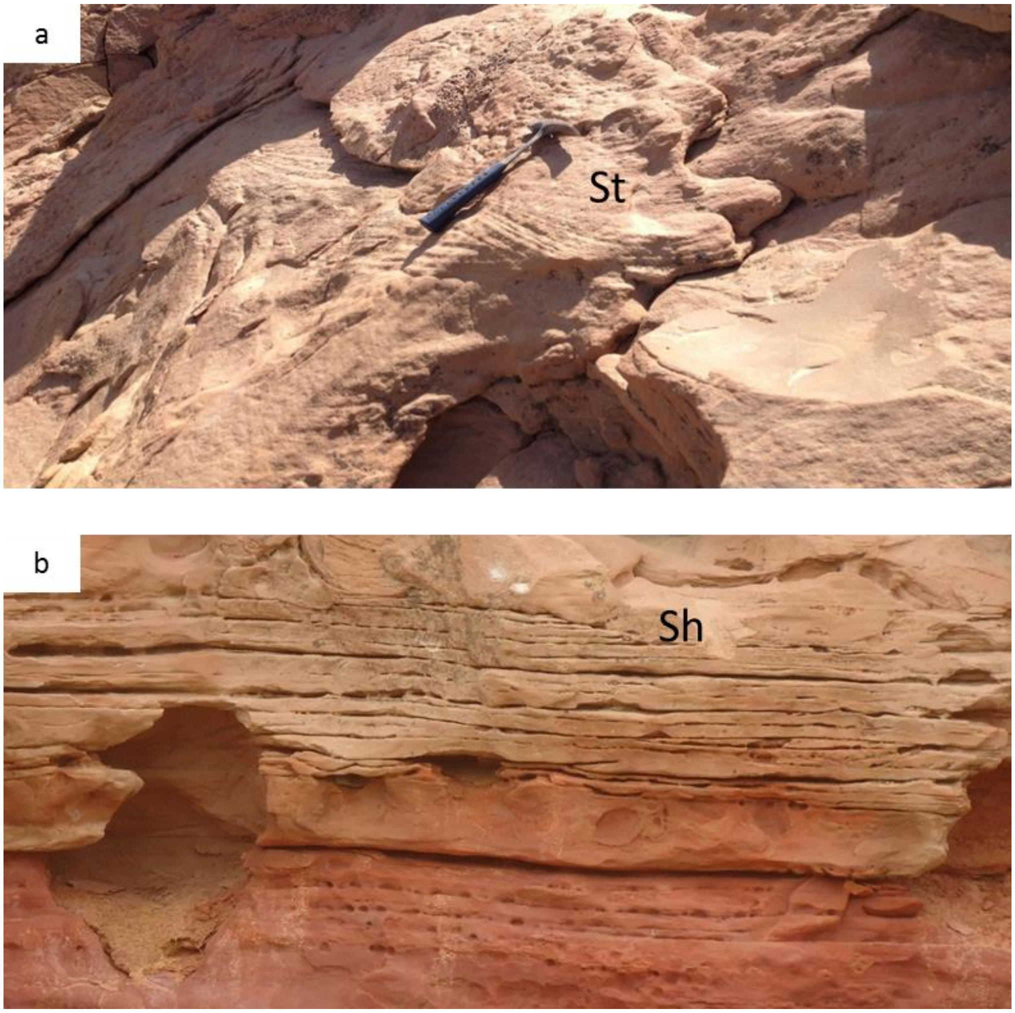

Figure 3-23: Photographs for the outcrop No. 8 of Sarah Formation at Al-Quwarah, Sarah paleovalley (26° 47' 22.8'' N, 43° 28' 5.2'' E) showing the dominant lithofacies: (a) fine-grained horizontally bedded sandstone at the top, (b) fine to very fine-grained trough cross-bedded sandstone.

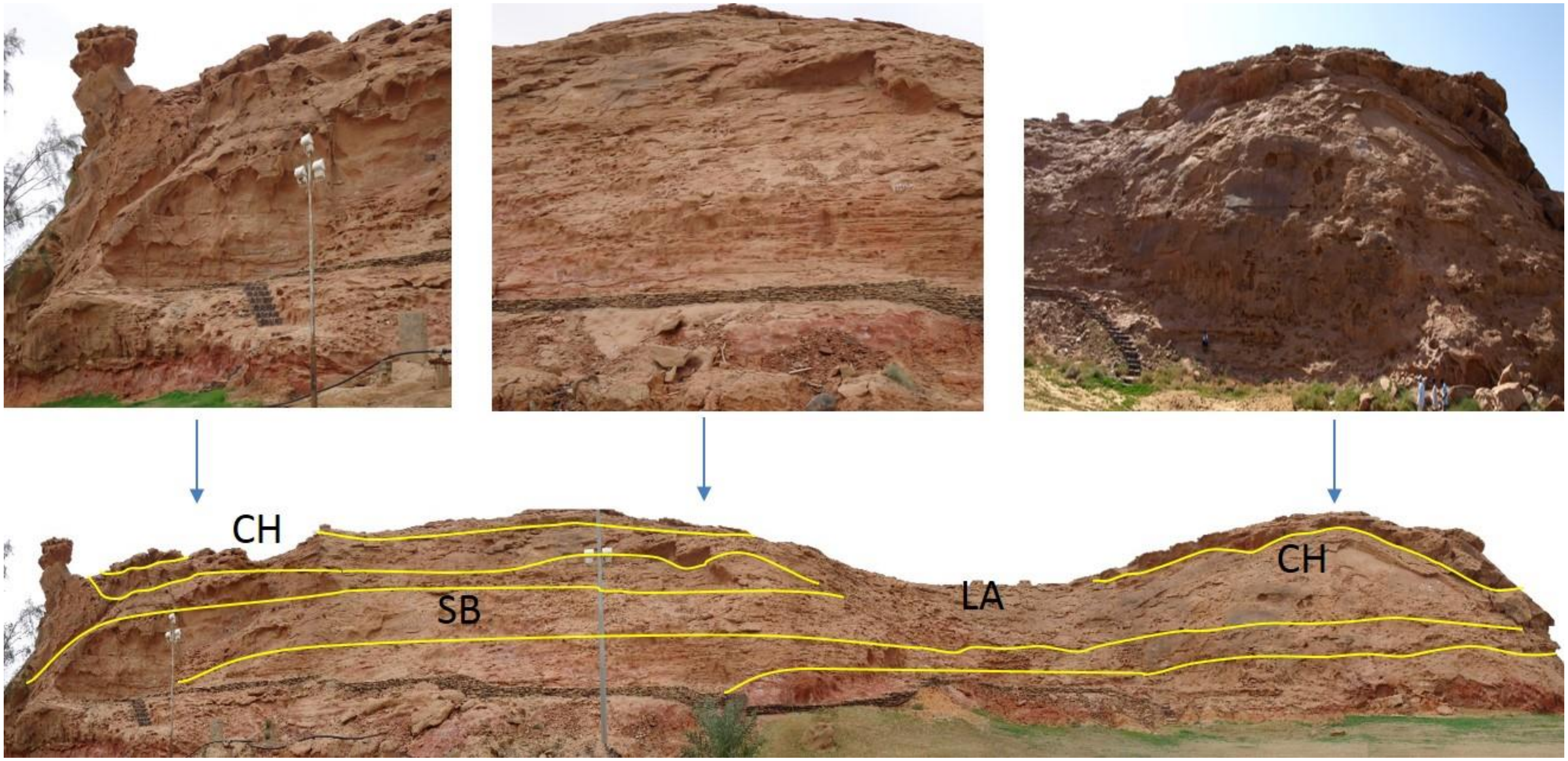

Figure 3-24: Panorama for the complete lateral profile of outcrop No. 8 of Sarah Formation at Al-Quwarah, Sarah paleovalley (26° 47' 22.8'' N, 43° 28' 5.2'' E). Note: the main architectural elements are annotated; CH: channel, SB: sandy bedforms, LA: lateral accretion.

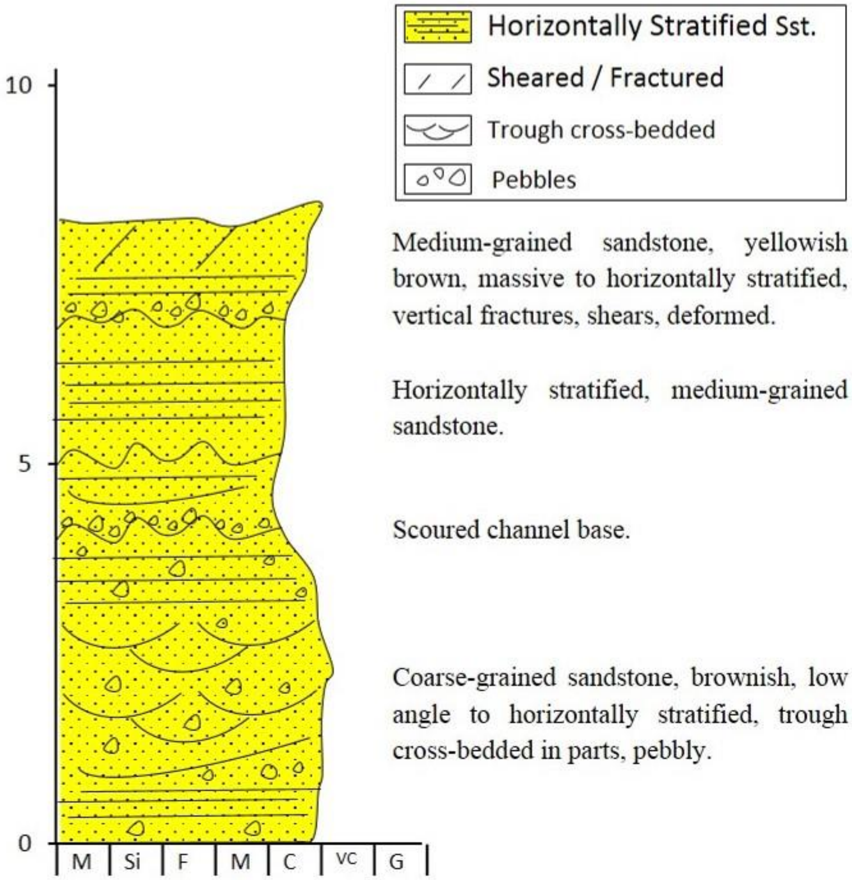

Medium-grained sandstone, yellowish brown, massive to horizontally stratified, vertical fractures, shears, deformed.

Horizontally stratified, medium-grained sandstone.

Scoured channel base.

Coarse-grained sandstone, brownish, low angle to horizontally stratified, trough cross-bedded in parts, pebbly.

Figure 3-25: The vertical profile of outcrop No. 9 of Sarah Formation at Sarah Ridge (Khanasir Sarah).

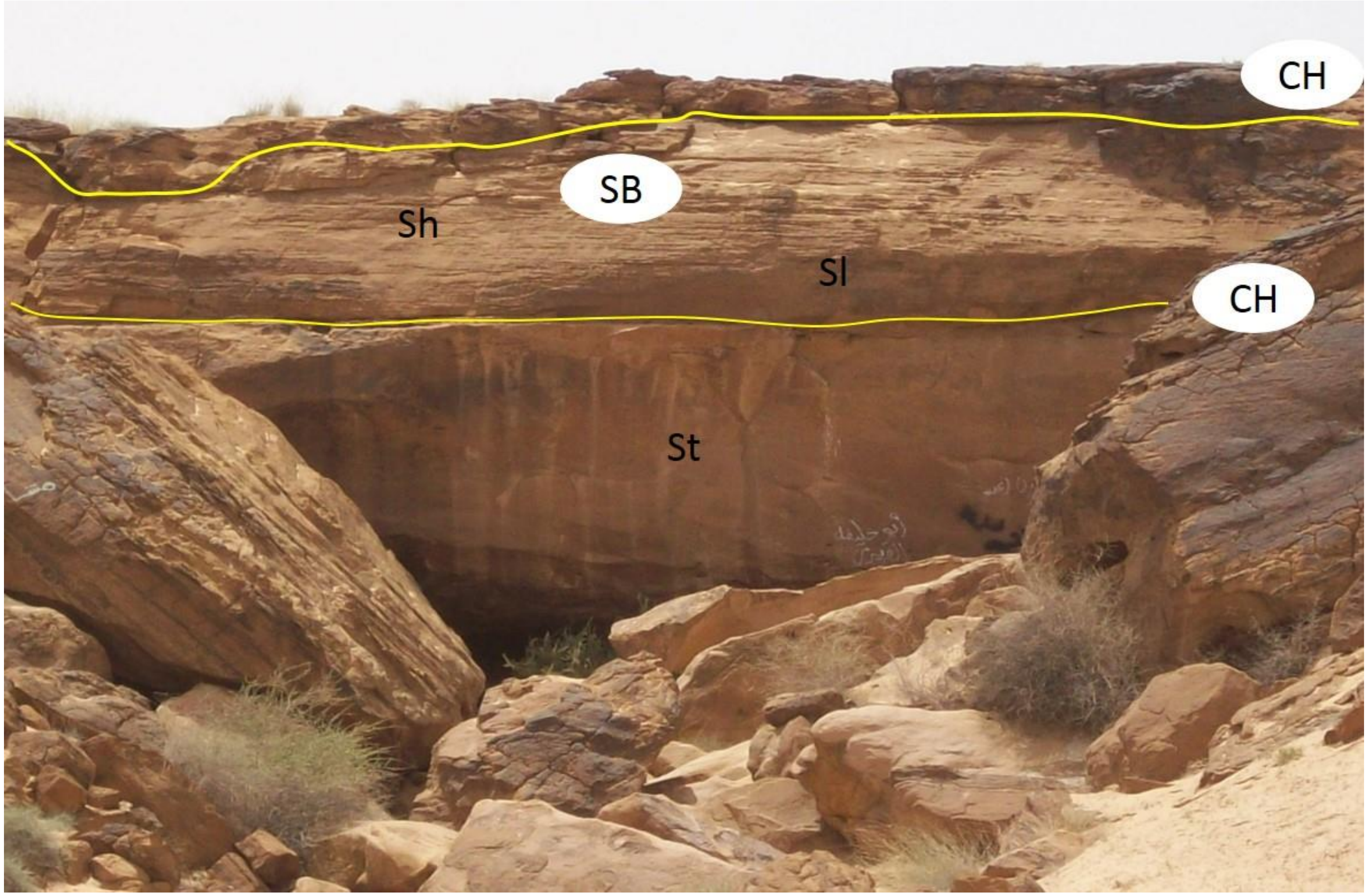

Figure 3-26: Photograph of outcrop No. 9 of Sarah Formation at Sarah Ridge (Khanasir Sarah) showing the facies and architectural elements of Sarah Formation. CH: channel, SB: sandy bedforms, Sh: horizontally laminated medium-grained sandstone, St: large-scale trough cross-bedded coarse-grained pebbly sandstone.

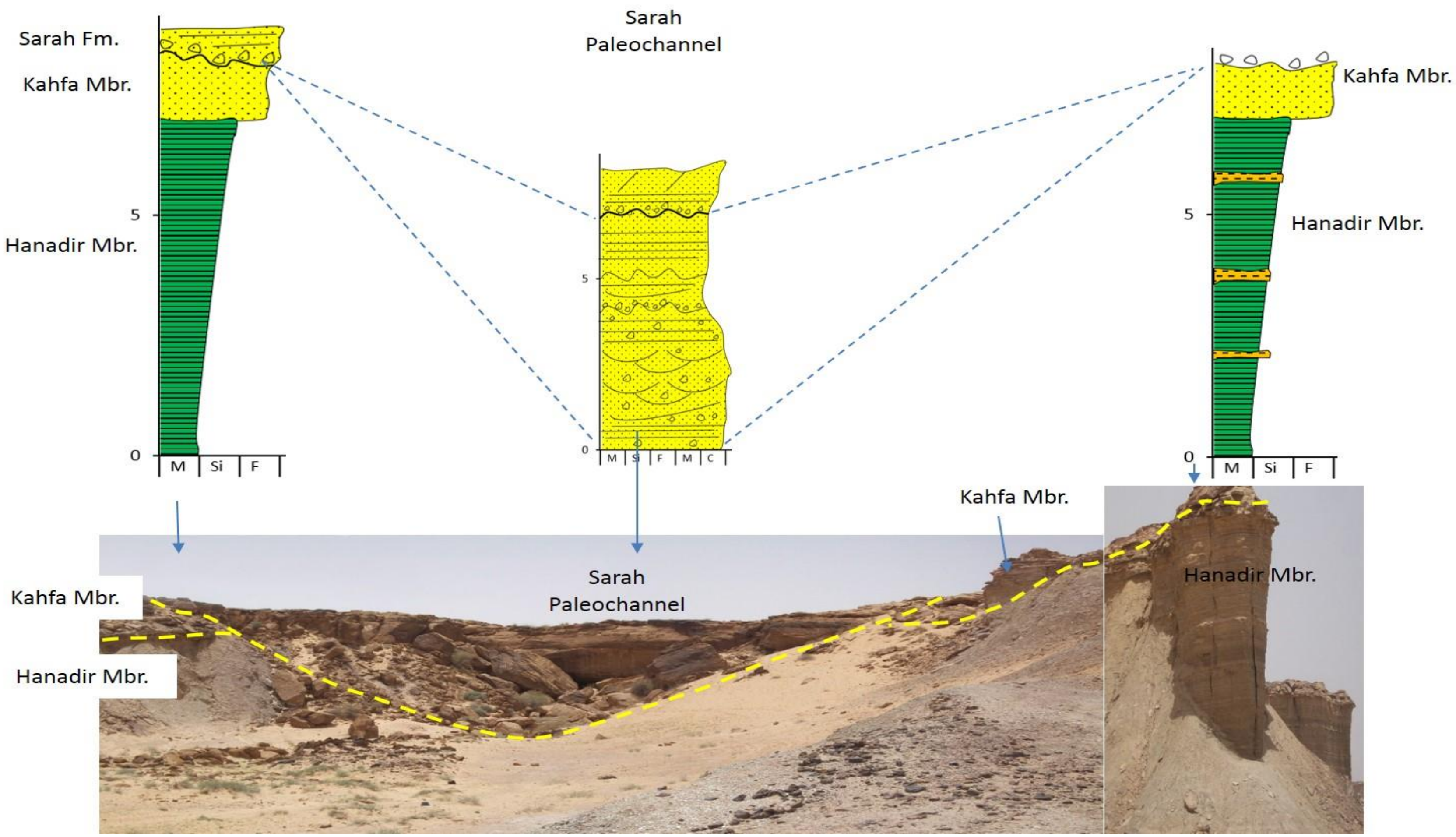

Figure 3-27: Photomosaic for the lateral profile of outcrop No. 9 of Sarah Formation at Khanasir Sarah with correlation of sedimentologic logs at different positions of the outcrop to illustrate the relationship with other Paleozoic formations.

Table 3-2: Facies codes (modified after Miall, 1996), classification and interpretation of facies as recognized in the Sarah Formation

Facies code	**Facies**	**Sedimentary structures**	**Interpretation**
Sh	Sand, very fine to very coarse, may be pebbly	Horizontal lamination parting or streaming lineation	Plane-bed flow (critical flow)
St	Sand, fine to very coarse, may be pebbly	Solitary or grouped trough cross-beds	Sinuous-crested and linguoid (3-D) dunes
Sl	Sand, fine to coarse, may be pebbly	Low-angle (<15°) cross-beds	Scour fills, humpback or washed-out dunes, antidunes
Sm	Sand, fine to coarse	Massive, or faint lamination	Sediment-gravity flow deposits
Ss	Sand, fine, may be pebbly	Broad, shallow scours	Scour fills
Sp	Sand, medium to coarse, pebbly	Solitary planar cross-beds	Transverse and linguoid bedforms (2D dunes)
Sb	Sand	Bioturbation, roots, vertical burrows, commonly *Scolithos*	High energy sandy shore line
Fl	Silt	Fine lamination, very small ripples	Overbank, abandoned channel, or waning flood deposits
Fr	Silt	Massive, roots, bioturbation	Root bed, incipient soil
Dm	Glacial diamictite	Stratified,	Ice-contact sediments

3.7. Facies Analysis of Sarah Formation

Based on their color, grain size, grain sorting, sedimentary structures, composition, and fossil content, the lithofacies characterizing Sarah Formation were identified and classified. Following Miall's facies classification scheme (Miall, 1996), 11 lithofacies were identified from Sarah paleovalleys. Table 3-2 shows a brief description and interpretation of facies as recognized in the Sarah Formation.

3.7.1. Sandstone Facies

The sandstone lithofacies were classified into Sh, St, Sm, Sl, Ss, Sp, and Sb. The horizontally bedded sandstone (Sh) lithofacies is characterized by flat, parallel lamination with parting lineation occurring on bedding plane. This lithofacies is the dominant one occurring in all the paleovalleys. It was observed in Bukayriyah (Figure 3-3 b, e), Rawd Al-Jawa (Figure 3-11 a, and Figure 3-14 b), Hanadir (Figure 3-17 a, Figure 3-18, and Figure 3-20), Sarah (Figure 3-23 b), and Khanasir Sarah (Figure 3-26) paleovalleys.

The trough cross-bedded sandstone (St) lithofacies occurred in fine to very coarse-grained sandstones in local beds of all the paleovalleys, ranging in scale from small to large. The St lithofacies was noted in Bukayriyah (Figure 3-3 f), Rawd Al-Jawa (Figure 3-11 e), Hanadir (Figure 3-17 d, and

Figure 3-18), Sarah (Figure 3-23 a), and Khanasir Sarah (Figure 3-26) paleovalleys. The massive sandstone (Sm) lithofacies occurred in the fine and medium-grained sandstone of Bukayriyah paleovalley (Figure 3-8 c, d, e), while in Hanadir paleovalley it was observed in coarse to very coarse-grained sandstone (Figure 3-20). The massive sandstone beds were difficult to pick out their faint lamination. Such beds are usually deposited by sediment-gravity flow. However, being commonly associated with soft-sediment deformation structures, the massive texture might have been produced by post-depositional modification such as clay de-watering. The massive sandstone of in paleovalley is interbedded with thin trough cross-bedded sandstone (lithofacies St, Figure 3-8)

The low-angle (<15°) cross-bedded sandstone (Sl) lithofacies was found in fine to medium-grained sandstone of Bukayriyah paleovalley (Figure 3-3 a), in the medium-grained sandstone of Rawd Al-Jawa paleovalley (Figure 3-11 a), and in the coarse-grained pebbly sandstone in Khanasir Sarah paleovalley (Figure 3-26). It is usually associated with scoured channel fills and washed-out sand bedforms. Few scour hollows were observed in Bukayriyah paleovalley (Figure 3-3 c, d) filled with fine-grained sand (lithofacies Ss).

In Rawd Al-Jawa paleovalley, planar cross-bedded medium-grained solitary sandstone bed (lithofacies Sp) was observed (Figure 3-11 e, f) in addition to the bioturbated, *Scolithos*-rich very fine-grained sandstone (Sb) associated with iron concretions and iron-cemented nodules. The *Scolithos* burrows are also cemented with iron oxides. Clark-Lowes (2005) interpreted the *Scolithos* clasts to be transported from the Kahfah *Scolithos*-sandstone by mudflows. Meanwhile, the iron concretions may be due to subaerial weathering which took place during the erosion of the paleovalley.

3.7.2. Fine-grained clastic facies

Deposits of mud, silt and very fine sand indicate deposition in flood-plain areas, abandoned channels and abandoned areas of normally active channels (Boggs, 2010; Miall, 1996). Fine-grained clastic facies was only detected in Rawd Al-Jawa paleovalley. It consists of two lithofacies; the fine-laminated siltstone with very small ripples (Fl) (Figure 3-11 b, c, d, e), and the massive siltstone containing roots and bioturbation (Fr) (Figure 3-14 a).

3.7.3. Glacial Facies

The glacio-fluvial deposits of Sarah Formation contain significant amount of sediments deposited by glacial melt-water river. The evidence of glacial origin of the Sarah Formation as witnessed in the studied outcrops include the following criteria:

1. The striated surfaces within the basal Sarah Formation and striated pavements with deep grooves on top of Quwarah Member at its

contact with Sarah Formation indicate the movements of ice sheets over the unlithified sandy beds of Quwarah (Figure 3-28 a).

2. The ice flow created a large shallow depression in Sarah sandstones at Al-Qar'a (Figure 3-28 b). Senalp and Al-Laboun (2000) described it as excavated by the ice movement or due to the impact of weight of the ice block that resulted in deepening this depression.
3. In almost all the studied outcrops Sarah Formation lies unconformably above the older members of Qasim Formation. In other outcrops, the base of Sarah Formation represent a regional unconformity marked by erosional surface. In addition to that, each outcrop is subdivided into several units by scoured channel surfaces. These multiple erosional processes indicate stages of deglaciation during the tilting of the Arabian platform (Senalp and Al-Laboun, 2000).
4. The matrix-rich diamictites, composed of conglomerates in a fine clay matrix, found at the basal part of Sarah Formation, sometimes cutting as long dykes marking the erosional surface at the contact between Sarah Formation and Quwarah Member of Qasim Formation (Figure 3-7 b, Figure 3-11 d) have the characteristics of ice contact deposits (Edwards, 1986; Clark-Lowes, 2005; Boggs, 2010).

Figure 3-28: (a) Glacially striated pavement in outcrop No. 3 of Sarah Formation at Al-Qar’a (43° 45' 19'' N; 43° 45' 19'' E) indicating the glacial origin of Sarah Formation, (b) Shallow depression in Sarah sandstones at Al-Qar’a excavated by the ice flow.

5. Deformation structures in trough cross-bedded or massive proximal outwash sandstones are observed in almost all the studied outcrops.

3.8. Architectural Element Analysis of Sarah Formation

An architectural element is defined by Miall (1996) as “a component of a depositional system equivalent in size to, or smaller than a channel fill, and larger than an individual facies unit, characterized by a distinctive facies assemblage, internal geometry, external form, and, in some instances, vertical profile”. 11 lithofacies from Sarah Formation are grouped into seven architectural elements (Table 3-3). These elements focus on the primary facies assemblages and geometry relationships.

Furthermore, lateral profiles were constructed based on photomosaics from the studied outcrops, and the architectural elements have been annotated on them (Figure 3-3, Figure 3-4, Figure 3-9, Figure 3-12, Figure 3-15, Figure 3-18, Figure 3-20, Figure 3-24, Figure 3-26). These lateral profiles and photomosaics are significant in understanding the architectural elements and also the lateral continuity of Sarah Formation and its relationship with other Paleozoic formations. This may help to predict and understand the reservoir quality, paleogeography and heterogeneity of Sarah Formation in the subsurface.

Table 3-3: Architectural elements encountered in paleovalleys of Sarah Formation (modified after Miall, 1996). Note: the facies code is illustrated in Table 3-2

Architectural element	Symbol	Facies assemblage	Geometry and relationships
Channel	CH	Sh, St, Sm, Sl, Ss, Sb, Fl, Fr, Dm	Concave-up erosive base; scale and shape highly variable
Sandy bedforms	SB	Sh, St, Sm, Sl, Ss, Sb, Sp	Lens, sheet, blanket, wedge; occurs as channel fill, minor bars
Lateral-accretion deposits	LA	Sh, St, Sb	Wedge, sheet, lobe; characterized by internal lateral accretion 3rd-order surfaces
Downstream-accretion macroform	DA	Sh, St, Sb	Lens resting on flat or channeled base, with convex-up 3rd-order internal erosion surfaces and upper 4th-order bounding surface.
Overbank fines	FF	Fl, Fr, Dm	Thin to thick blankets; commonly interbedded with SB; may fill abandoned channels
Scour hollows	HO	Ss, Sh	Scoop-shaped with asymmetric fill

3.9. Outcrop Analog Guide to Subsurface Paleogeography and Reservoir Heterogeneity of Sarah Formation

The heterogeneity of the Sarah Formation reflects the complexity of facies, paleoenvironments and paleogeography of the Late Ordovician deposits. Such complexity is observed also in the subsurface and was previously reported by many authors, e.g., Al-Mahmoud and Al-Ghamdi (2010) and Briner et al. (2010), which makes the prediction of reservoir quality difficult, especially relying on insufficient borehole data. The borehole data cannot resolve the relationship of such multiple closely spaced rock bodies. On the other hand, the outcrop analog of the Sarah Formation helped investigating such complexity, as it provided information about rock body dimension, size and orientation, as well as relationship with other Paleozoic formation at a resolution unavailable from the subsurface. Understanding the geologic controls on the variation of reservoir quality is a key factor for predicting reservoir properties in the subsurface. This will increase the understanding of reservoir heterogeneity in the subsurface and can help predicting the distribution of the potential reservoir facies, and their petrophysical properties.

The heterogeneity of Sarah Formation was observed and studied here in different scales; the mega-scale (paleogeography and sedimentary position within the Paleozoic deposits, and relationship with other Paleozoic formations like Qasim Formation), macro-scale (the architectural elements), meso-scale (the lithofacies types), and micro-scale (the textural, compositional, depositional, and diagenetic factors controlling the variation of petrophysical properties). The micro-scale heterogeneity is illustrated, in detail, in chapters four and five.

Figure 3-29 shows the locations of outcrop sections within the Sarah paleovalleys. The map shows the vertical and lateral heterogeneity, and the variation of facies among the different paleovalleys. As explained earlier in outcrop sections No. 3, 7 and 9, the Sarah paleochannels are incised deeply through various depositional environments, cutting in the storm-dominated, shallow-marine depositional system of Hanadir and Kahfah, and the upper progradational sequence of the offshore marine Ra’an shale and the tide-dominated Quwarah sandstone. In addition to that, the Sarah Formation cuts more deeply into the fluvial and shallow marine sandstones of Saq Formation in the Sarah Ridge paleovalley (Clark-Lowes, 2005). This indicates the heterogeneity in terms of depositional environments that may be detected in a single borehole.

Figure 3-30 is a schematic diagram that illustrates the heterogeneity of Sarah Formation in terms of vertical and lateral facies variability and relationships with the unconformably underlying Qasim and Saq formations and the overlying Qusaiba Member of Qaliba Formation. Table 3-4 shows the variation in macro- and meso-scale in terms of architectural elements and lithofacies observed in the different paleovalleys of Sarah Formation.

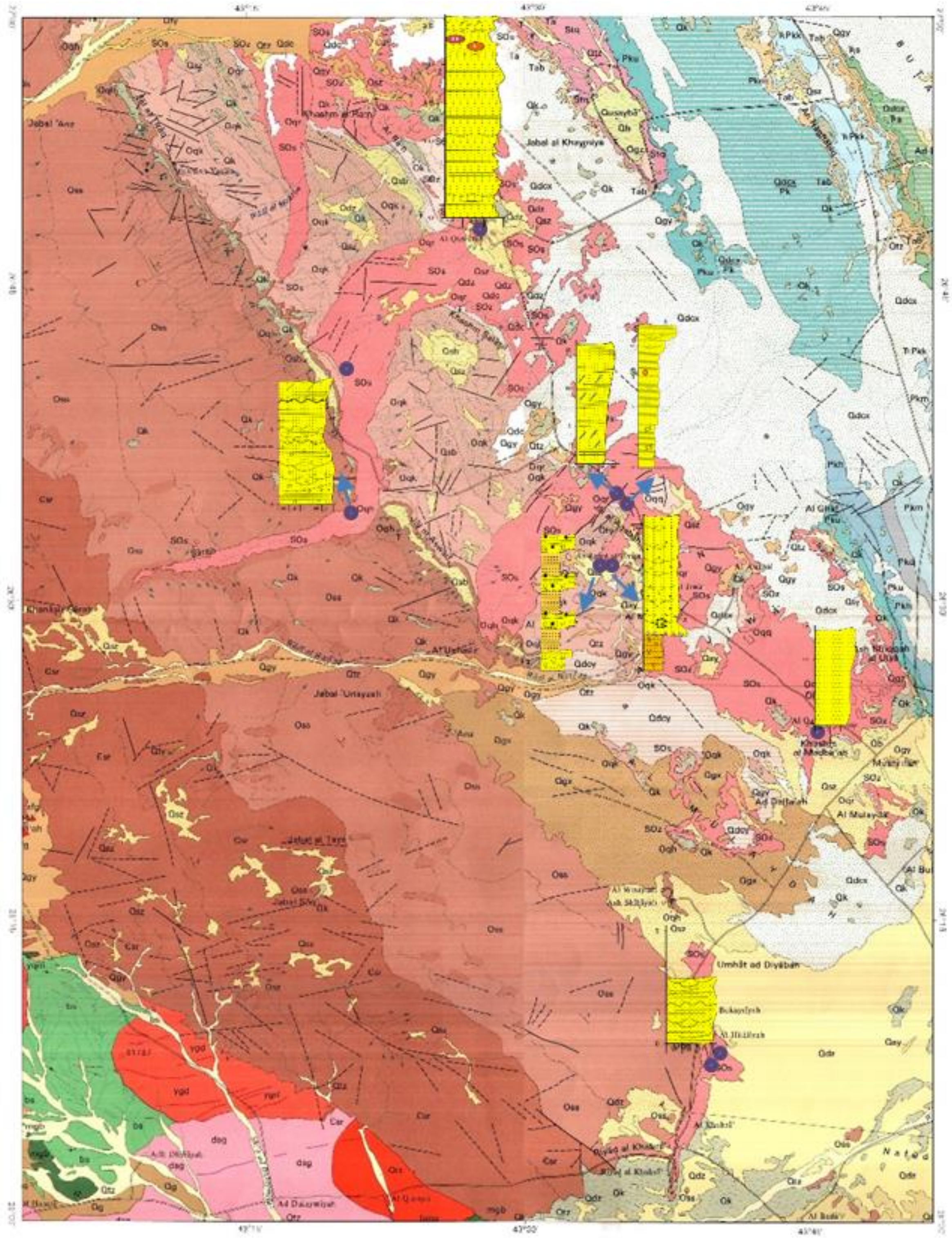

Figure 3-29: Map showing the Sarah outcrop locations within the Late Ordovician paleovalleys. The base map is modified after Manivit et al., 1986.

Table 3-4: Correlation of facies and architectural elements in Sarah paleovalleys. Note: facies codes are explained in Table 3-2, abbreviations of architectural elements are illustrated in Table 3-3

Paleovalley	Facies	Architectural elements
Bukayriyah	Sh, St, Sm, Sl, Ss, Dm	Ch, SB, HO
Rawd Al-Jawa	Sh, St, Sb, Sp, Fl, Fr, Dm	Ch, SB, LA, FF
Hanadir	Sh, St, Sm, Sb	CH, SB, LA, DA
Sarah	Sh, St	CH, SB, LA
Khanasir Sarah	Sh, St, Sl	CH, SB

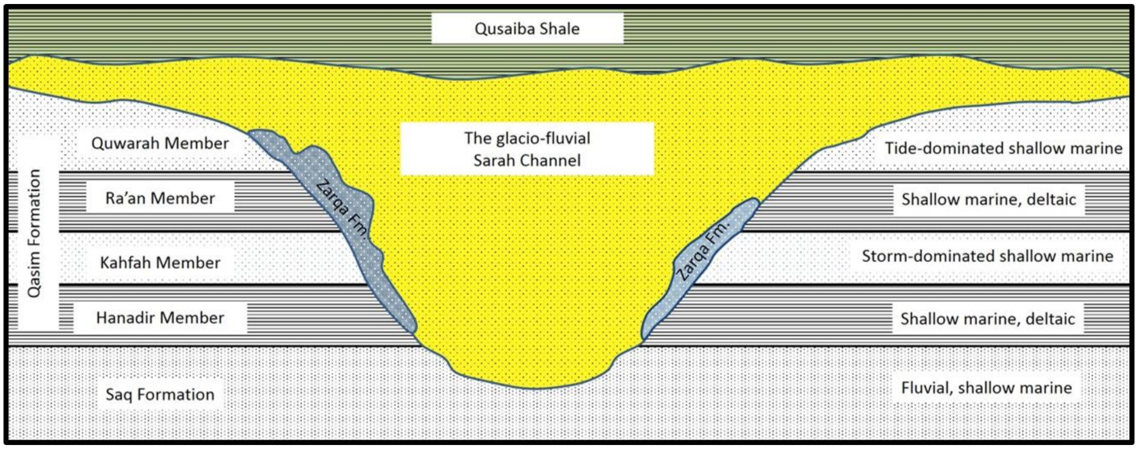

Figure 3-30: Schematic diagram illustrating the Heterogeneity of Sarah Formation in terms of vertical and lateral facies variability and relationships with other Paleozoic formations.

CHAPTER FOUR

PETROGRAPHY

4.1. Introduction

This chapter discusses the results of petrographic analysis. These results include: thin section petrography and modal analysis, SEM, XRD and sandstone classification. The depositional and diagenetic controls on poro-perm measurements are discussed briefly in this chapter and in details in the next chapter.

4.2. Thin Section Petrography

The sandstones are dominantly fine to medium-grained, moderately- to well-sorted, quartz arenites (Figure 4-1a). The quartz grains are generally mono-crystalline, while the poly-crystalline grains are rare. Alkali-feldspars and plagioclase are the main components of the detrital feldspars in the samples (Figure 4-1b, c). Lithic fragments are absent in most samples. Mica grains range from 0-5 percent (Figure 4-1d). Heavy minerals were not observed in the thin sections. The grains are mainly sub-angular to sub-rounded. Mud is the dominant matrix, generally less than 2%. The cementing materials (5-10%) include clay and iron oxides. The results from the modal analysis are shown in Table 4-1 to 4.5. The results will be discussed and investigated in this chapter.

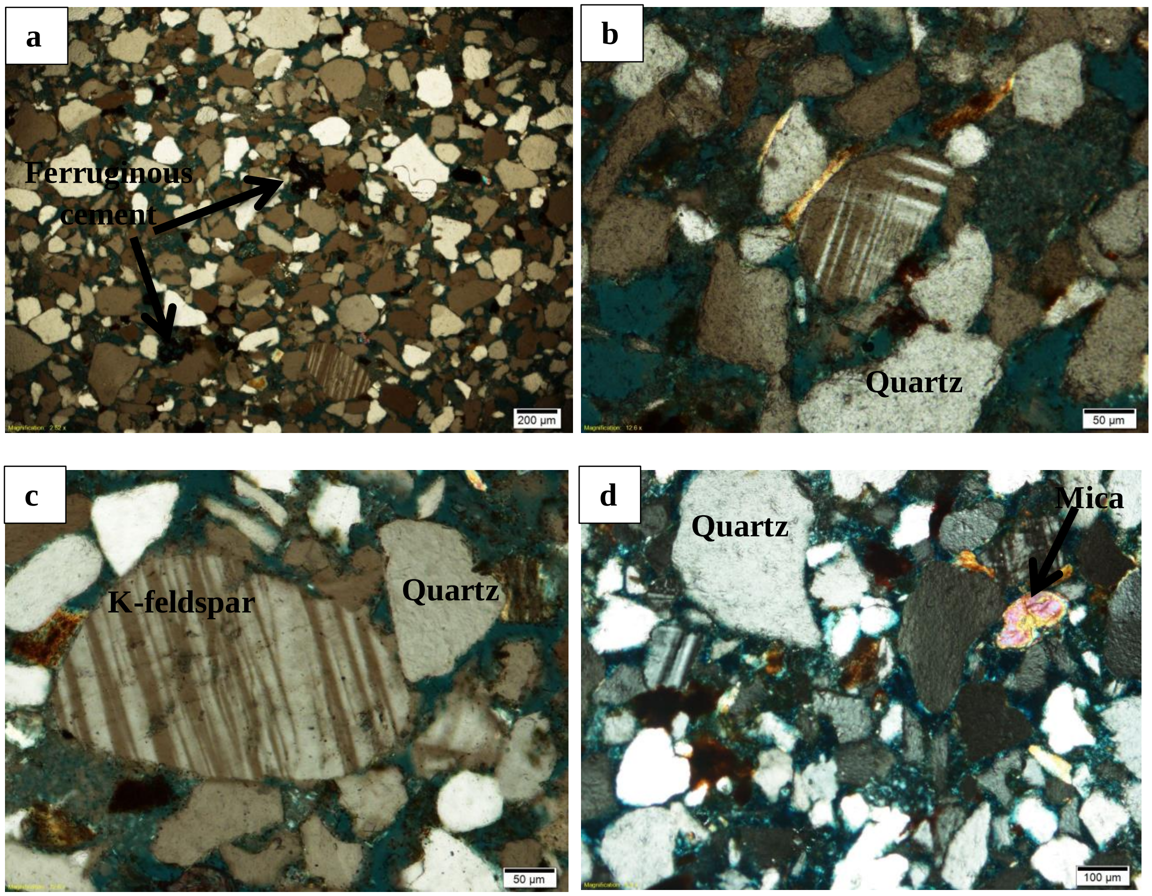

Figure 4-1: Photomicrographs of (a) thin section # RC2-V1-2 arenitic composition of Sarah Formation sandstones, moderately sorted sub-angular to sub-rounded quartz grains, ferruginous cement, inter-granular porosity around 20 %, (b) thin section # RC2-H1-6, (c) thin section # RC2-V1-1 showing the presence of large angular K-feldspar grains which may indicate extremely cold climate (e.g., Folk, 1974; Boggs, 2010), and (d) thin section # RC2-V2-4 showing the presence of mica grains which tend to align themselves within the framework grains.

Table 4-1: The compositional modal analysis for samples of Bukayriyah paleovalley

Sample ID	Φ (%)	MGS	Sorting	Roundness	Matrix	Cement	Quartz Crystals (%)		Mineral Composition (%)							φ (%)	K (md)
	Visual				(%)	(%)	Mono	Poly	Qz	Alk-Fld	Plag	Mica	Lith frag	HV-Mnrls	FeO	Measured	
S1-H3	26	0.35	Mod-well	SubAng-SubRnd	-	9	95	5	90	1	0	5	0	0	4	26.50	11.12
S1-H8	25	0.3	Well	SubAng-SubRnd	-	10	96	4	90	2	0	3	0	0	5	24.87	3.44
S1-H13	22	0.3	Well	SubAng	-	5	95	5	92	1	0	2	0	0	5	25.89	3.82
S1-V2	25	0.4	Well	SubAng	-	4	93	7	92	1	1	2	0	0	4	26.60	8.28
S1-V5	24	0.35	Well	SubAng	-	3	94	6	94	1	0	2	0	0	3	26.99	13.27
S1-V9	15	0.35	Well	SubAng-SubRnd	-	4	97	3	94	0.5	0.5	1	0	0	4	27.06	2.38
S2-H1	29	0.3	Well	SubAng-SubRnd	-	2	95	5	93	3	1	1	0	0	2	28.08	23.02
S2-H3	24	0.25	Well	SubAng-SubRnd	-	5	95	5	91	3	0	1	0	0	5	29.73	27.10
S2-H7	26	0.35	Well	SubAng	-	8	96	4	88	2	0	2	0	0	4	29.87	18.26
S2-H8	27	0.35	Mod-well	SubAng-SubRnd	-	5	97	3	90	3	0	2	0	0	5	24.72	10.29
S2-H10	26	0.4	Well	SubAng-SubRnd	-	6	98	2	89	2	1	2	0	0	6	26.67	13.53
S2-V2	25	0.4	Mod-well	SubAng-SubRnd	-	4	96	4	91	3	1	1	0	0	4	29.58	16.88
S2-V4	19	0.3	Mod	SubAng-SubRnd	-	4	94	6	91	4	0	1	0	0	4	24.58	9.19
S2-V6	28	0.35	Well	SubAng	-	5	97	3	89	3	1	2	0	0	5	28.47	11.82
S2-V10	23	0.35	Well	SubAng-SubRnd	-	3	97	3	94	2	0	1	0	0	3	27.58	13.31

Table 4-2: The compositional modal analysis for samples of Sarah paleovalley

Sample ID	Φ (%)	MGS	Sorting	Roundness	Matrix	Cement	Quartz Crystals (%)		Mineral Composition (%)							φ (%)	K (md)
	Visual				(%)	(%)	Mono	Poly	Qz	Alk-Fld	Plag	Mica	Lith frag	HV-Mnrls	FeO	Measured	
S3-H1	24	0.35	Mod-well	SubAng-SubRnd	-	10	95	5	87	2	0	1	0	0	6	22.81	9.89
S3-H2	27	0.45	Well	SubAng-SubRnd	-	8	97	3	90	1	0.5	0.5	0	0	5	24.28	10.89
S3-H4	22	0.5	Well	SubAng-SubRnd	-	7	97	3	90	1	1	1	0	0	4	20.21	11.41
S3-H6	23	0.4	Mod-well	SubAng-SubRnd	-	4	96	4	94	1	0	1	0	0	3	23.21	11.63
S3-H8	30	0.35	Well	SubAng-SubRnd	-	5	95	5	93	1	0	1	0	0	3	22.92	11.17
S3-V1	22	0.25	Mod-well	SubAng-SubRnd	-	7	98	2	91	1	0	1	0	0	3	22.82	9.45
S3-V3	17	0.35	Mod-well	SubAng-SubRnd	-	10	98	2	89	0.5	0	0.5	0	0	4	22.41	8.33
S3-V5	18	0.35	Mod-well	SubAng-SubRnd	-	6	97	3	93	0.5	0	0.5	0	0	3	21.82	10.74
S3-V8	20	0.45	Mod-well	SubAng-SubRnd	-	6	97	3	90	1	0	2	0	0	3	23.94	11.03
S3-V10	20	0.35	Mod-well	SubAng-SubRnd	-	8	95	5	90	1	0	1	0	0	3	20.69	9.52
SQ-1A-V1	30	0.5	poorly	SubRnd	5	7	95	5	89	3	5	0	0	0	5	21.31	30.68
SQ-1B-V2	20	0.45	moderate	SubAng	7	5	90	10	92	2	3	-	0	0	2	23.48	723.88
SQ-1C-H1	15	0.45	poorly	SubRnd	5	9	50	50	90	4	3	3	0	0	-	22.89	62.22
SQ-1C-H4	20	0.5	moderate	SubRnd	4	5	70	30	93	3	1	1	0	0	1	24.26	60.46
SQ-2-V1	15	0.35	poorly	SubAng	3	7	90	10	91	3	5	1	0	0	0.5	30.45	52.33
SQ-2A-V1	20	0.35	moderate	SubAng	3	15	99	1	85	0.5	3	-	0	0	1	26.31	45.60
SQ-2A-V4	15	0.5	poorly	SubRnd	4	8	95	5	88	3	1	1	0	0	1	56.71	49.33
SQ-3-V3	10	0.37	poorly	SubRnd	5	8	80	20	91	1	0	2	0	0	3	24.02	26.57
SQ-4-V3	10	0.42	moderate	SubRnd	10	5	80	20	93	3	2	0	0	0	2	20.10	22.46
SQ-5-H4	10	0.4	moderate	SubRnd	8	12	90	10	84	2	1	0	0	0	1	51.13	20.32
SQ-5-H6	15	0.46	moderate	SubRnd	8	10	90	10	87	2	2	0	0	0	1	55.70	25.19
SQ-6B-V1	30	0.47	poorly	SubRnd	5	7	90	10	91	10	5	0	0	0	5	53.42	32.75
SQ-7-H1	25	0.5	well	Rnd	20	7	80	20	91	3	3	0	0	0	1	19.37	22.68

Table 4-3: The compositional modal analysis for samples of Hanadir paleovalley

Sample ID	Φ (%)	MGS	Sorting	Roundness	Matrix	Cement	Quartz Crystals (%)		Mineral Composition (%)							φ (%)	K (md)
	Visual				(%)	(%)	Mono	Poly	Qz	Alk-Fld	Plag	Mica	Lith frag	HV-Mnrls	FeO	Measured	
RC1-H6	18	0.45	Mod-well	SubAng-SubRnd	0	8	96	4	89.6	0.5	0.5	3	0	0.1	5	30.21	26.81
RC1-V6	15	0.4	Mod	SubAng-SubRnd	0	8	98	2	88.8	1	0	2	0	0.1	5	30.02	20.52
RC2-H1	12	0.4	Mod-well	SubAng-SubRnd	0	10	98	2	97	0	0	1	0	0.1	7	31.74	13.04
RC2-V1	18	0.35	Mod-well	SubAng	0	7	96	4	97	0.5	0.5	0.5	0	0.2	3	30.78	11.44
RC2-V2	15	0.28	Mod-well	SubAng-SubRnd	0	1	93	7	98	0.5	0	1	0	0.1	4	30.31	14.49
RC3-H4	15	0.3	Mod	SubAng	0	9	96	4	99	0	0	0	0	0.3	10	32.84	3.83
RC3-V1	12	0.25	Mod-well	SubAng	0	3	96	4	99	0	0	4	0	0.1	3	31.52	7.69
RC3-V2	12	0.25	Well	SubAng-SubRnd	0	5	97	3	98	0	0	1	0	0.3	2	30.12	4.37
RC3-V3	18	0.3	Well	SubRnd	0	5	96	4	96	0.5	0.5	1	0	0.2	2	29.37	4.12
RC3-V4	15	0.42	Mod-well	SubRnd	0	20	96	4	99	0	1	3	0	0.2	7	30.18	2.79
RC4-H1	15	0.35	Well	SubAng-SubRnd	0	15	97	3	99	0.5	0.5	2	0	0.2	7	34.62	16.76
RC4-H2	10	0.25	Well	SubRnd	0	8	97	3	98	0.5	0.5	1	0	0.2	5	32.70	16.25
RC4-V4	15	0.25	Well	SubRnd	0	1	96	4	99	0.5	0.5	1	0	0.1	5	29.82	13.39
RC5-H6	15	0.25	Well	SubRnd	0	2	96	4	98	0	0	2	0	0.4	3	29.02	8.32
RC5-V2	15	0.35	Well	SubRnd	0	1	95	5	99	0.5	0.5	2	0	0.2	4	35.13	5.12

Table 4-4: The compositional modal analysis for samples of Hanadir paleovalley (continued)

Sample ID	Φ (%)	MGS	Sorting	Roundness	Matrix	Cement	Quartz Crystals (%)		Mineral Composition (%)							φ (%)	K (md)
	Visual				(%)	(%)	Mono	Poly	Qz	Alk-Fld	Plag	Mica	Lith frag	HV-Mnrls	FeO	Measured	
SR-1-V1	27	0.25	well	Rnd	0	10	98	2	98	1	2	0	0	0.5	3	25.98	597.56
SR-1-H2	30	0.2	Mod-well	Well Rnd	3	3	95	5	97	1	2	0	0	0.5	15	23.62	437.20
SR-1-H4	20	0.3	well	V.Well Rnd	0	2	98	2	99	0	2	0	0	0	5	27.76	963.76
SR-2-V1	35	0.25	well	Well Rnd	1	5	98	2	99	1	0	0	0	0.5	6	29.5	61.64
SR-2-H2	27	0.3	Mod-well	Well Rnd	0	2	97	3	98	0	1	0	0	0.5	2	28.61	1857.60
SR-2-H5	30	0.25	Mod-well	Rnd	0	10	98	2	96	0	2	0	0	0.5	5	30.98	2040.80
SR-3-V2	30	0.25	Mod-well	Rnd-SubRnd	0	15	96	5	90	5	3	0	0	0.5	3	29.89	1585.10
SR-3-H2	27	0.2	well sorted	Rnd	0	10	98	2	97	1	0	0.5	0	0.5	4	27.97	814.86
SR-4-V1	30	0.2	Mod-well	SubAng	0	5	98	2	98	0	1	0.3	0	1	3	29.20	1485.30
SR-5-V2	20	0.25	Mod	SubRnd	0	7	98	2	99	1	1	0	0	0.3	10	27.02	327.51
SR-6-V1	35	0.7	v. well	V.Well Rnd	0	5	90	10	98	1	0	0	0	1	2	24.10	401.90
SR-6-V3	35	0.7	v.well	Well Rnd	1	20	80	20	98	1	0	0	0	0.3	3	55.25	401.57
SR-6-H2	35	0.7	v.well	V.Well Rnd	0	10	60	40	97	0	1	0	0	1	5	22.37	297.63
SR-6-H5	25	0.3	Mod	Well Rnd	3	3	95	5	97	0	2	0	0	0.8	4	19.10	232.07
SR-7-H2	25	0.15	well	Rnd	0	10	98	2	97	1	2	0.3	0	0.5	3	30.32	1193.20
SR-7c-H3	35	0.35	Mod-well	WellRnd	0	15	92	8	99	1	0	0	0	0.5	3	24.84	1576.60
SR-9-V1	25	0.15	very well	SubAng	0	10	100	0	99	1	0	0	0	0.5	5	29.68	1000.50

Table 4-5: The compositional modal analysis for samples of Khanasir Sarah

Sample ID	Φ (%)	MGS	Sorting	Roundness	Matrix	Cement	Quartz Crystals (%)		Mineral Composition (%)							φ (%)	K (md)
	Visual				(%)	(%)	Mono	Poly	Qz	Alk-Fld	Plag	Mica	Lith frag	HV-Mnrls	FeO	Measured	
KS1-V1	10	0.17	well	Rnd	20	5	80	20	90	20	80	0	1	0	0	29.13	46.62
KS1-V3	20	0.17	well	SubAng	10	10	90	10	90	60	40	0	20	0	0	29.06	39.42
KS3-A-H1	30	0.7	mod	Rnd	10	10	80	20	95	0	100	0	2	0	0	27.87	910.64
KS3-C-V3	26	0.3	mod	Rnd	15	5	70	30	90	50	50	0	5	0	0	32.24	1056.50
KS3-C-V4	25	0.3	well	SubRnd	25	5	90	10	95	0	100	0	0	0	2	28.42	1628.70
KS9-V2	20	0.3	poorly	SubRnd	5	5	95	5	95	0	0	0	5	0	0	20.95	7.41
KS9-H2	30	0.7	poorly	well	25	5	90	10	99	0	0	0	1	0	2	23.12	70.50
KS9-H6	25	0.7	poorly	SubRnd	5	10	95	5	99	0	0	0	1	0	0	24.79	191.46

4.3. Sandstone Classification

QFL diagram in accordance with Williams et al. (1982) and Pettijohn et al. (1987) shows that all the samples that were subjected to thin section petrography analysis (about 80 thin sections) from the studied paleovalleys are quartz arenites (Figure 4-2). The QFL values range between 90-100 % for quartz, 0-10 % for feldspar, and 0-5 % for lithic fragments. QFL diagrams were generated by the *Excel spreadsheet method* (Graham and Midgley, 2000).

4.4. X-Ray Diffraction (XRD)

The results of XRD analysis on 20 selected samples representing the four studied paleovalleys show that the mineralogical phases are dominated by quartz with subordinate amount of kaolinite. Calcite and dolomite are limited to very few samples from Hanadir and Sarah paleovalleys.

Table 4-6 shows a summary of the XRD results. Figure 4-3 shows examples for X-ray diffractograms of two samples, one containing no clays, and the other containing 2.4 % clay. Complete XRD results are included in Appendix A.

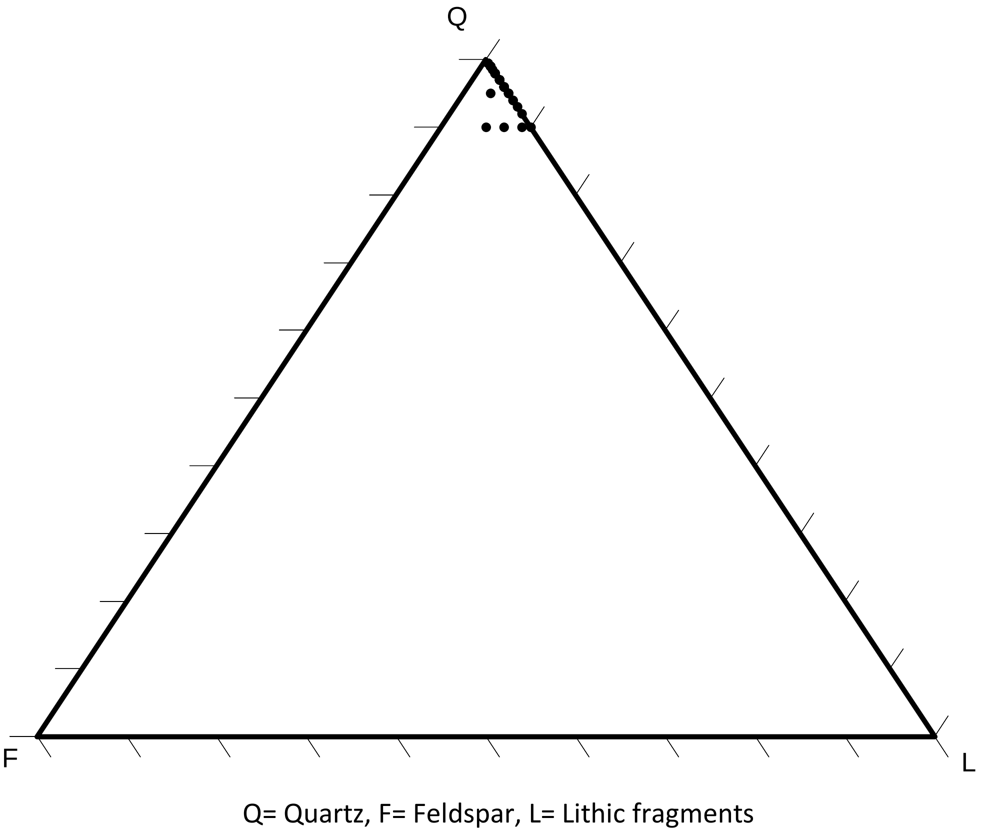

Figure 4-2: QFL diagram for all the thin section studied samples. The QFL diagram shows that all the samples are quartz arenites.

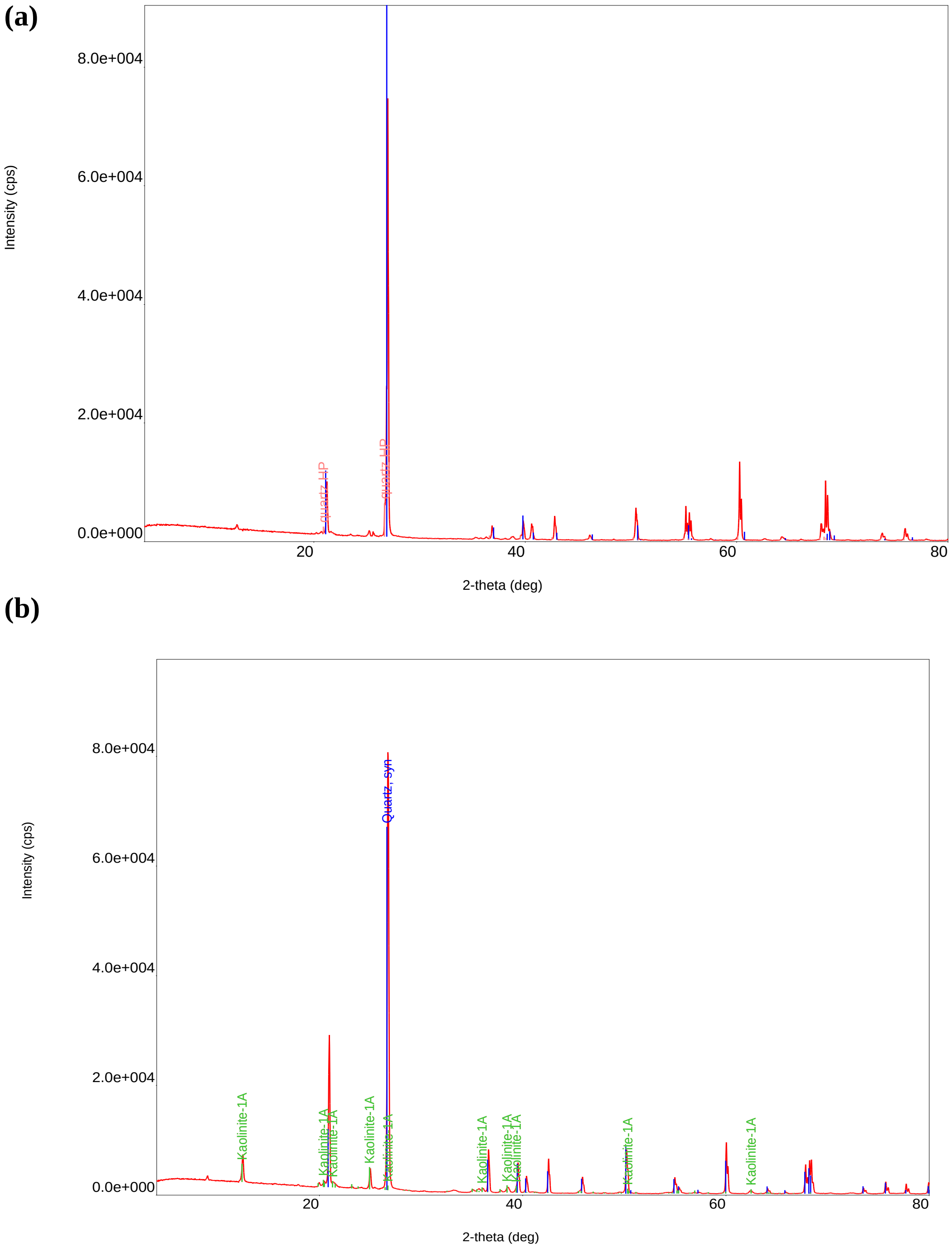

Figure 4-3: X-ray diffractograms for (a) sample # KS-3C-V3 with 100 % quartz, φ = 32.24 %, K = 1056.5 md, (b) sample # S1H8 containing 97.6 % quartz and 2.4 % kaolinite, φ = 24.87 %, K = 3.44 md.

Table 4-6: XRD results for representative samples from the studied paleovalleys of Sarah Formation

	Sample #	Compounds		Wt. %
Bukayriyah Paleovalley	S1H1	SiO_2 $Al_2Si_2O_5(OH)_4$	Quartz Kaolinite	100 0
	S1H6	SiO_2 $Al_2Si_2O_5(OH)_4$	Quartz Kaolinite	100 0
	S1H8	SiO_2 $Al_2Si_2O_5(OH)_4$	Quartz Kaolinite	97.6 2.4
	S2H3	SiO_2 $Al_2Si_2O_5(OH)_4$	Quartz Kaolinite	100 0
	S2H4	SiO_2 $Al_2Si_2O_5(OH)_4$	Quartz Kaolinite	NA*
	S2H7	SiO_2 $Al_2Si_2O_5(OH)_4$	Quartz Kaolinite	NA
Quwarah Paleovalley	S3H4	SiO_2 $Al_2Si_2O_5(OH)_4$	Quartz Kaolinite	99 1
	S3H6	SiO_2 $Al_2Si_2O_5(OH)_4$	Quartz Kaolinite	NA
	S3V8	SiO_2 $Al_2Si_2O_5(OH)_4$	Quartz Kaolinite	NA
	S3V9	SiO_2 $Al_2Si_2O_5(OH)_4$	Quartz Kaolinite	NA
Khanasir Sarah	KS-3C-V3	SiO_2 $Al_2Si_2O_5(OH)_4$	Quartz Kaolinite	100 0
	KS-9-V2	SiO_2 $Al_2Si_2O_5(OH)_4$	Quartz Kaolinite	100 0
Hanadir Paleovalley	RC-1-H6	SiO_2 $Al_2Si_2O_5(OH)_4$ $CaMg(CO_3)_2$ $CaCO_3$	Quartz Kaolinite Dolomite Vaterite	98 0 1.9 0.1
	RC-3-V2	SiO_2 $Al_2Si_2O_5(OH)_4$	Quartz Kaolinite	NA
	RC-4-H2	SiO_{10} $Al_2Si_2O_5(OH)_{12}$	Quartz Kaolinite	100 0
	SR-7A-H4	SiO_2 $Al_2Si_2O_5(OH)_4$	Quartz Kaolinite	NA
	SR-9-V1	SiO_2 $Al_2Si_2O_5(OH)_4$	Quartz Kaolinite	100 0
Sarah Paleovalley	SQ-1C-H4	$Be_{0.67}$ $Co_{0.33}$ $AlPO_4$	Beryllium Cobalt Berlinite	80 20
	SQ-4-V3	SiO_2 $Al_2Si_2O_5(OH)_4$ $CaCO_3$	Quartz Kaolinite Calcite	89.9 10.1
	SQ-7A-H4	SiO_2 VO2	Quartz Vanadium Oxide	NA

* NA = not available

4.5. Scanning Electron Microscopy (SEM)

15 samples were subjected to SEM analysis. Texture and mineralogy of the samples were clarified by photomicrographs of both low and high magnification. Low magnification photomicrographs (down to 500 µm) show the overall texture and porosity-cement relationship. High magnification photomicrographs (up to 1 µm) were used to focus on some surface details and morphology of crystals at discrete particles.

Surface morphology and grain contacts of the quartz grains as well as the nature of the cementing materials and their type are shown in Figure 4-4. The presence of authigenic kaolinite cement filling the pores associated with quartz overgrowth (Figure 4-5) usually occurs in sands that have been flushed by acidic waters (Selley, 1998). SEM photomicrographs also show the delicate book-stack and granular morphology of kaolinite cement (Figure 4-6).

The energy dispersive spectrometry (EDS) results show that all samples are rich in silica and hence in quartz. Significant amounts of Al (Figure 4-7a) indicate that the dominant cement is from the kaolinite group. Fe is present in very few samples, mostly from Hanadir paleovalley (Figure 4-7b).

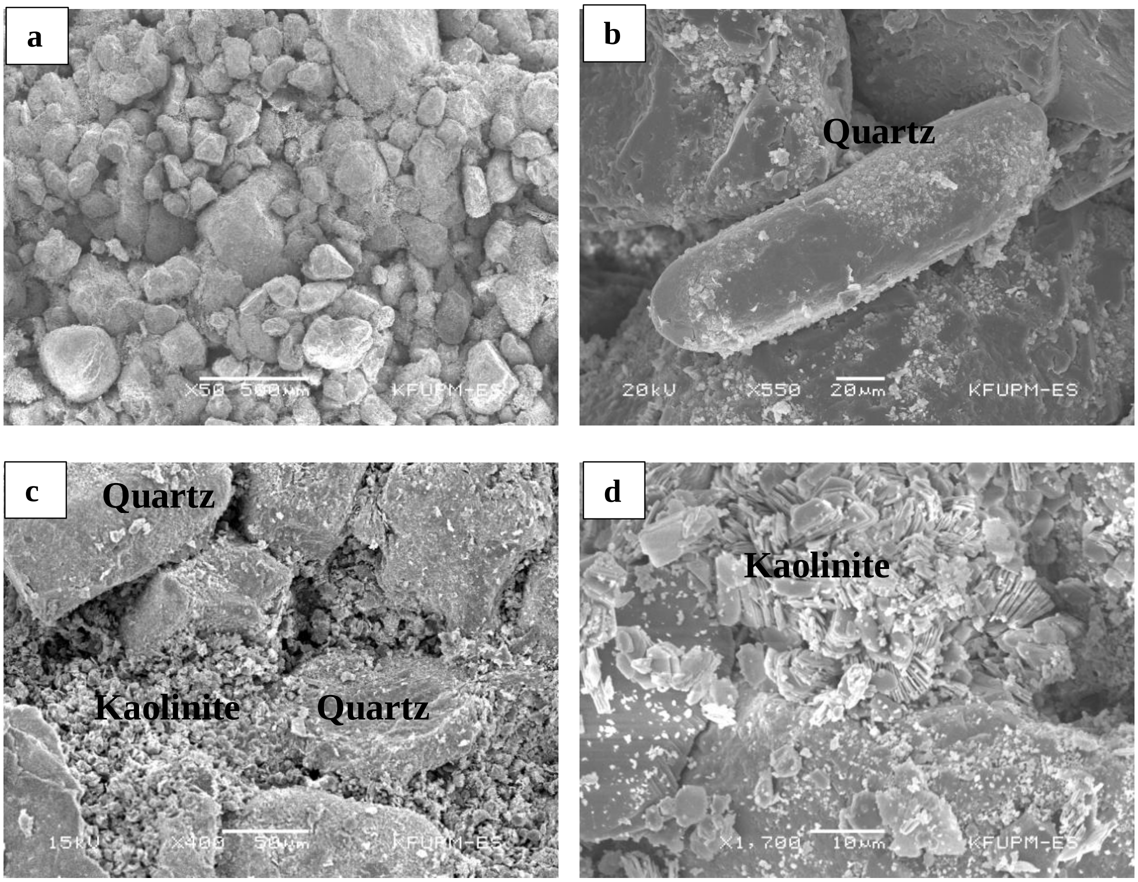

Figure 4-4: SEM micrograph of (a) overall view of rounded to sub-rounded quartz grains with very few sub-angular grains (sample KS3-C-V3-1, φ = 32.24 %, K = 1056.5 md), (b) grain surface morphology and type of contact of the grains (sample S3-V9-7, φ = 8.63 %, K = 21.32 md), (c) kaolinite cement blocking the pore spaces between the quartz grains (sample S1-V8-2, φ = 27.69 %, K = 1.87 md), and (d) grain-coating kaolinite on the surface of quartz grains (sample KS3-C-V3-1, φ = 32.24 %, K = 1056.5 md). The dense packing of quartz grains may explain why the samples have high porosity and low permeability values, which is typical for glacio-fluvial facies.

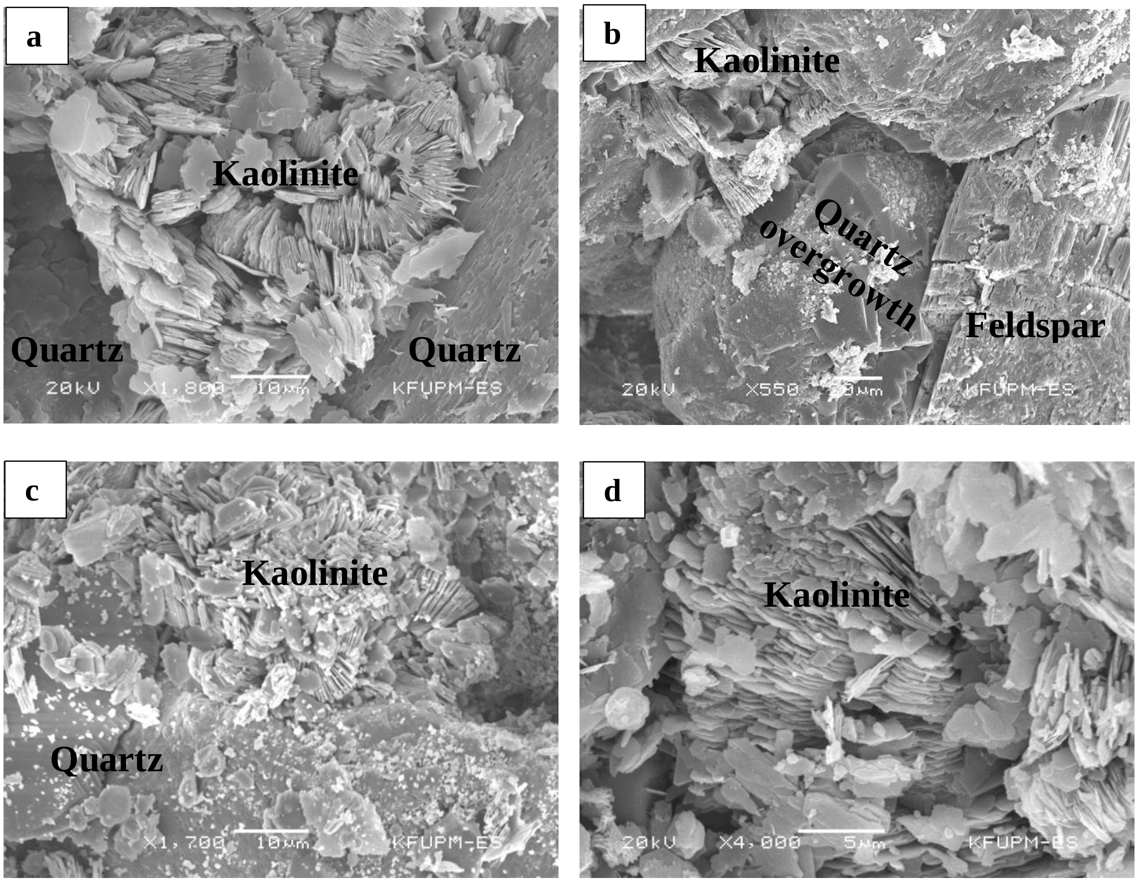

Figure 4-5: (a) SEM micrograph of sample # S3-V9-8 (φ = 21.32 %, K = 8.63 md) showing the pore-filling kaolinitic material in-between quartz grains. This reduces permeability between the grains. (b) Photomicrograph of sample # S3-H4-5 (φ = 20.21 %, K = 11.41 md) showing kaolinite booklets, quartz overgrowth and partially dissolved feldspar grain. (c) Photomicrograph of sample # KS3-C-V3-3 (φ = 32.24 %, K = 1056.5 md) showing kaolinite grain-coating on the surface of quartz grains. (d) Photomicrograph of sample # S2-H8-6 (φ = 24.72 %, K = 10.29 md) showing kaolinite book-stack textural morphology.

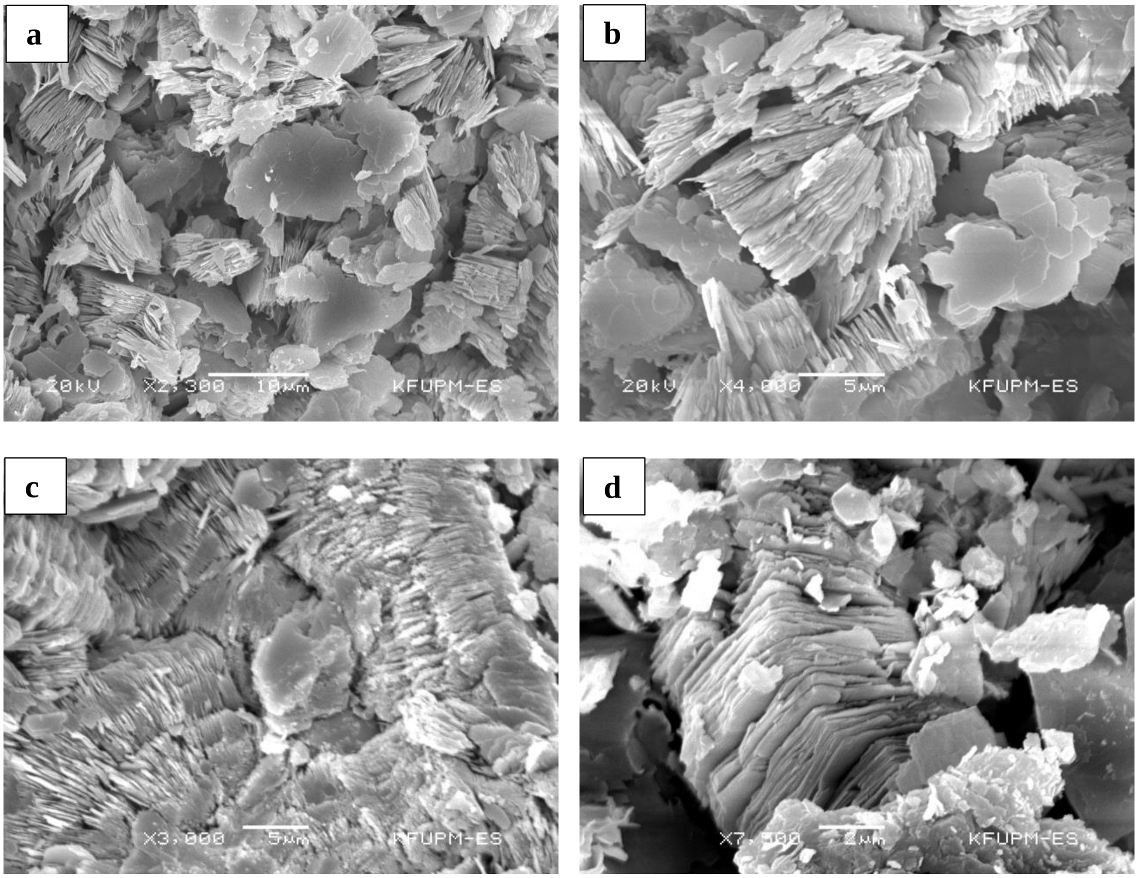

Figure 4-6: SEM micrograph of (a) sample # S3-H6-3 (φ = 23.21 %, K = 11.63 md) showing thin idiomorphic platelets and book-stack of kaolinite, (b) sample # S3-V9-3 (φ = 21.32 %, K = 8.63 md) showing typical book-stack with some discrete platy textural morphology of kaolinite, (c) sample # KS9-V2-6 (φ = 20.95 %, K = 7.41 md) showing typical book-stacked vermiculite-type kaolinite cement, (d) sample # RC3-V2-6 (φ = 30.12 %, K = 4.37 md) showing stacks of pseudohexagonal-shaped kaolinite platelets.

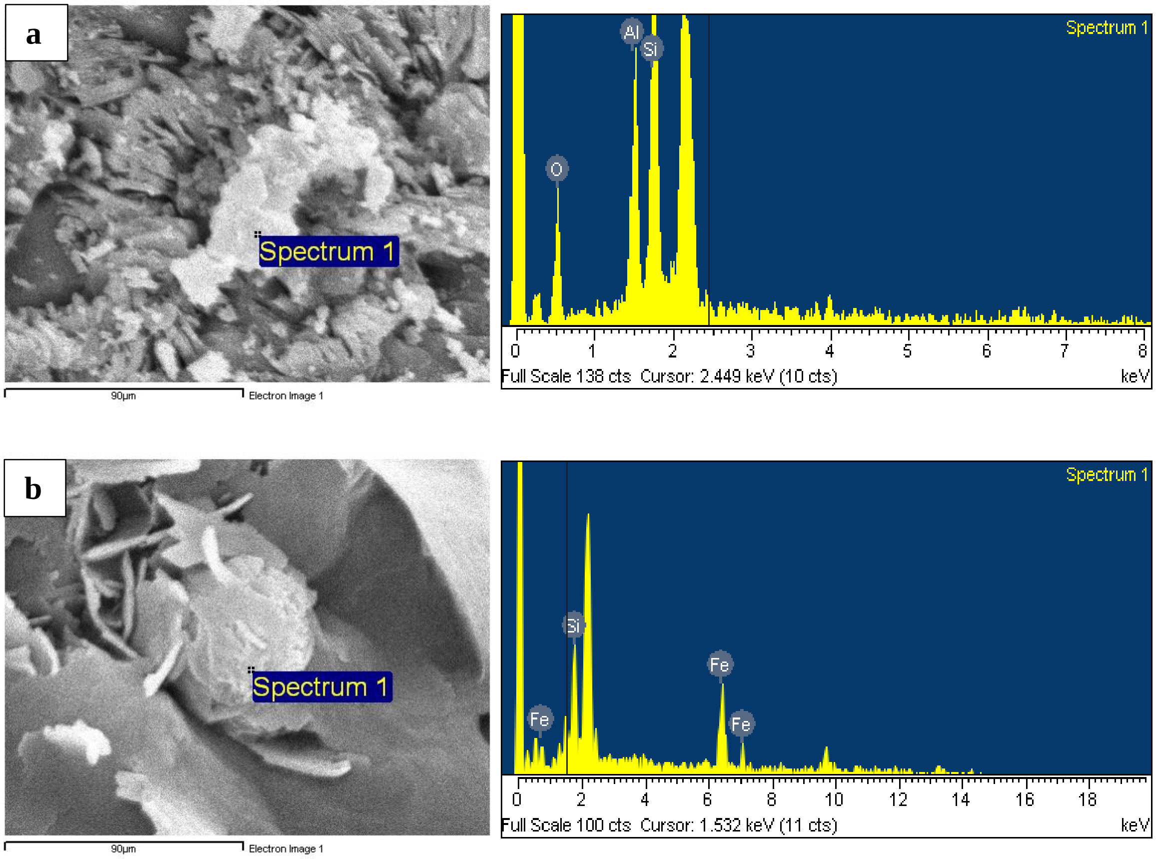

Figure 4-7: SEM micrograph of (a) sample # KS9-V2 (φ = 20.95 %, K = 7.41 md) showing kaolinite cement coating quartz grains, (b) sample # RC4-H2 (φ = 32.70 %, K = 16.25 md) showing iron cement aggregated into rosette-like clusters between the grains. Note the EDS beside the photomicrographs confirm the presence of kaolinite and iron in (a) and (b) respectively.

4.6. Diagenesis

Diagenesis is a sequence of processes that take place after deposition of sediments. These processes involve organic reworking, physical and chemical compaction, cementation and mineral replacement, dissolution by pore fluids; and clay mineral authigenesis (Boggs, 2010; Selley, 1998; Pettijohn et al., 1987).

4.6.1. Compaction

As the sediments are buried deeper, the overburden pressure increases the tightening of grain packing; which results in a significant loss of porosity (Boggs, 2010). This loss of porosity occurs during early burial (Selley, 1998). Chemical compaction, also known as pressure solution, results from partial dissolution of the grains due to the increased pressure at the contact point between the grains.

The grain contacts in the studied samples are dominantly point/tangential and long, with low number of grain-to-grain contacts. Concavo-convex contacts are rare in the samples (Figure 4-8). This may indicate that the grains had undergone minor pressure solution (low degree of compaction) (Pettijohn et al., 1987).

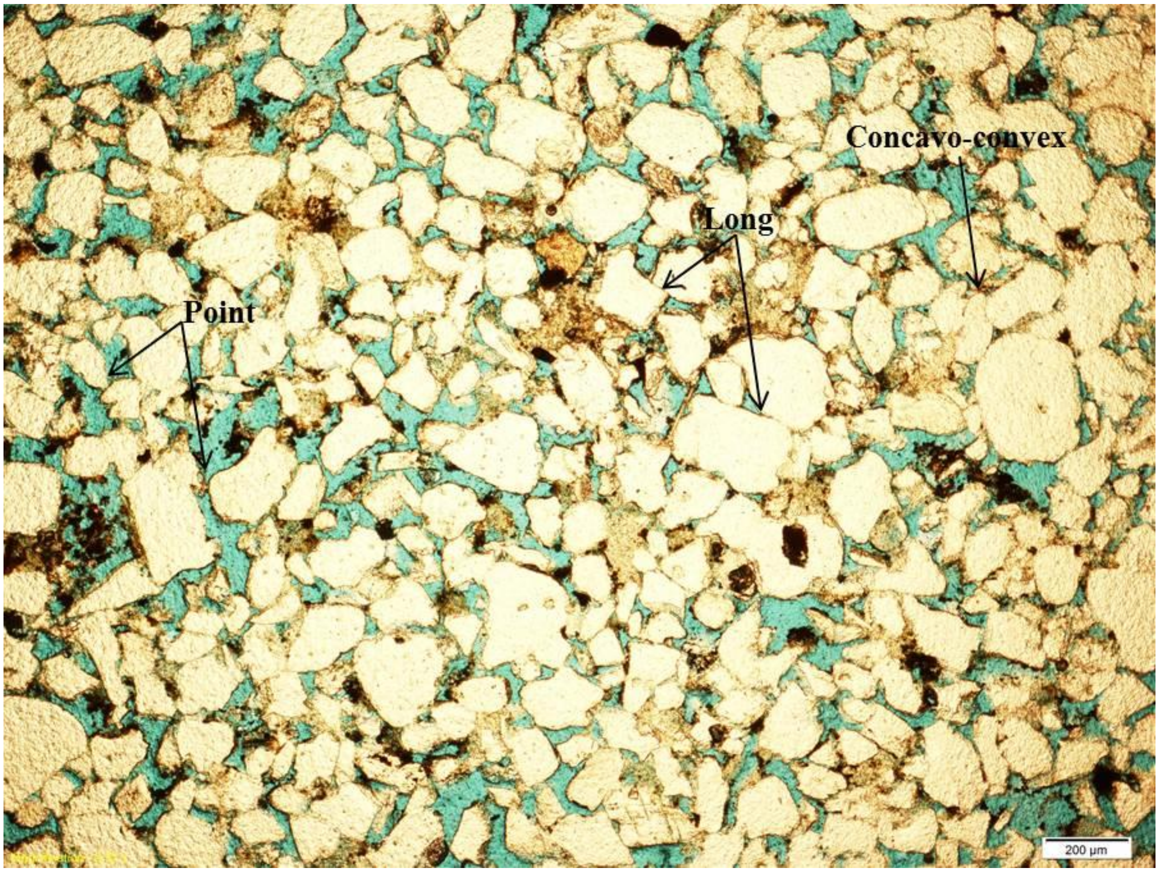

Figure 4-8: Thin section micrograph portrays the nature of grain contacts (sample # S3V1-1), measured porosity in the sample is 22.8 %, permeability is 9.45 md.

4.6.2. Cementation

During the process of sediment lithification, authigenic minerals tend to precipitate within the pore spaces between the detrital grains. This behavior causes porosity reduction due to the blockage of inter-granular rock volume. Being a tight gas sandstone reservoir (Al-Mahmoud and Al-Ghamdi, 2010; Briner et al., 2010; Bukhamseen et al., 2010), Sarah Formation might have undergone through extensive episodes of cementation (Clarkson et al., 2012; Naik, 2003).

The amount of cementing material in the studied samples of Sarah outcrops is generally less than 10 %. Kaolinite is the main cementing material (Figure 4-4c, Figure 4-4d, Figure 4-5, Figure 4-6, and Figure 4-7a). It usually occurs as blocky crystals within the pores between quartz grains. Authigenic kaolinite cement blocks the pore spaces and diminishes porosity. It is also an indication that sandstone has been flushed by acidic water. Ferruginous materials occur as important cement as well (Figure 4-1a, Figure 4-7b). Their penetrating nature may be an indication of replacement of silica cement, and reducing the porosity as a result. Silica is also observed in the samples. Quartz, being the most common silicate mineral acting as cement, is usually attached to the detrital quartz grains as quartz overgrowth (Figure 4-5b, Figure 4-10). It occurs as a line of bubbles around the surface of the original grain. Quartz overgrowth is very rare due to the low degree of compaction that was proved earlier. Silica cement is an indication of flushing by acid fluids, because the solubility of silica tends to increase with increasing pH (Selley, 1998).

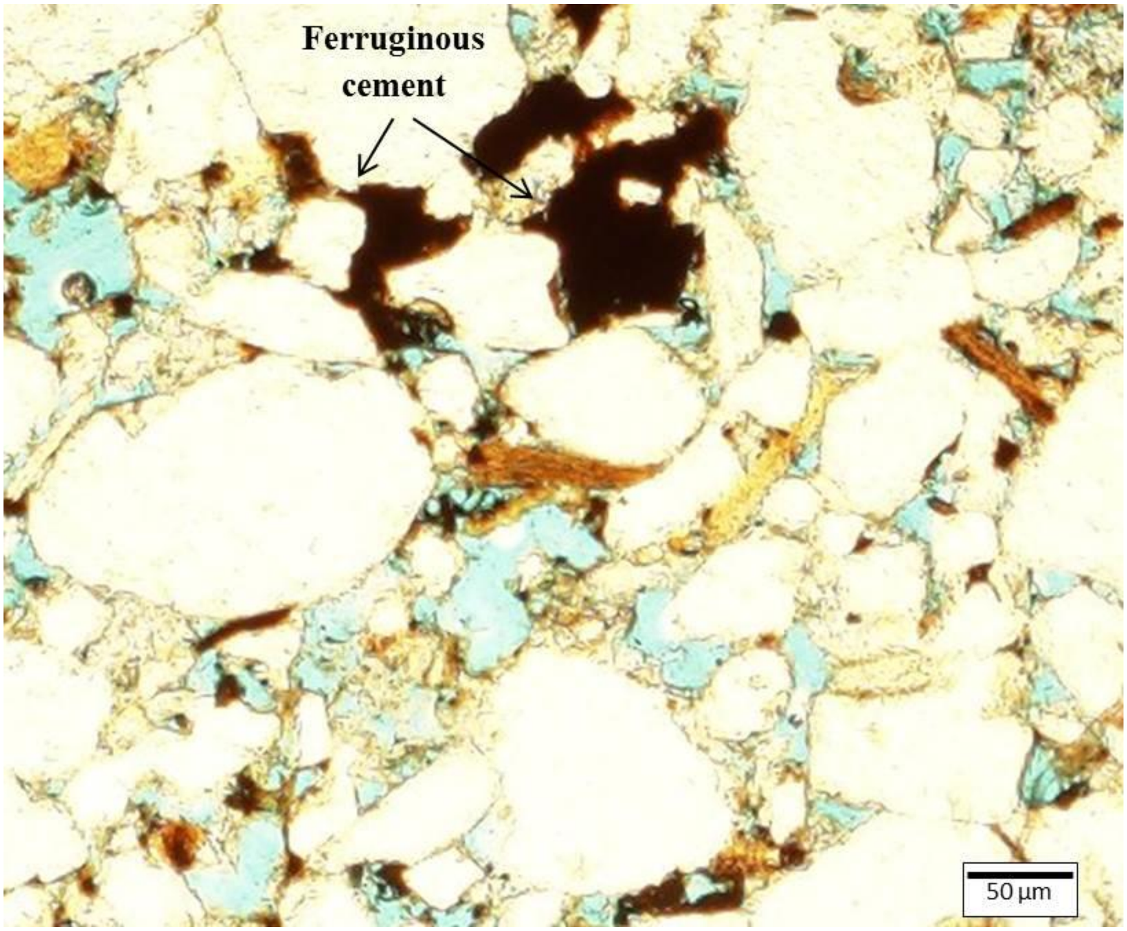

Figure 4-9: Thin section micrograph of sample # RC1-H6-3 showing an example of the presence of ferruginous cement within the quartz grains in the samples, (φ = 30.21 %, K = 26.81 md).

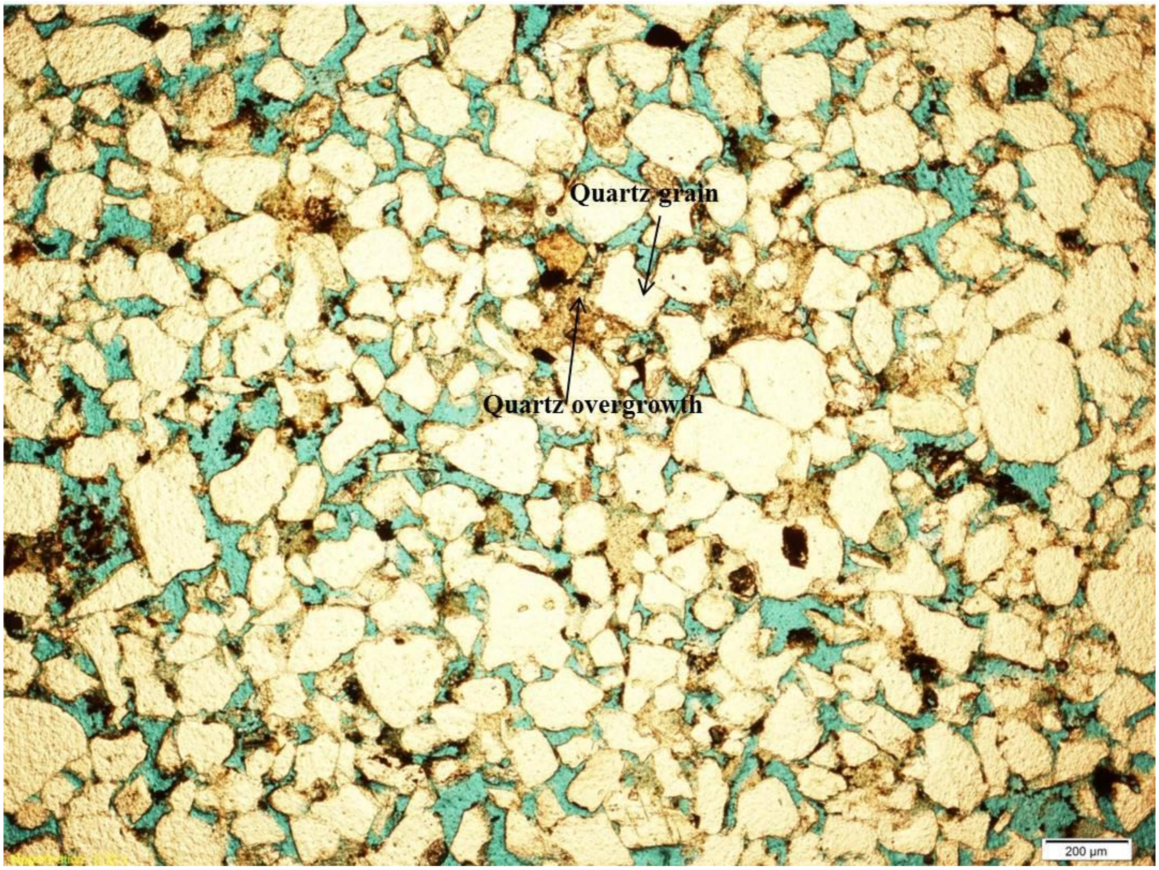

Figure 4-10: Thin section micrograph of sample # S3V1 showing an example of quartz overgrowth around the detrital quartz grains, moderately to well sorted (φ = 22.82 %, K = 9.45 md).

4.6.3. Dissolution and Mineral Replacement

The reduction of porosity and permeability due to cementation can be compensated by dissolution of cements or grains. This process involves leaching of feldspar and other unstable detrital minerals. This leads to increase in porosity, which in this case is called secondary porosity. Furthermore, porosity might be affected by mineral replacement.

The absence of carbonate cement and the lack of feldspars in the studied samples might be as a result of dissolution and replacement by other minerals. The presence of partially kaolinitized feldspars in some samples may also act as an evidence of this process. What greatly supports this concept is the inhomogeneous packing of the framework grains. Since the studied samples are collected from outcrops, meteoric water may be responsible for the dissolution of feldspars and unstable minerals.

Although dissolution tends to increase porosity, it may also reduce it. This happens when feldspars are replaced by clay minerals, which usually plugs the pore throats and cause porosity reduction. Chamley (1994) referred to K-feldspars and micas as the most probable sources of Si and Al needed for kaolinite formation.

CHAPTER FIVE

PETROPHYSICAL PROPERTIES

5.1. Introduction

To characterize the quality of a sandstone reservoir, two important characteristics must be studied, described and analyzed deeply. Those are: *porosity* and *permeability*, the keys. If you got those keys, you got the secrets of the reservoir. As a sandstone reservoir, Sarah Formation exhibits a heterogeneous character in terms of petrophysical properties. Much effort has been done to analyze the degree and patterns of such heterogeneity in the studied samples.

This section serves to determine relationships among depositional texture, mineral composition and diagenesis in Sarah Formation, and to relate these attributes to porosity and permeability. For this purpose, porosity and permeability measurements were conducted in the laboratory on about 200 sample plugs using helium porosimeter and permeameter. In addition, Mercury injection capillary pressure tests were carried out on 10 representative samples.

5.2. Porosity

The measured porosity values from sample plugs range between 17 % and 56.7 % with an average value of 28 %. Both primary and secondary porosities have been registered. As discussed earlier, leaching and dissolution created secondary intergranular porosity and intragranular microporosity. Figure 5-1 shows that the most frequent porosity measurements in the studied samples are between 25-35 %.

5.3. Permeability

The studied samples showed very wide range of permeability values ranging from 0.1 md to 2.27 Darcy, with an average of 0.25 Darcy. As permeability depends on the effective porosity of the rock, so it is affected by the rock grain size, shape, sorting, packing and the degree of compaction and cementation (Tiab and Donaldson, 2004). Figure 5-2 shows that permeability values less than 200 md are the most common.

5.4. Porosity-Permeability Relationship

Each paleovalley of Sarah Formation exhibits generally limited range of porosity values and a unique wide range of permeability values. Therefore, it is difficult to define a continuous porosity-permeability trend.

For none of the four groups of samples could I find a meaningful mathematical relation between log K and φ. For any kind of fitting (linear, logarithmic, exponential, polynomial, etc.), R^2 was close to zero (Figure 5-7). However, the log K – φ plot shows an interesting clustering. From the frequency curves in Figure 5-7, one can notice that φ values are mostly between 25 and 35 percent for the four groups, except some samples from Sarah paleovalley. Meanwhile, log K values show wide range of variation according to the different abundance of cements and packing as discussed earlier in Chapter Four.

Samples of Sarah paleovalley are clustered into three groups, the first two with the same range of φ but with different log K range. The third group of Sarah paleovalley has higher φ values (50-60 %). With further revision of these samples of the third group, it was found that they have very well sorted coarse grains, with less cement content, and composed of friable grains which account for the high porosity values.

Samples of Hanadir paleovalley are clustered into two groups, one is correlated with those of Bukairiyah paleovalley ($20<\varphi<40$ %, $2.5<\log K<3.5$ md), and the other is correlated with the first group of Sarah paleovalley ($20<\varphi<40$ %, $0.5<\log K<2.0$ md). Samples of of Khanasir Sarah are distributed also within the last two groups.

This clear clustering of the four paleovalleys could not be observed on the petrographic plots (Figure 5-8-5.9). This clustering is someway related to the different locations of samples.

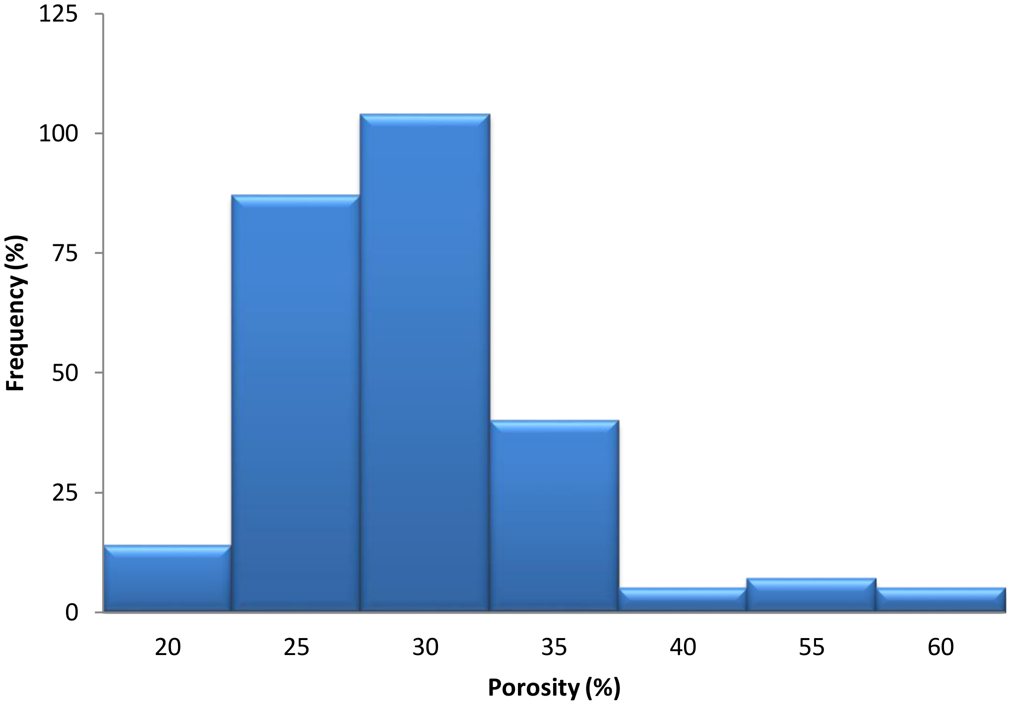

Figure 5-1: Histogram of porosity values for all the samples.

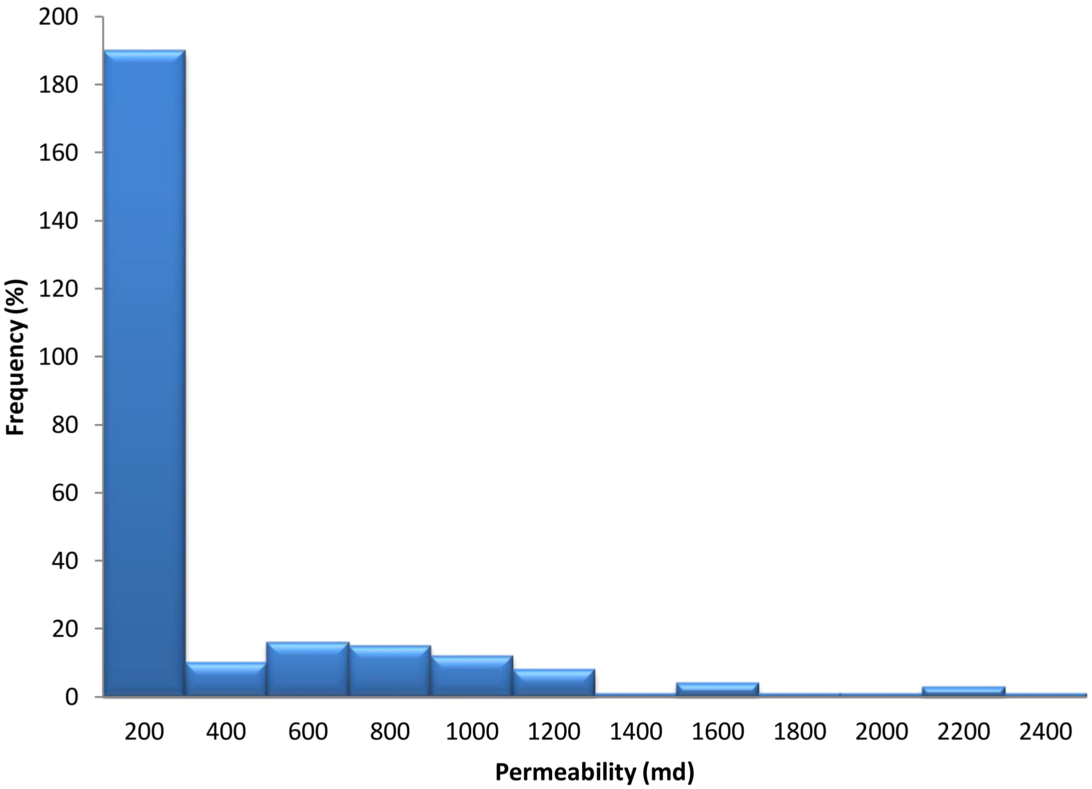

Figure 5-2: Histogram of permeability values for all the samples.

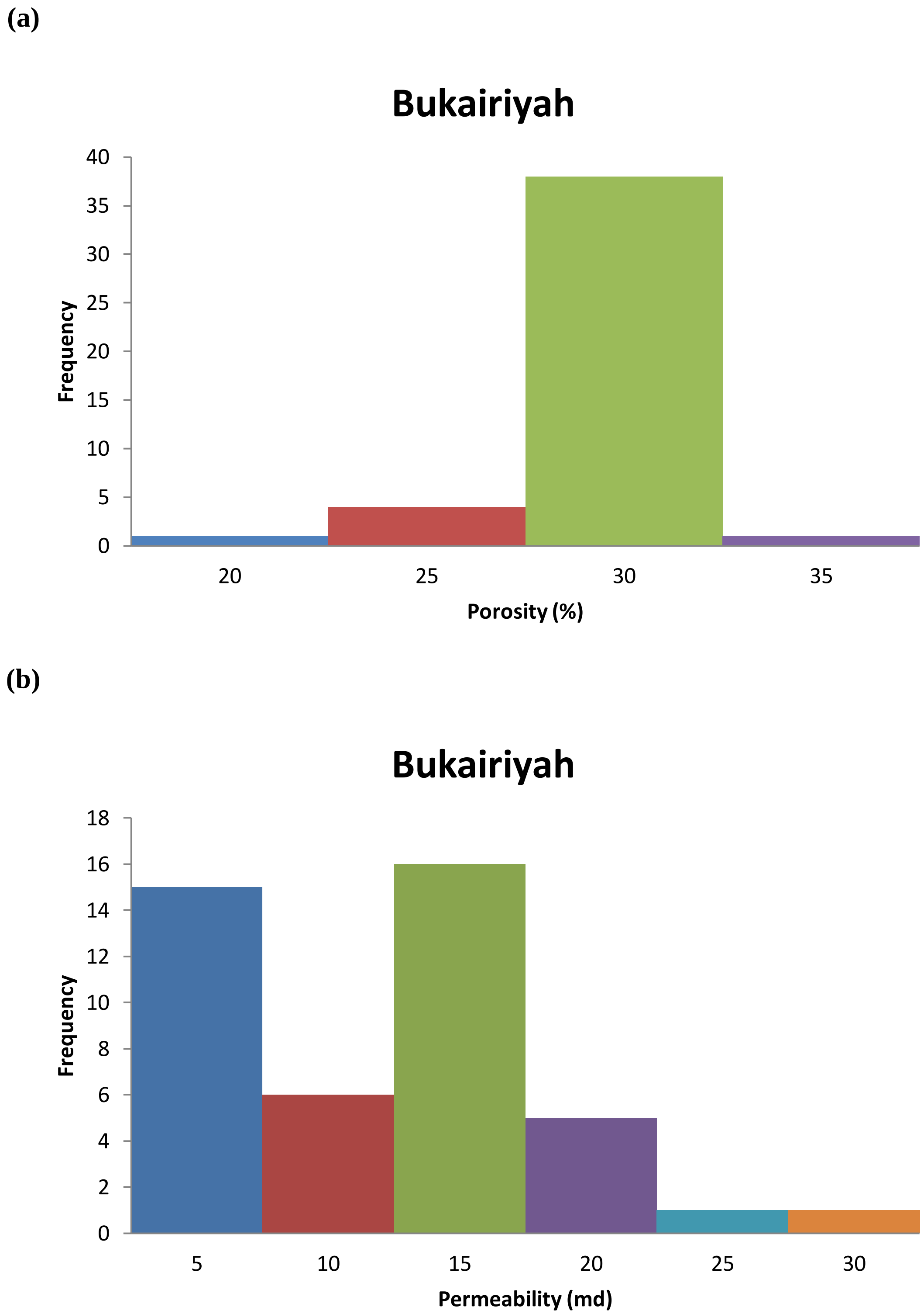

Figure 5-3: (a) Histogram of porosity values for samples of Bukairiyah paleovalley, (b) Histogram of permeability values for samples of Bukairiyah paleovalley.

(a)

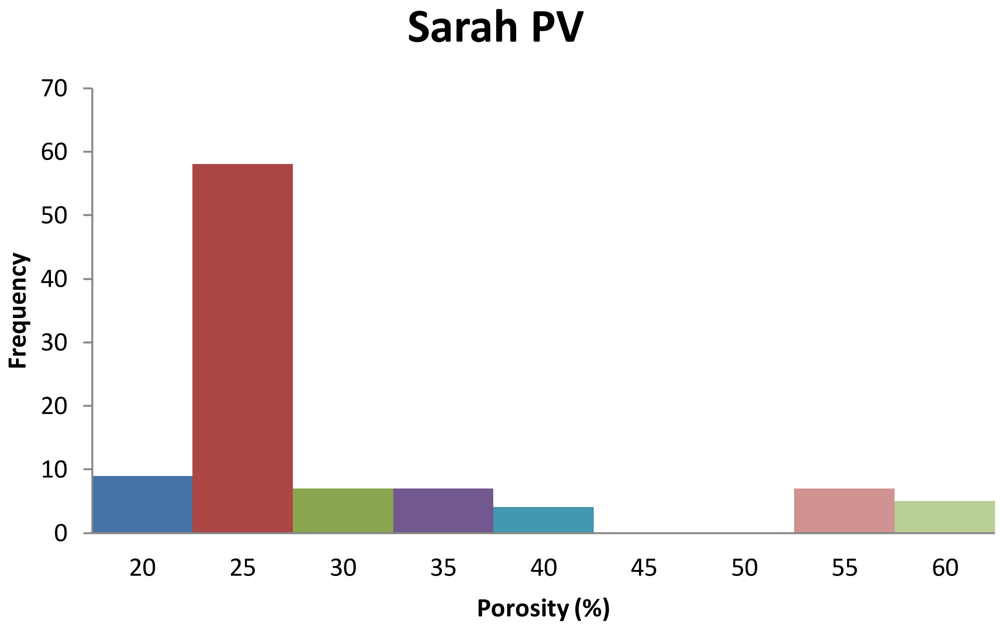

(b)

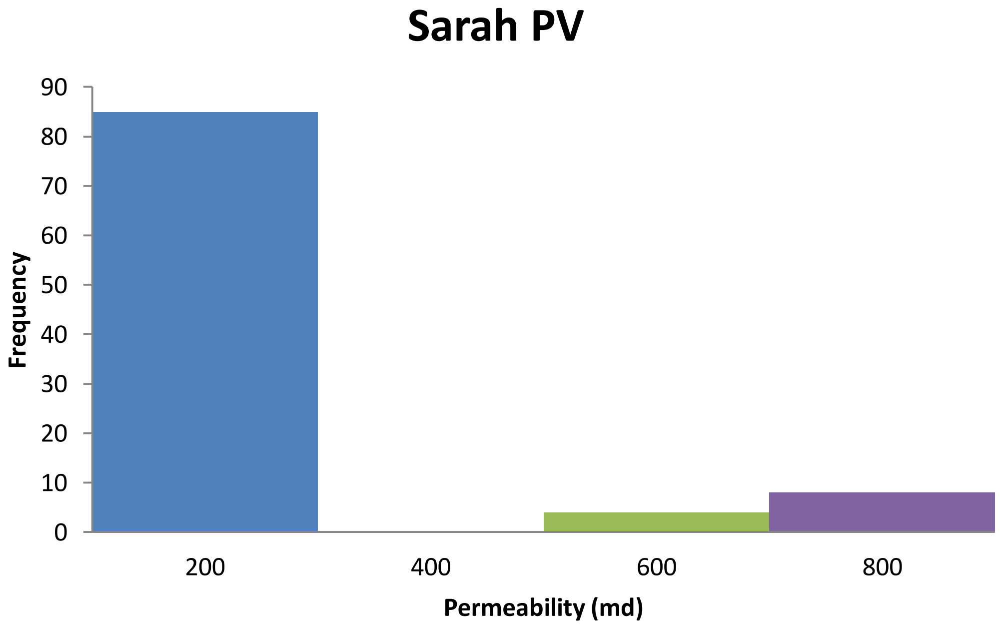

Figure 5-4: (a) Histogram of porosity values for samples of Sarah paleovalley, (b) Histogram of permeability values for samples of Sarah paleovalley.

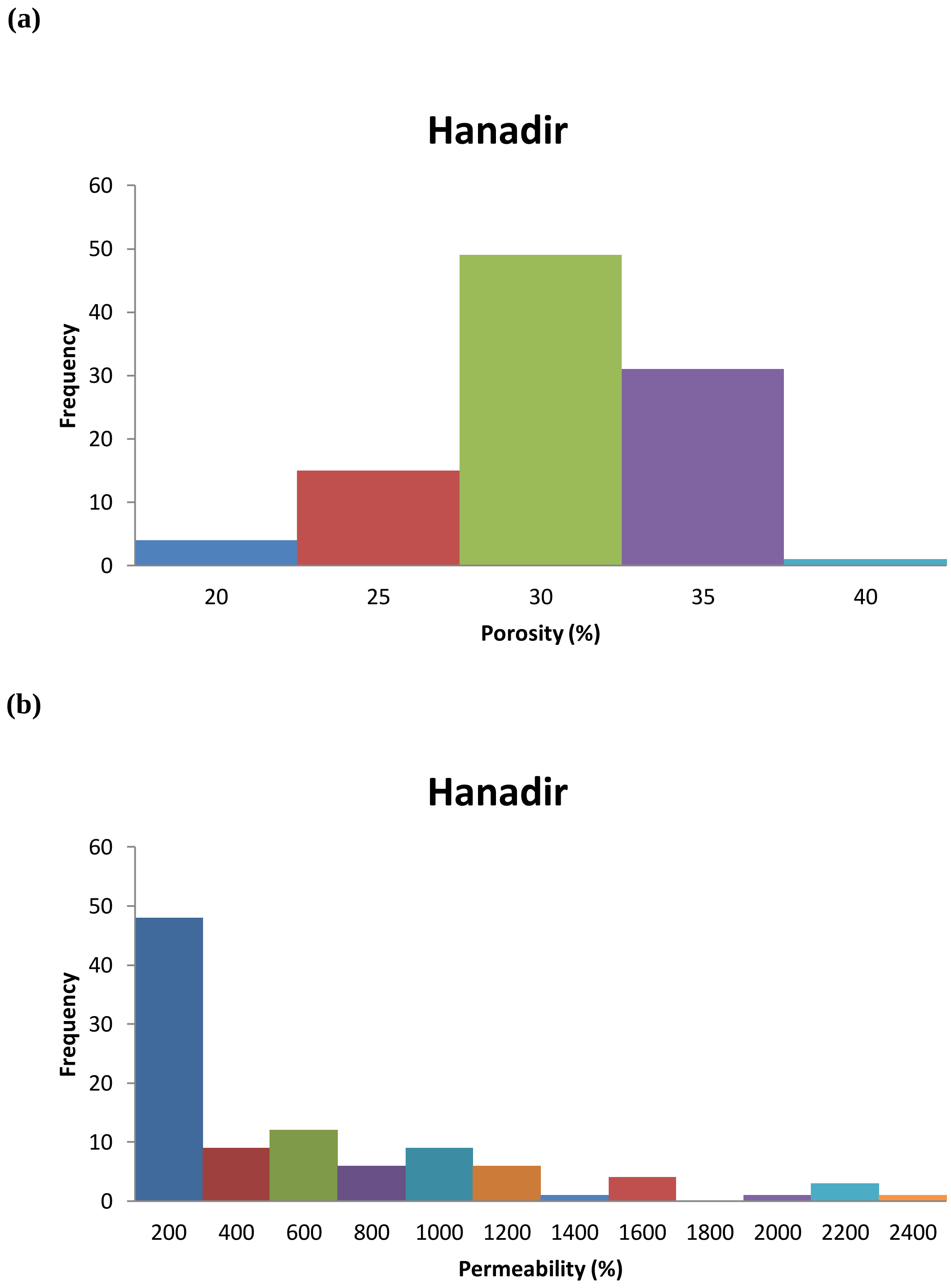

Figure 5-5: (a) Histogram of porosity values for samples of Hanadir paleovalley, (b) Histogram of permeability values for samples of Hanadir paleovalley.

(a)

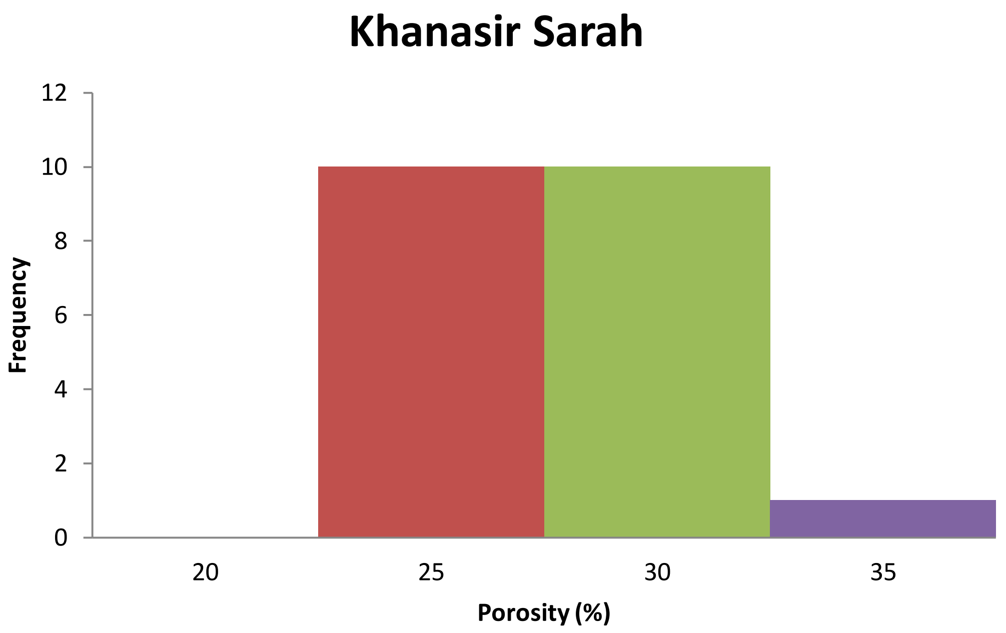

(b)

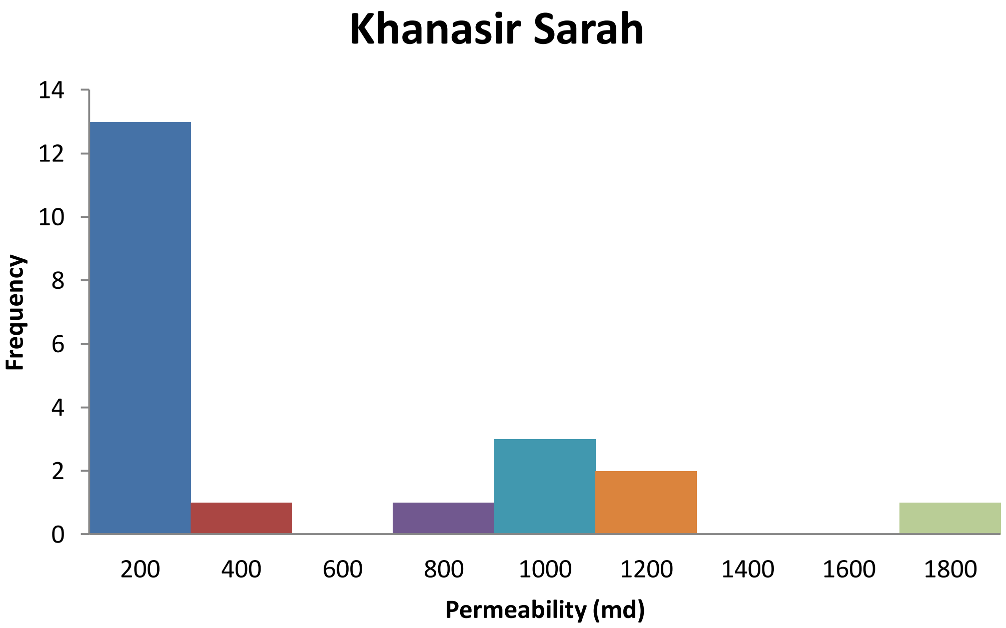

Figure 5-6: (a) Histogram of porosity values for samples of Sarah Ridge, (b) Histogram of permeability values for samples of Sarah Ridge.

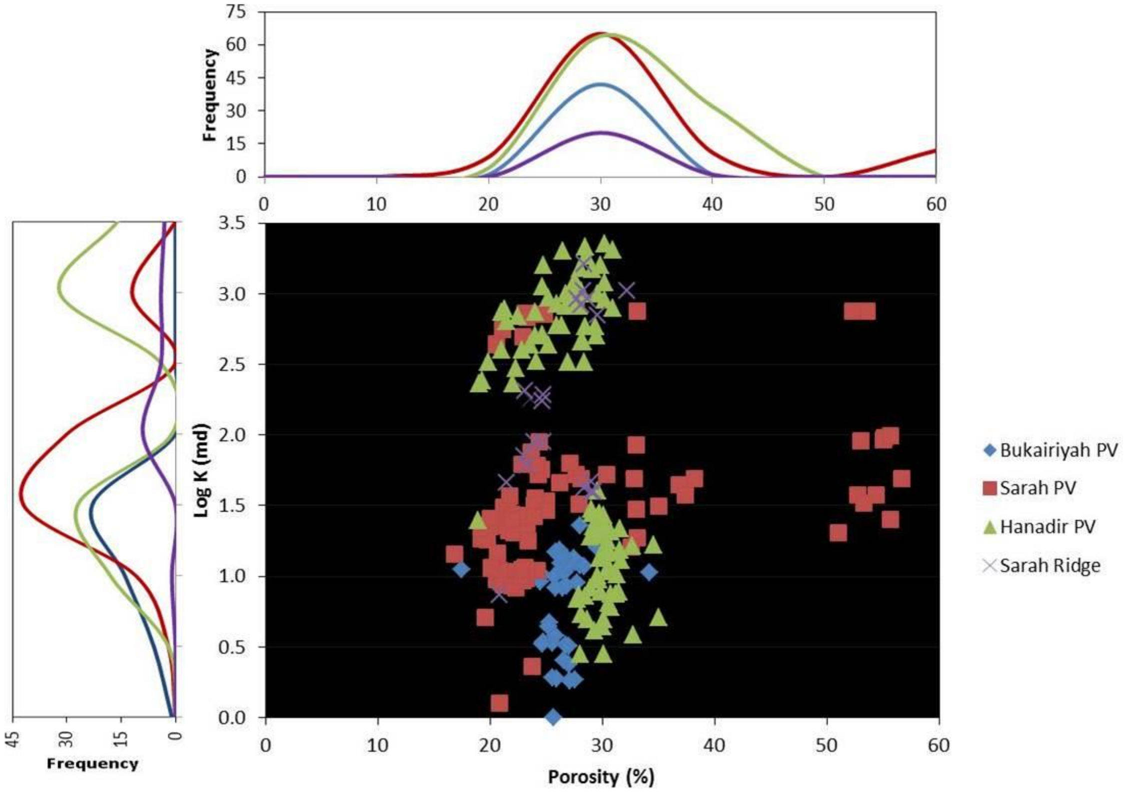

Figure 5-7: φ – log K cross-plot showing the relationship between porosity and logarithm of permeability in the studied paleovalleys of Sarah Formation. Frequency curves of φ and log K are shown in side and top panels of the cross-plot respectively.

5.5. Factors Controlling Porosity-Permeability

The analysis of 75 selective samples of Sarah Formation, representing the various paleovalleys, through thin section petrography, SEM and XRD showed that porosity and permeability values are greatly affected by both depositional and post-depositional processes. The main factors controlling porosity and permeability in Sarah Formation include: grain size variation, degree of sorting, cementation, leaching and dissolution. These factors are discussed in the following sections.

5.5.1. Texture

Studying the texture of the rock samples collected from the different paleochannels of Sarah Formation gives a good idea about the original depositional conditions of sedimentation and their impact on the petrophysical properties. Porosity and permeability values show some correlation with the texture of the studied samples. Grain size and grain sorting are the most important textural parameters that affected porosity and permeability of Sarah Formation.

- *Grain Size`*

Tiab and Donaldson (2004) pointed out that pore sizes usually retain a correlation with the grain size in sandstones. Theoretically, grain size has no effect on porosity for uniformly packed sands (Rogers and Head, 1961).

However other factors when combined with grain size like sorting and/or cementation may affect the porosity (Selley, 1998). Meanwhile, permeability is directly proportional to grain size. As grain size decreases, permeability decreases (Krumbein and Monk, 1943) .Grain size in Sarah samples varies from fine to medium and coarse.

- *Grain Sorting*

As mentioned earlier, grain size and sorting commonly show a good correlation. In a poorly sorted sandstone, the smaller grains tend to infill the pore spaces between the larger grains, and hence both porosity and permeability decrease.

However, the relationship of the size and sorting of the grains with both φ and K stays unclear in the studied samples (Figure 5-8 - Figure 5-11). This may be because the sediments have undergone high degree of diagenesis that changed the original physical properties that had been controlled by size and sorting of the detrital grains.

5.5.2. Diagenesis

As discussed earlier in Chapter Four, the studied outcrops of Sarah Formation had undergone low degree of compaction, so compaction might have a slight effect on porosity and permeability. Meanwhile, both cementation and leaching have a clear effect on porosity and permeability.

The poor correlation between φ and log K shown in Figure 5-7 is typical in samples where mechanical and chemical diagenesis have greatly affected and altered the original properties resulting in complex pore geometry (Comisky et al., 2007). Although Sarah Formation is considered as a tight gas reservoir in the subsurface (Al-Mahmoud and Al-Ghamdi, 2010), its outcrop analog shows relatively high porosity and permeability values (Figure 5-1 – Figure 5-7). This is probably due to important diagenetic factors such as burial depth, type and amount of cement, leaching by meteoric water, dissolution and mineral replacement, etc. For example in some of the studied samples, the coating of quartz grains by authigenic kaolinites (Figure 4-5 – Figure 4-7) prevented quartz overgrowth; and thus preserved the initial porosity and permeability. In addition, when dealing with outcrop samples, one should take into consideration the effects of meteoric water in leaching and dissolution of minerals. Therefore, the cement percent, when studied alone and separately, may not give either a proper interpretation or a clear relationship with φ and/or log K (Figure 5-12 – Figure 5-13). Thus, understanding the role of the diagenetic effects may help solving the difficulty of predicting reservoir quality of Sarah Formation. Al-Mahmoud and Al-Ghamdi (2010) and Briner et al. (2010) attributed this difficulty to other factors, as well, like complexity of facies, environments and paleogeography of Sarah Formation (see Chapter 3).

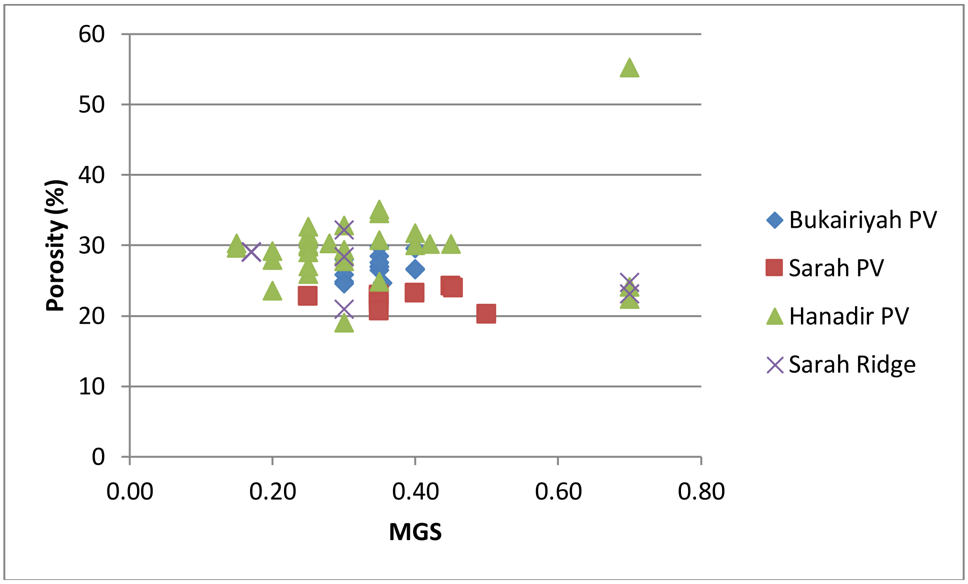

Figure 5-8: Relationship between porosity and grain size in samples of Sarah paleovalleys.

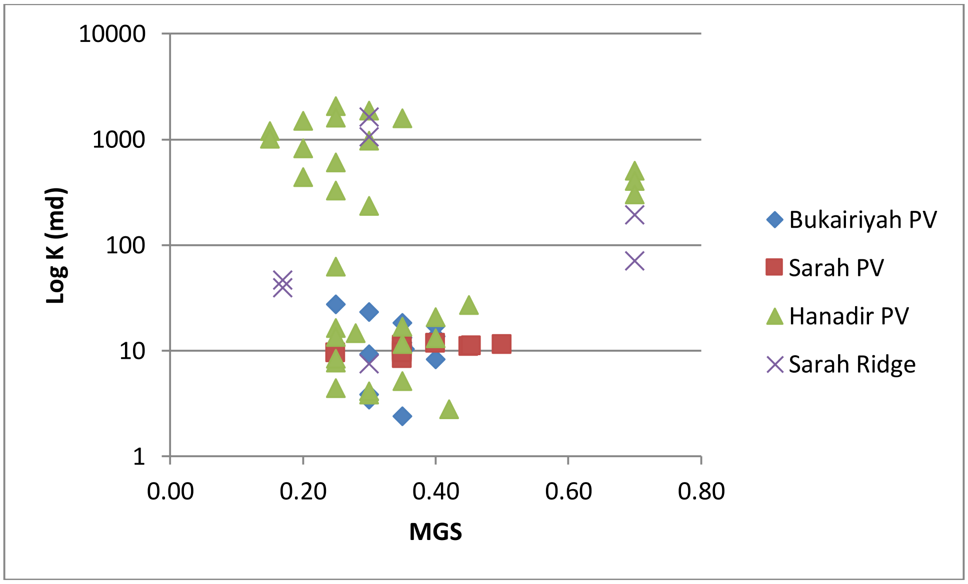

Figure 5-9: Relationship between logarithm of permeability and grain size in samples of Sarah paleovalleys.

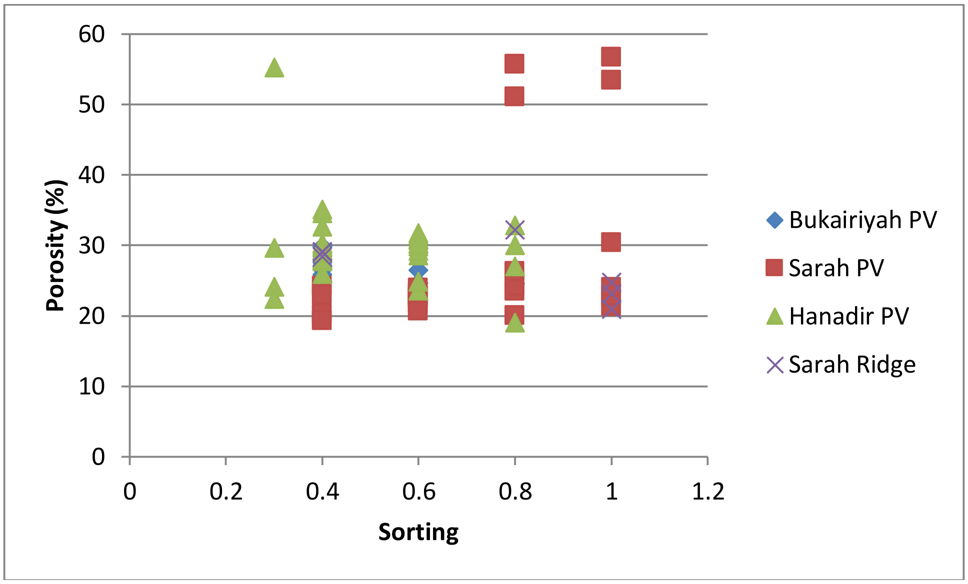

Figure 5-10: relationship between porosity and sorting in samples of Sarah paleovalleys.

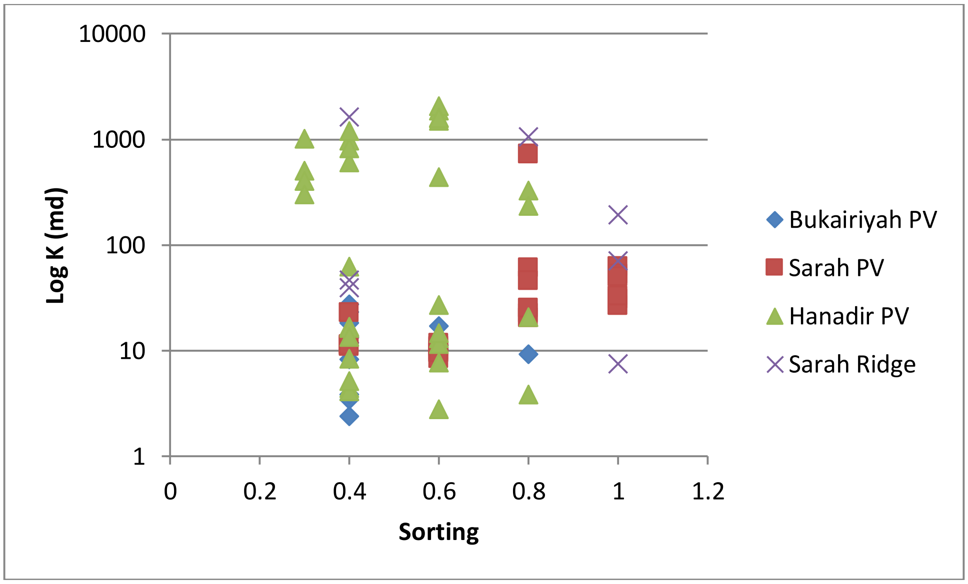

Figure 5-11: Relationship between logarithm of permeability and sorting in samples of Sarah paleovalleys.

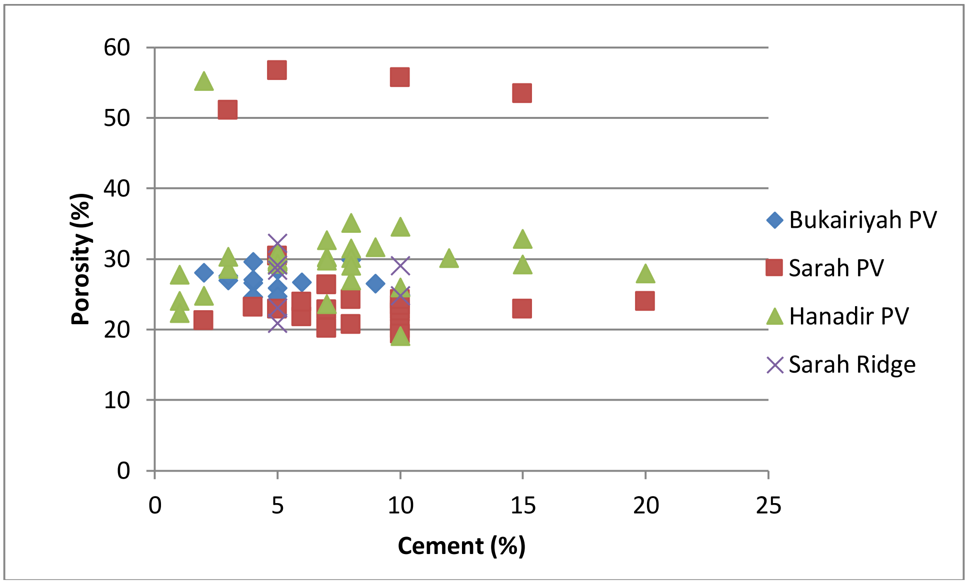

Figure 5-12: Relationship between porosity and cement in samples of Sarah paleovalleys.

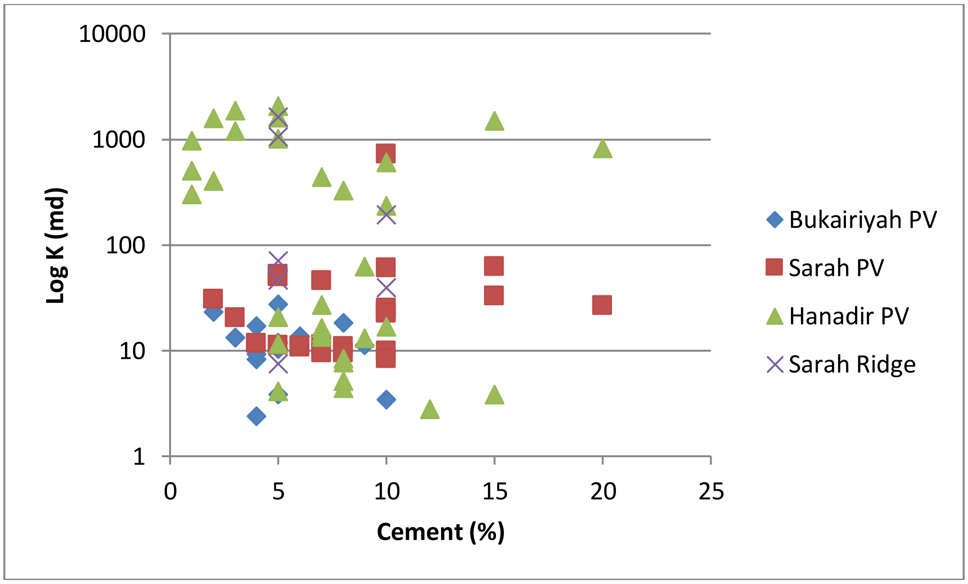

Figure 5-13: Relationship between logarithm of permeability and cement % in samples of Sarah paleovalleys.

5.6. Mercury Injection Capillary Pressure (MICP)

MICP tests were performed for 10 representative samples using a penetrometer stem volume of 1.06 to 1.7 mL. Contact angle is 140 degrees and the mercury surface tension is 480 dynes/cm. Two corrections are usually done; those are: Blank, and conformance corrections.

During MICP tests, different materials undergo varying degrees of compression recorded as small but measurable intrusion/extrusion data. In Figure 5-14, note the deviation of the uncorrected capillary pressure curve from the expected asymptotic trend. This behavior is corrected by the blank correction. We used an “operator generated” blank correction file. The correction is done by analyzing a non-porous sample with the bulk volume and composition similar to the porous sample being tested. For analyzing quartz-rich sandstone, amorphous quartz is used.

When mercury is injected into the sample, the intrusion is recorded at each pressure step. As mercury surrounds or conforms to the sample surface irregularities, this is recorded as intrusion without actual intrusion of mercury into the pores. In conformance correction, all intrusion data recorded prior to the initial entry pressure, at which mercury intrudes the actual pore system, are subtracted. This correction is necessary if MICP curves are used for further estimation of permeability. Since this is beyond the scope of our work, conformance correction was not really necessary.

So, after mercury starts to intrude into the pores, each step of intrusion is recorded with the corresponding pressure needed for intrusion. Figure 5-15 shows the incremental intrusion of mercury versus pore-throat diameter. Generally, the curves show a bimodal distribution of pore-throat sizes. In addition, a composite plot of cumulative intrusion against pressure is presented in Figure 5-16. Table 5-1 shows a summary of the results of MICP in addition to the corresponding Helium porosity and permeability measurements for each sample. It is obvious that as the permeability decreases, the pressure needed for intrusion of mercury is increased. By comparing the permeability values with MICP curves in Figure 5-16, one can justify the variance in the curves. For example, the permeability for sample # RC3-H3 equals 6.04 md, so it needs higher pressure for mercury to intrude into the pore system than in case of sample # SR9-V3 which has permeability of 111.5 md.

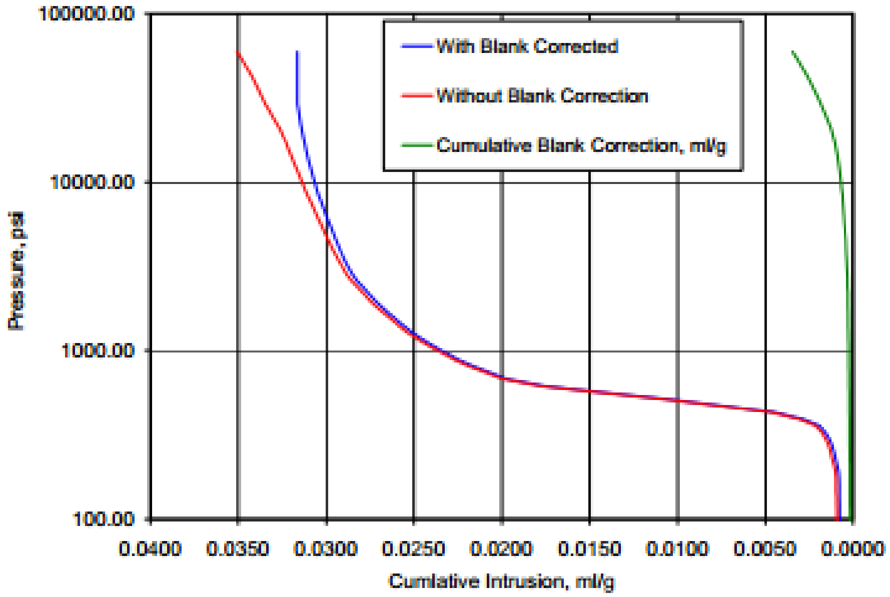

Figure 5-14: Illustration of blank correction. The blue curve is "Blank" corrected, the red one is uncorrected. The blank correction is the green curve. (Comisky et al., 2007).

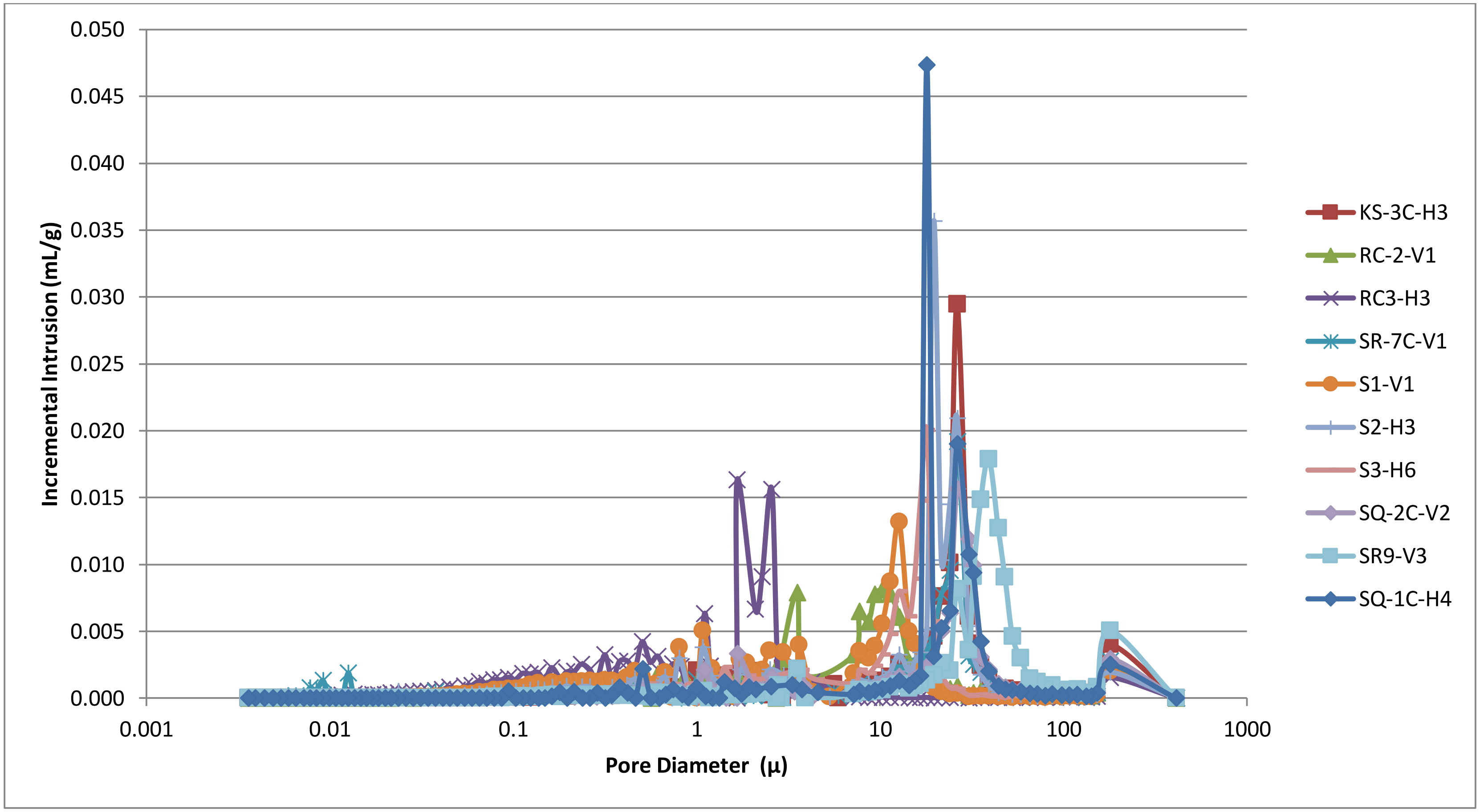

Figure 5-15: Composite plot of incremental Hg intrusion at each pore diameter for all the MICP tested samples.

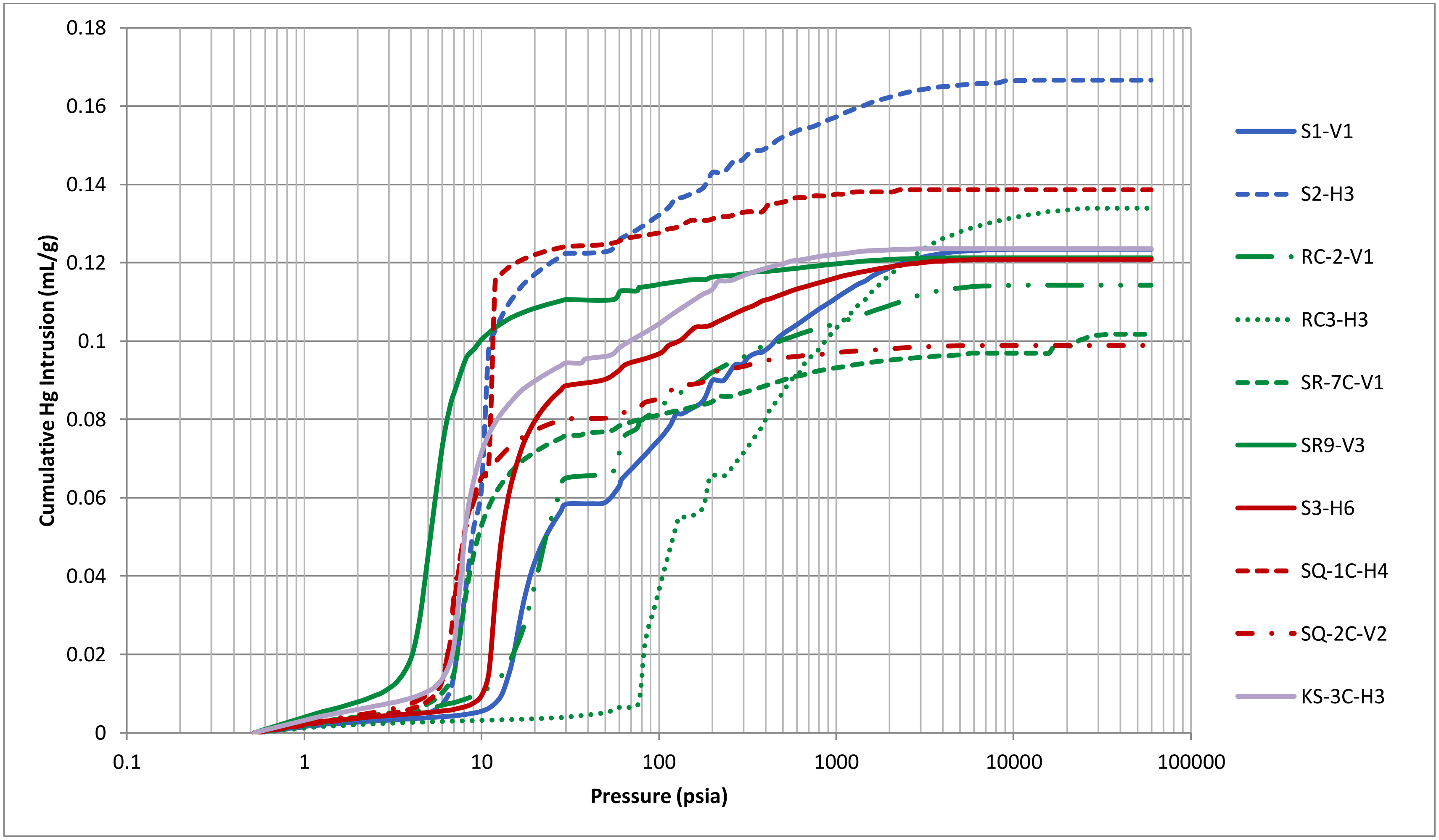

Figure 5-16: A composite plot of MICP curves versus cumulative intrusion. The curves are color coded – blue, green, red, and purple for Bukairiyah, Hanadir, Sarah, and Khanasir Sarah, respectively.

Table 5-1: Summary of MICP results compared with measured helium porosity and permeability

Sample #	**S1-V1**	**S2-H3**	**RC-2-V1**	**RC3-H3**	**SR-7C-V1**	**SR9-V3**	**S3-H6**	**SQ-1C-H4**	**SQ-2C-V2**	**KS-3C-H3**	
Total Intrusion Volume =	0.12	0.1667	0.11	0.1339	0.1018	0.1213	0.1209	0.1387	0.0989	0.12	mL/g
Total Pore Area =	0.78	0.676	0.626	2.625	2.213	0.105	0.337	0.122	0.153	0.16	m²/g
Median Pore Diameter (Volume) =	37394.00	204589	83656	8550	222352	390851	151722	194818	272427	245792.00	A
Median Pore Diameter (Area) =	1431.00	1002	999	551	104	2245	1786	4728	2253	5048.00	A
Average Pore Diameter (4V/A) =	6373.00	9864	7304	2040	1840	46171	14339	45526	25815	30499.00	A
Bulk Density at 0.52 psia =	3.59	2.8016	3.4929	3.2440	3.8347	3.1888	4.1485	2.9274	2.9271	3.19	g/mL
He Porosity =	26.56	29.73	30.78	30.81	21.53	24.76	23.21	24.26	28.17	28.37	%
He Permeability =	9.00	27.10	11.44	6.04	635.54	1111.50	11.63	60.46	49.27	1047.10	md

5.7. Reservoir Heterogeneity

Both sedimentologic and petrologic heterogeneity defines the reservoir quality. Heterogeneity in a sandstone reservoir depends on various controlling factors, e.g. sandstone geometry, reservoir structural parameters, distribution of facies, sedimentary structures, lamination and bedding, as well as the effects of diagenesis on both porosity and permeability (Ahmed Tarek, 2001; Higley et al., 1997). The diagenetic factors, e.g. compaction, cementation, leaching and dissolution, may affect the petrophysical parameters either by preservation, destruction or enhancement. Thus, heterogeneity occurs at different scales, from microscopic to gigascopic, i.e., from pore-scale to basin-scale (Adams et al., 2011; Jennings et al., 2007; Pranter et al., 2006; Tiab and Donaldson, 2004).

Heterogeneity measures are geostatistical characteristics that provide a numerical value for describing heterogeneity in a data distribution and use that value for comparing heterogeneity with other distributions or reservoirs (Jensen, 2000; Lake and Jensen, 1989). The heterogeneity of Sarah Formation as a sandstone reservoir is discussed in this section based on the three most common static measures, namely coefficient of variation, Dykstra-Parsons coefficient, and Lorenz coefficient.

5.7.1. Coefficient of Variation

The coefficient of variation (CV) equals the standard deviation divided by the mean. It is used as indication of heterogeneity. With regard to permeability, CV is less than 0.5 in a homogenous medium, between 0.5 and 1.0 in a heterogeneous one, and greater than 1.0 if the distribution is very heterogeneous (Lake and Jensen, 1989).

Permeability distributions of Bukairiyah, Sarah, Hanadir, and Khanasir Sarah paleovalleys have CV values equal to 0.62, 1.94, 1.24 and 1.17, respectively. These values indicate heterogeneous to very heterogeneous distributions for permeability in these paleovalleys.

5.7.2. Dykstra-Parsons Coefficient

The Dykstra-Parsons coefficient (Dykstra and Parsons, 1950) is also known as “coefficient of permeability variation” or “Reservoir Heterogeneity Index”. The Dykstra-Parsons coefficient is the most common heterogeneity measure. Tiab and Donaldson (2004) described it as an excellent tool for characterizing a reservoir’s heterogeneity. It is based mainly on permeability variations. This coefficient can be obtained from the equation

$$\mathbf{V_{DP} = \frac{k_{0.50} - k_{84.1}}{k_{0.50}}}$$

where $k_{0.50}$ is the median permeability, and $k_{84.1}$ is the permeability value one standard deviation above $k_{0.50}$ on a log-permeability plot. V_{DP} equals zero for an ideally homogeneous reservoir, 0-0.25 for a slightly homogeneous one, 0.25-0.5 for a heterogeneous distribution, 0.5-0.75 if it is very heterogeneous, 0.75-1 in an extremely heterogeneous reservoir, and greater than one if the reservoir is perfectly heterogeneous (Tiab and Donaldson, 2004).

The Dykstra-Parsons coefficient was calculated from a set of permeability values from Sarah paleovalleys. The permeability measurements from each outcrop were sorted in a descending order. Then, the percent of permeability values greater than each permeability value in the distribution was computed (Tables 5-2 to 5-6). What comes next is plotting the results on a log probability paper (Figure 5-17-5.17). The Dykstra-Parsons coefficient was then calculated for each paleovalley.

Dykstra-Parsons coefficient of permeability variation

For Bukairiyah paleovalley;

$k_{0.50}$ = 7.2, $k_{84.1}$= 3.2; V_{DP} = $(k_{50} - k_{84.1})/k_{50}$ = (7.2 – 3.2)/7.2 = 0.56

For Hanadir paleovalley;

$k_{0.50}$ = 95, $k_{84.1}$= 11; V_{DP} = $(k_{50} - k_{84.1})/k_{50}$ = (95 – 11)/95 = 0.88

For Sarah paleovalley;

$k_{0.50}$ = 34.05, $k_{84.1}$= 9.56; V_{DP} = $(k_{50} - k_{84.1})/k_{50}$ = (34.05 – 9.56)/7.2 =0.72

For Sarah Ridge;

$k_{0.50}$ = 147.47, $k_{84.1}$= 31.72; $V_{DP} = (k_{50} - k_{84.1})/k_{50}$ = (147.47 – 31.72)/7.2 = 0.78

Hence, the Dykstra-Parsons coefficients indicate that the Sarah Reservoir is very to extremely heterogeneous. The Bukairiyah and Sarah paleovalleys represent very heterogeneous reservoirs, whereas the Hanadir paleovalley and Sarah Ridge extremely heterogeneous reservoir.

Table 5-2: Frequency distribution for the permeability measurements in Bukairiyah paleovalley

Sample No.	probability	K (md)	Sample No.	probability	K (md)
S2H3	0.00	27.10	S2H8	0.50	10.29
S2H1	0.02	23.02	S1H1	0.52	9.98
S2H7	0.05	18.26	S2V4	0.55	9.19
S2V3	0.07	17.46	S1H6	0.57	9.03
S2V2	0.09	16.88	S1H4	0.59	8.56
S2V6 (c)	0.11	15.75	S1V2	0.61	8.28
S2H5	0.14	15.21	S1H2	0.64	8.21
S2H4	0.16	14.93	S1V12	0.66	4.68
S2H11	0.18	13.88	S1V13	0.68	4.37
S2H10	0.20	13.53	S1H13	0.70	3.82
S2V10	0.23	13.31	S1H8	0.73	3.44
S1V5	0.25	13.27	S1V11	0.75	3.38
S1V4	0.27	12.65	S1H9	0.77	3.33
S2H9	0.30	12.41	S1H7	0.80	3.27
S2V11	0.32	11.97	S1H12	0.82	3.22
S2V9	0.34	11.93	S1H11	0.84	2.52
S1V6	0.36	11.84	S1V9	0.86	2.38
S2V6 (a)	0.39	11.82	S1V7	0.89	1.91
S1H3	0.41	11.12	S1H10	0.91	1.89
S2V6 (b)	0.43	11.10	S1V8	0.93	1.87
S2V5	0.45	10.65	S1V10	0.95	1.81
S1H5	0.48	10.54	S1V3	0.98	1.00

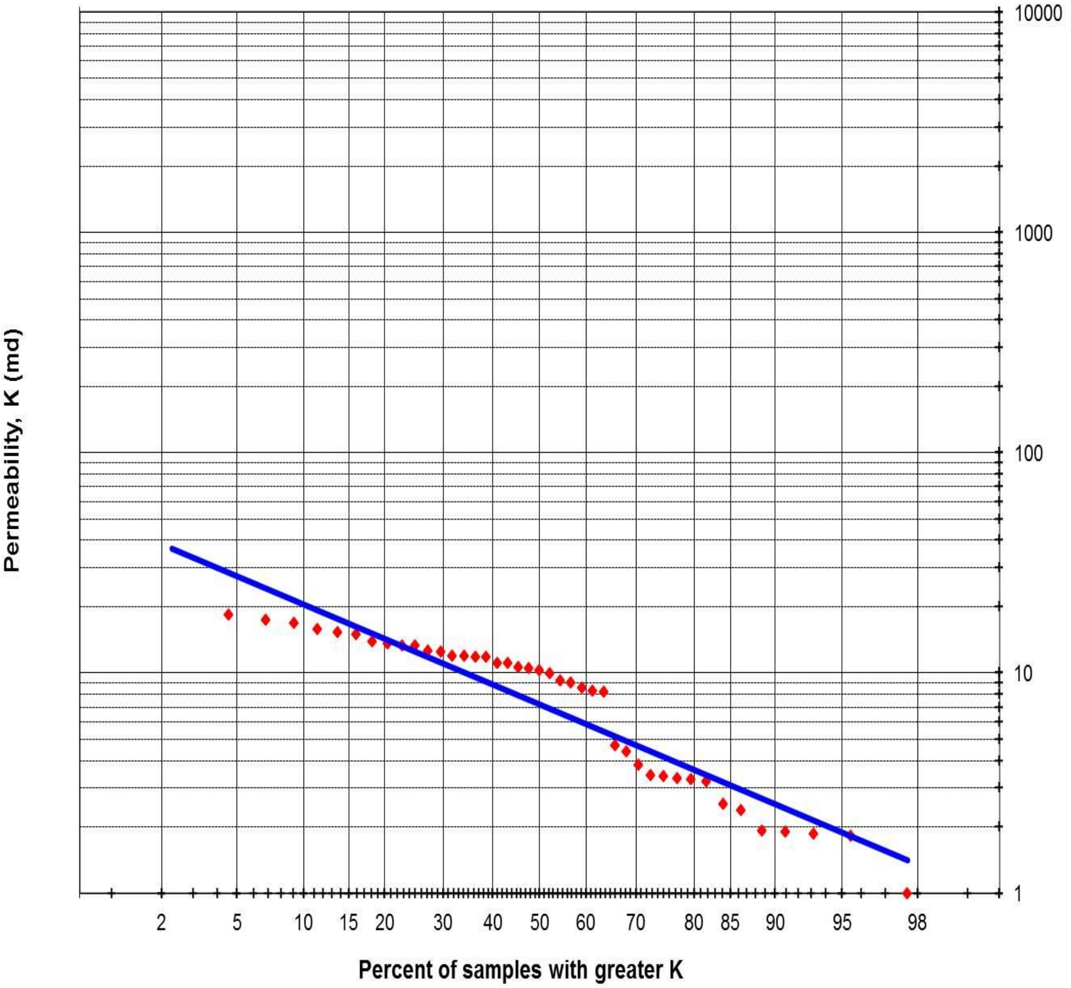

Figure 5-17: Dykstra-Parsons plot for permeability measurements from Bukairiyah paleovalley. $\mathbf{k}_{0.50}$ = 7.2, and $\mathbf{k}_{84.1}$= 3.2.

Table 5-3: Frequency distribution for the permeability measurements in Hanadir paleovalley

Layer No.	probability	K (md)	Layer No.	probability	K (md)
SR-2-V3	0	2252	SR-5-H4	0.25	787.22
SR-2-H4	0.01	2160.1	SR-7C-H2	0.26	780.64
SR-2-H5	0.02	2040.8	SR-9-V2	0.27	736.7
SR-2-H1	0.03	2004.2	SR-7C-V3	0.28	736.01
SR-2-H2	0.04	1857.6	SR-7C-V2	0.29	689.37
SR-3-V2-C	0.05	1585.1	SR-7C-V1	0.3	635.54
SR-7C-H3	0.06	1576.6	SR-1-V1	0.31	597.56
SR-4-V2	0.07	1503.7	SR-1-V2	0.32	592.18
SR-4-V1	0.08	1485.3	SR-5-V4	0.33	584.46
SR-4-V3	0.09	1240.2	SR-5-H3	0.34	584.15
SR-7B-H2	0.1	1193.2	SR-1-H1	0.35	515.57
SR-2-H3	0.11	1147.2	SR-6-V1	0.36	504.9
SR-9-V3	0.12	1111.5	SR-5-H1	0.37	501.24
SR-4-H1	0.13	1055.1	SR-5-H2	0.38	458.22
SR-3-V4	0.14	1003	SR-5-V3	0.39	455.56
SR-9-V1	0.15	1000.5	SR-1-H2	0.4	437.2
SR-2-V2	0.16	996.48	SR-6-H1	0.41	436.4
SR-4-H2	0.17	963.76	SR-6-V2	0.42	401.25
SR-3-V2-A	0.18	939.52	SR-7A-H2	0.43	399.23
SR-3-V2-B	0.19	897.46	SR-6-H3	0.44	332.12
SR-3-H3	0.2	870.87	SR-5-V1	0.45	328.71
SR-3-H1	0.21	839.26	SR-5-V2	0.46	327.51
SR-3-V1	0.22	832.58	SR-7A-H3	0.47	326.83
SR-3-H2	0.23	814.86	SR-6-H2	0.48	297.63
SR-4-H3	0.24	810.52	SR-7A-H1	0.49	243.33

Table 5-4: Frequency distribution for the permeability measurements in Hanadir paleovalley (Contd.)

Layer No.	probability	K (md)	Layer No.	probability	K (md)
SR-7A-H4	0.5	232.07	RC-2-H2	0.75	11.719
SR-7A-V3	0.51	229.69	RC-2-V1	0.76	11.442
SR-3-V5	0.52	40.178	RC-2-H4	0.77	10.821
RC-1-H3	0.53	29.905	RC-4-V1	0.78	10.354
RC-1-H1	0.54	28.018	RC-5-H2	0.79	10.099
RC-1-H2	0.55	27.677	RC-3-H1	0.8	9.4909
RC-1-H6	0.56	26.805	RC-5-H6	0.81	8.3195
SR-7B-H1	0.57	24.733	RC-3-H2	0.82	7.7348
RC-4-H4	0.58	23.498	RC-3-V1	0.83	7.6898
RC-1-H8	0.59	22.28	RC-4-V3	0.84	7.5434
RC-1-V4	0.6	21.719	RC-4-V2	0.85	7.4648
RC-1-V3	0.61	20.763	RC-5-H1	0.86	7.3419
RC-1-V5	0.62	20.622	RC-5-H3	0.87	7.3026
RC-1-V6	0.63	20.521	RC-5-H5	0.88	6.9235
RC-1-V8	0.64	19.562	RC-4-V5	0.89	6.4892
RC-1-V7	0.65	18.867	RC-3-H3	0.9	6.0436
RC-1-V2	0.66	17.761	RC-5-V5	0.91	5.3379
RC-4-H1	0.67	16.755	RC-5-V2	0.92	5.1234
RC-4-H2	0.68	16.249	RC-5-V1	0.93	4.9794
RC-4-H3	0.69	15.399	RC-5-V4	0.94	4.9101
RC-1-V1	0.7	14.893	RC-3-V2	0.95	4.3656
RC-2-H3	0.71	14.6	RC-3-V3	0.96	4.1178
RC-2-V2	0.72	14.489	RC-3-H4	0.97	3.8329
RC-4-V4	0.73	13.385	RC-5-V3	0.98	2.8056
RC-2-H1	0.74	13.044	RC-3-V4	0.99	2.7902

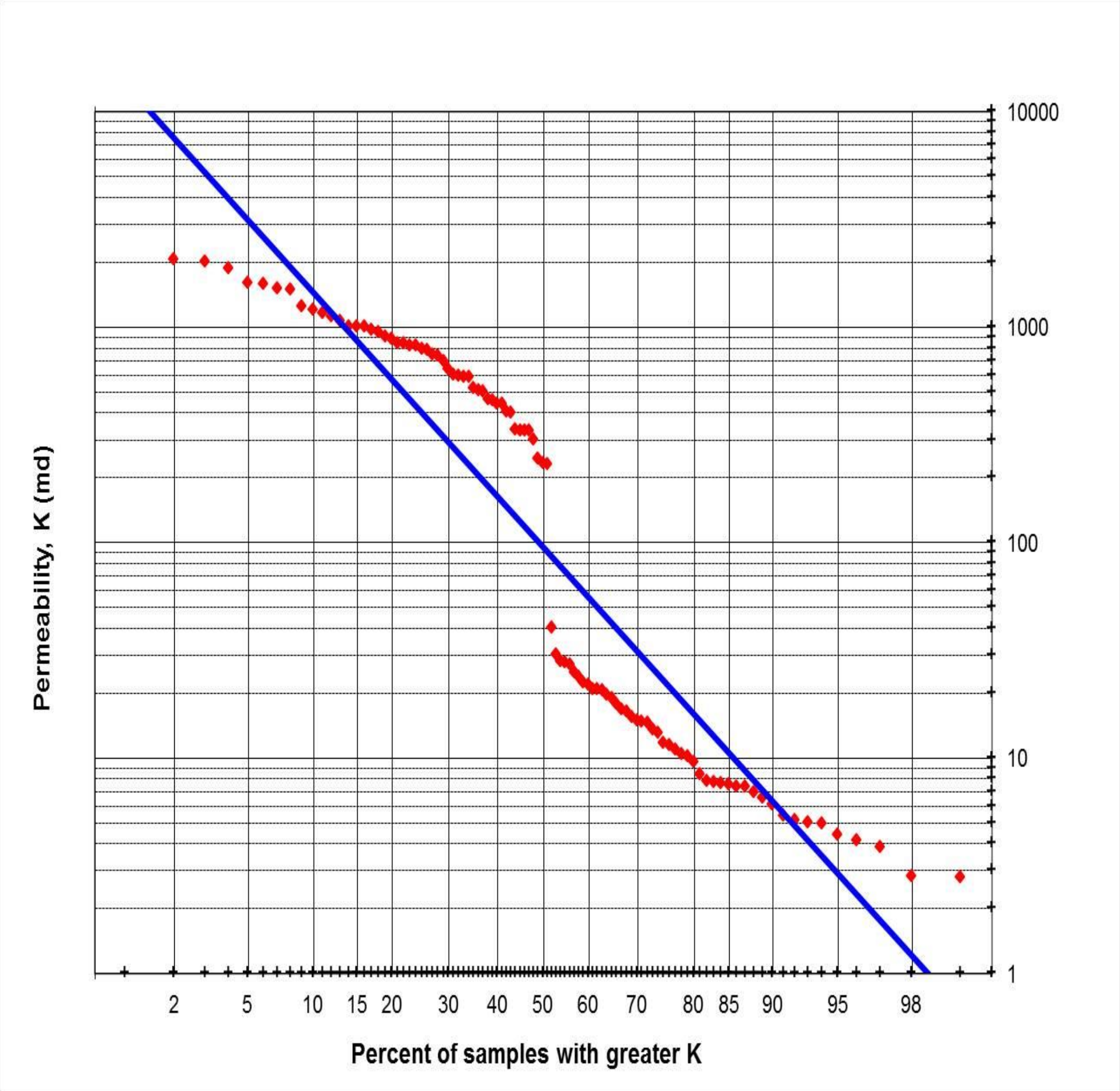

Figure 5-18: Dykstra-Parsons plot for permeability measurements from Hanadir paleovalley. $\mathbf{k_{0.50}}$ = 95, and $\mathbf{k_{84.1}}$= 11.

Table 5-5: Frequency distribution for the permeability measurements in Sarah paleovalley

Layer No.	probability	K (md)	Layer No.	probability	K (md)
SQ-1B-V1	0.00	757.48	SQ-1C-H2	0.25	52.58
SQ-1B-V5	0.01	755.60	SQ-2C-V1	0.26	52.33
SQ-1B-V6	0.02	750.41	SQ-2A-V4	0.27	49.33
SQ-1B-V2	0.03	723.88	SQ-2C-V2	0.28	49.27
SQ-1B-H1	0.04	721.37	SQ-2C-V3	0.29	49.20
SQ-1B-V4	0.05	717.09	SQ-2A-V2	0.30	48.84
SQ-1B-V3	0.06	713.88	SQ-2A-V1	0.31	45.60
SQ-1B-H2	0.07	675.06	SQ-2B-H2	0.32	44.31
SQ-1A-H1	0.08	559.27	SQ-3-V3	0.33	37.84
SQ-1A-V6	0.09	493.63	SQ-5B-H4	0.34	37.50
SQ-1A-H2	0.10	443.12	SQ-3-V4	0.35	37.36
SQ-1A-H3	0.11	432.28	SQ-3-H4	0.36	36.77
SQ-1C-V4	0.12	99.22	SQ-3-H1	0.37	35.98
SQ-1C-V2	0.13	94.81	SQ-3-V2	0.38	33.93
SQ-1C-V3	0.14	91.93	SQ-5B-V1	0.39	32.75
SQ-1C-V1	0.15	90.11	SQ-7-V2	0.40	32.42
SQ-1C-V7	0.16	90.01	SQ-5B-H3	0.41	32.04
SQ-1C-V5	0.18	84.60	SQ-5B-H1	0.42	31.88
SQ-1C-V6	0.19	75.92	SQ-7-V1	0.43	31.45
SQ-2A-H2	0.20	62.79	SQ-1A-V1	0.44	30.68
SQ-1C-H1	0.21	62.22	SQ-5B-V4	0.45	29.79
SQ-1C-H4	0.22	60.46	SQ-6-H6	0.46	29.21
SQ-1C-H3	0.23	56.64	SQ-1A-V2	0.47	28.91
SQ-2A-V3	0.24	52.61	SQ-4-H3	0.48	27.61

Table 5-6: Frequency distribution for the permeability measurements in Sarah paleovalley (Contd.)

Layer No.	probability	K (md)	Layer No.	probability	K (md)
SQ-4-H1	0.49	26.99	SQ-5B-H5	0.75	14.48
SQ-7-V3	0.51	26.57	SQ-6-H1	0.76	14.40
SQ-6-H4	0.52	26.15	S3H6	0.77	11.63
SQ-4-H2	0.53	26.04	SQ-5B-H6	0.78	11.53
SQ-7-H4	0.54	25.82	S3H4	0.79	11.41
SQ-7-V4	0.55	25.37	S3H8	0.80	11.17
SQ-5B-V3	0.56	25.28	S3H7	0.81	11.05
SQ-6-H5	0.57	25.19	S3V8	0.82	11.03
SQ-5A-H2	0.58	24.56	S3H5	0.84	11.01
SQ-1A-V3	0.59	22.94	S3H2	0.85	10.89
SQ-7-H2	0.60	22.78	S3V5	0.86	10.74
SQ-7-H1	0.61	22.68	S3V6	0.87	9.98
SQ-6-H2	0.62	22.67	S3H1	0.88	9.89
SQ-4-V3	0.63	22.46	S3V4	0.89	9.62
SQ-7-H3	0.64	21.59	S3V10	0.90	9.52
SQ-5B-H7	0.65	20.92	S3V1	0.91	9.45
SQ-5A-H4	0.66	20.32	S3V7	0.92	9.24
SQ-5B-H8	0.67	20.27	S3V11	0.93	9.08
SQ-4-V2	0.68	18.86	S3V9	0.94	8.63
SQ-5B-H2	0.69	18.59	S3V13	0.95	8.60
SQ-5A-H3	0.70	18.47	S3V3	0.96	8.33
SQ-4-V1	0.71	18.35	SQ-1A-V4	0.97	5.07
SQ-5A-H1	0.72	18.09	SQ-3-V1	0.98	2.30
SQ-5B-V5	0.73	17.87	SQ-1A-V5	0.99	1.26
SQ-5B-V2	0.74	16.10			

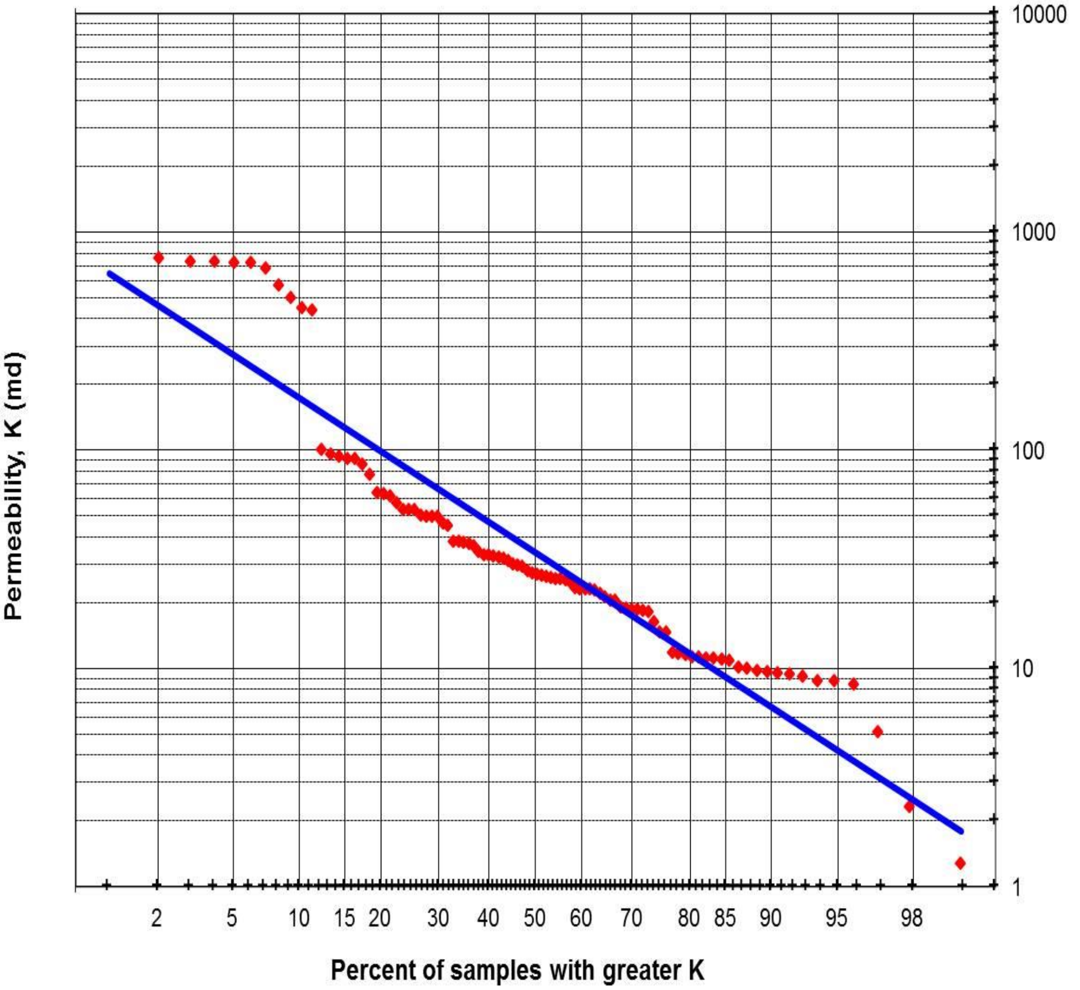

Figure 5-19: Dykstra-Parsons plot for permeability measurements from Hanadir paleovalley. $\mathbf{k_{0.50}}$ = 34.05, and $\mathbf{k_{84.1}}$= 9.56.

Table 5-7: Frequency distribution for the permeability measurements in Khanasir Sarah paleovalley

Layer No.	probability	K (md)
KS-3C-H4	0.00	1628.70
KS-3C-V3	0.05	1056.50
KS-3C-H3	0.10	1047.10
KS-3C-H1	0.14	910.64
KS-3C-H2	0.19	910.42
KS-3C-V2	0.24	825.51
KS-3C-V1	0.29	706.26
KS-9-H3	0.33	206.60
KS-9-H6	0.38	191.46
KS-9-H4	0.43	180.36
KS-9-H5	0.48	172.76
KS-9-V3	0.52	89.73
KS-9-V4	0.57	88.68
KS-9-H2	0.62	70.50
KS-9-H1	0.67	60.61
KS-1-V1	0.71	46.62
KS-9-V1	0.76	46.29
KS-1-V4	0.81	42.39
KS-2-V2	0.86	39.53
KS-1-V3	0.90	39.42
KS-9-V2	0.95	7.41

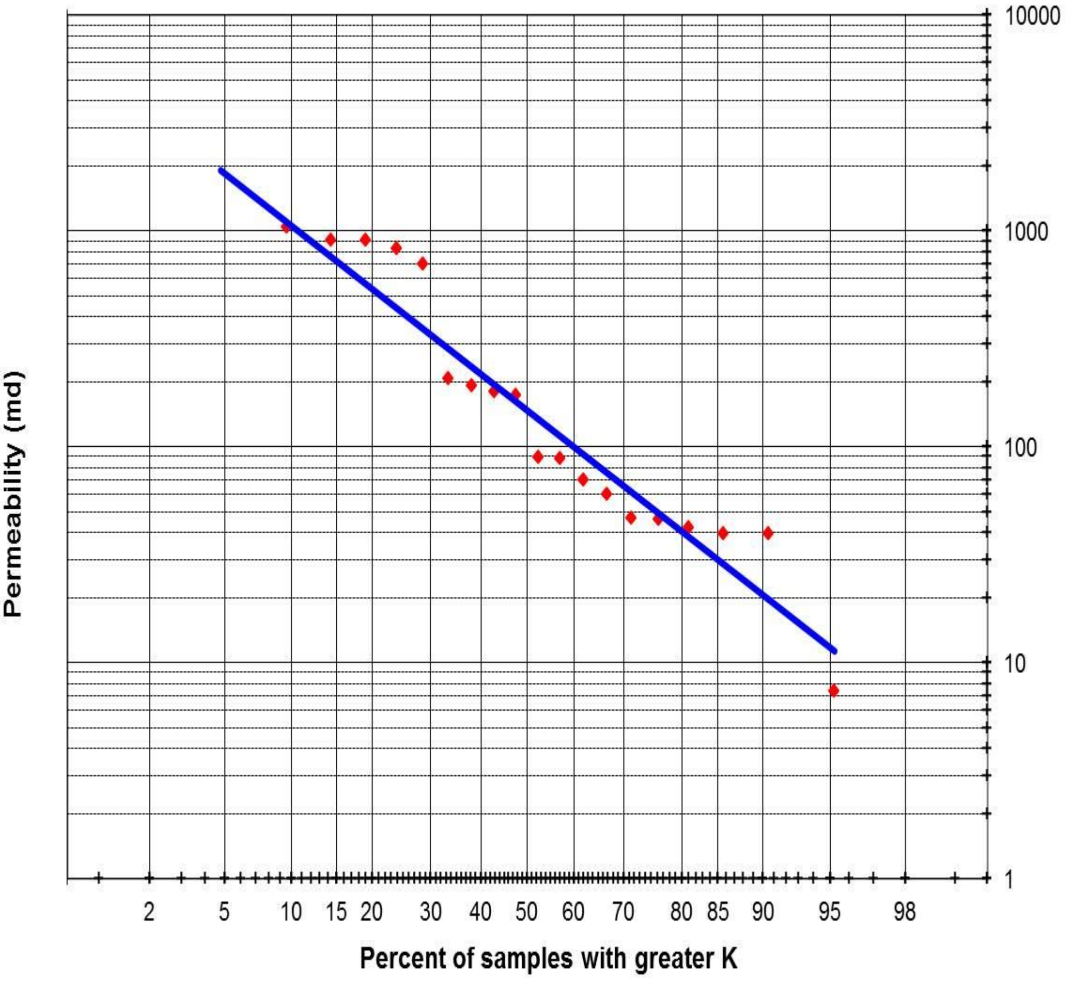

Figure 5-20: Dykstra-Parsons plot for permeability measurements from Hanadir paleovalley. $\mathbf{k_{0.50}}$ = 147.47, and $\mathbf{k_{84.1}}$= 31.72.

5.7.3. Lorenz Coefficient

Lorenz (1905) developed the Lorenz coefficient as a measure of the concentration of wealth. It was then introduced, as an important parameter for characterizing porosity and permeability heterogeneity within a reservoir (Schmalz and Rahme, 1950).

Generally, Lorenz coefficient is obtained by plotting cumulative flow capacity (F_m) against cumulative thickness (H_m). F_m and H_m are calculated from the following equations (Ahmed Tarek, 2001; Lake and Jensen, 1989; Peters, 2012; Schmalz and Rahme, 1950; Tiab and Donaldson, 2004)

$$F_m = \frac{\sum_{i=1}^{i=m} k_i h_i}{\sum_{i=1}^{i=n} k_i h_i}$$

$$H_m = \frac{\sum_{i=1}^{i=m} h_i}{\sum_{i=1}^{i=n} h_i}$$

However, suppose there are pairs of variables, all positive, every pair measured at same location, but the thickness (h) is not known, Fitch et al. (2013) developed an alternate version of Lorenz coefficient where the cumulative of the first variable, sorted in a descending order, is plotted against that of the other variable. So, Lorenz coefficient can be calculated using porosity and permeability directly.

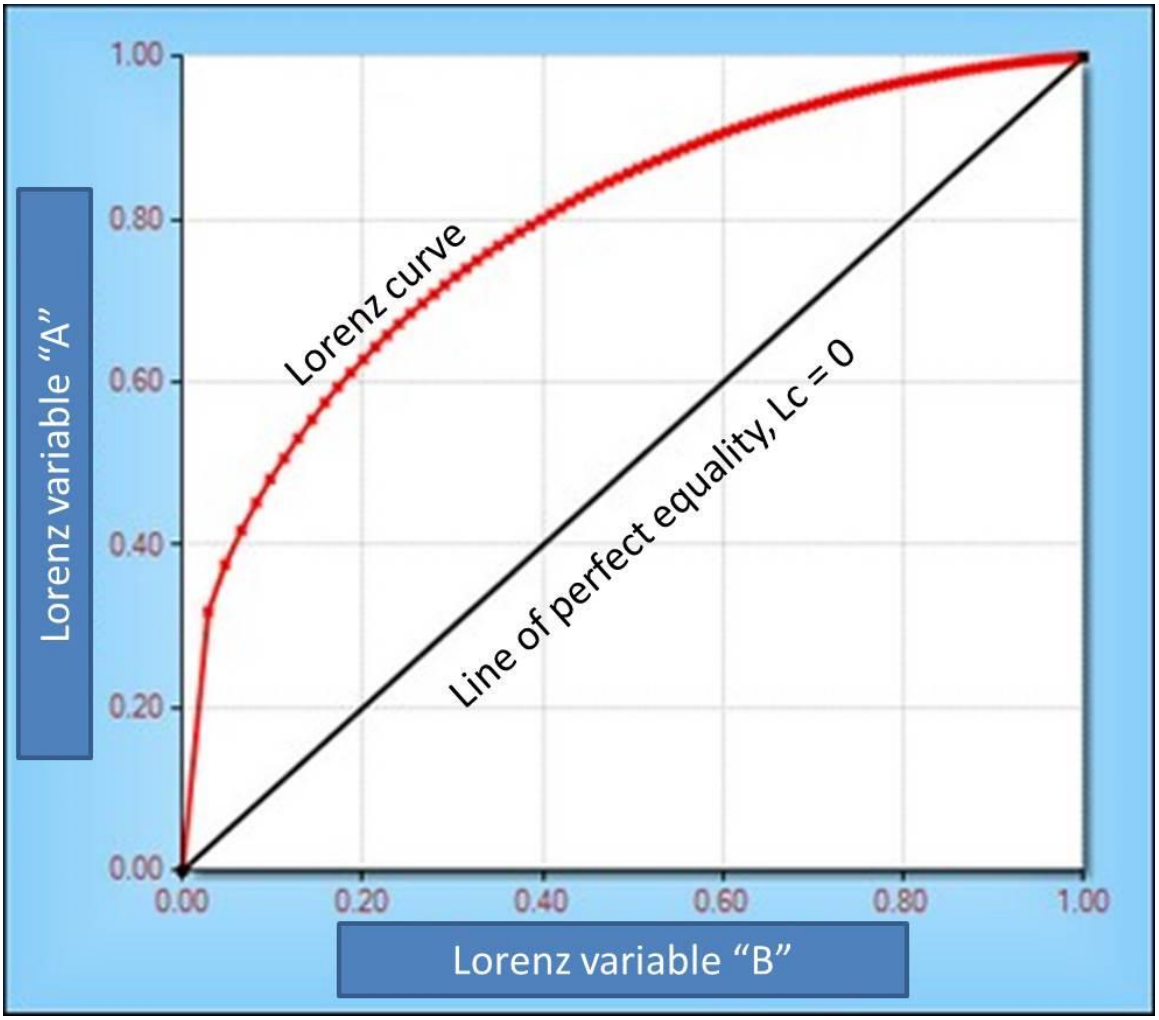

Figure 5-21: Schematic illustration of Lorenz plot, after (Fitch et al., 2013).

The Lorenz coefficient (Lc) ranges from zero, in a homogeneous reservoir, to one, in a heterogeneous reservoir. Lc equals twice the area between the Lorenz curve and the line of perfect equality (Figure 5-21). To compute this area, we do the following:

1. Calculate the total area below the Lorenz curve. This area equals
$$\sum_{i=1}^{i=n}\left(\emptyset_{cum,\ i+1}-\emptyset_{cum,\ i}\right) * \frac{K_{cum,\ i}+K_{cum,\ i+1}}{2}$$
2. The area of the triangle below the line of perfect equality equals half the total area of the square.
3. So, the area between the Lorenz curve and the line of perfect equality equals the total area below the Lorenz curve minus the area of the triangle below the line of perfect equality.

Lc was calculated for the Sarah paleovalleys. To compute Lc, the φ and k values for each paleovalley were arranged in a descending order. Then the cumulative sums were calculated and normalized to 1. Then, normalized ∑φ was plotted versus normalized ∑K on a Cartesian scale (Figure 5-22-Figure 5-25). As an example, Table 5-8 shows the calculations of Lc for the measurements of samples from Khanasir Sarah paleovalley. Complete calculations of Lc for the other paleovalleys are shown in APPENDIX B.

Table 5-8: Calculation of Lorenz coefficient for porosity and permeability measurements from Khanasir Sarah paleovalley

φ	Cumulative	% cumulative	K	Cumulative	% cumulative
32.24	0.00	0.00	1628.70	0.00	0.00
29.60	32.24	0.06	1056.50	1628.70	0.19
29.30	61.84	0.11	1047.10	2685.20	0.32
29.13	91.14	0.16	910.64	3732.30	0.45
29.06	120.27	0.22	910.42	4642.94	0.55
28.73	149.33	0.27	825.51	5553.36	0.66
28.45	178.06	0.32	706.26	6378.87	0.76
28.42	206.51	0.37	206.60	7085.13	0.85
28.37	234.93	0.42	191.46	7291.73	0.87
28.17	263.30	0.48	180.36	7483.19	0.89
27.87	291.47	0.53	172.76	7663.55	0.92
24.82	319.34	0.58	89.73	7836.31	0.94
24.79	344.16	0.62	88.68	7926.04	0.95
24.76	368.96	0.67	70.50	8014.72	0.96
24.04	393.71	0.71	60.61	8085.22	0.97
23.54	417.75	0.75	46.62	8145.83	0.97
23.36	441.29	0.80	46.29	8192.45	0.98
23.17	464.65	0.84	42.39	8238.73	0.98
23.12	487.82	0.88	39.53	8281.12	0.99
21.60	510.94	0.92	39.42	8320.65	0.99
20.95	532.54	0.96	7.41	8360.07	1.00
	553.49	1.00		8367.48	1.00

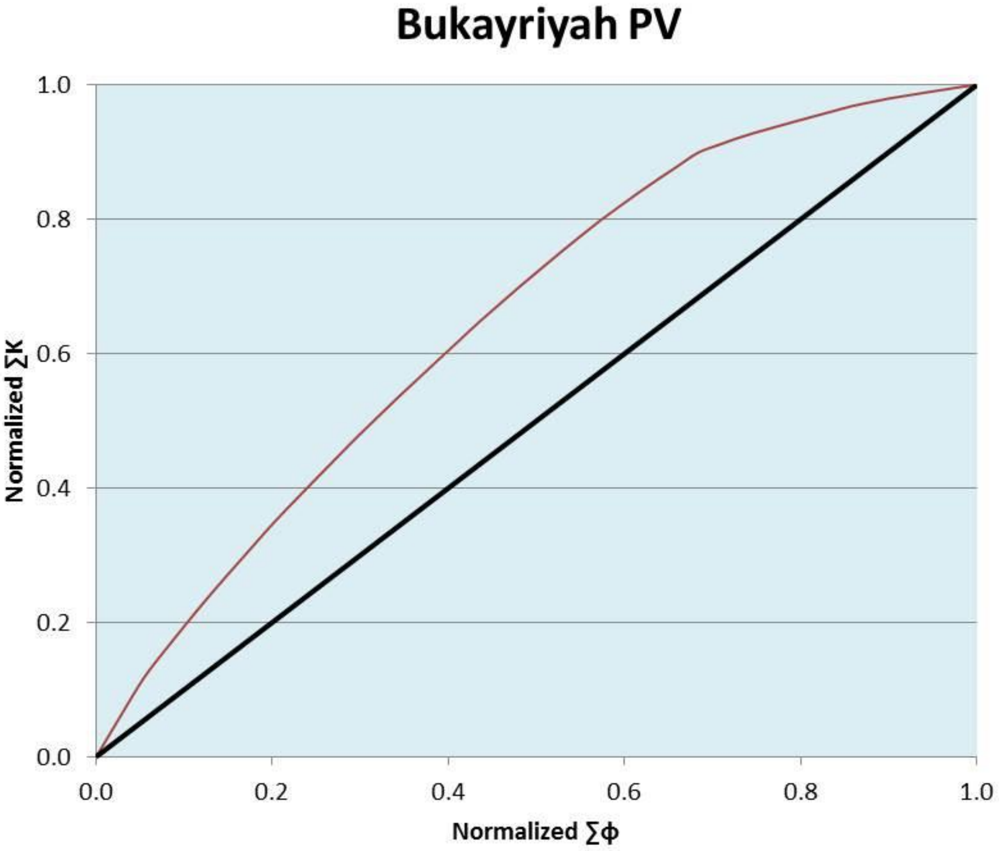

Figure 5-22: Lorenz plot for Bukayriyah paleovalley

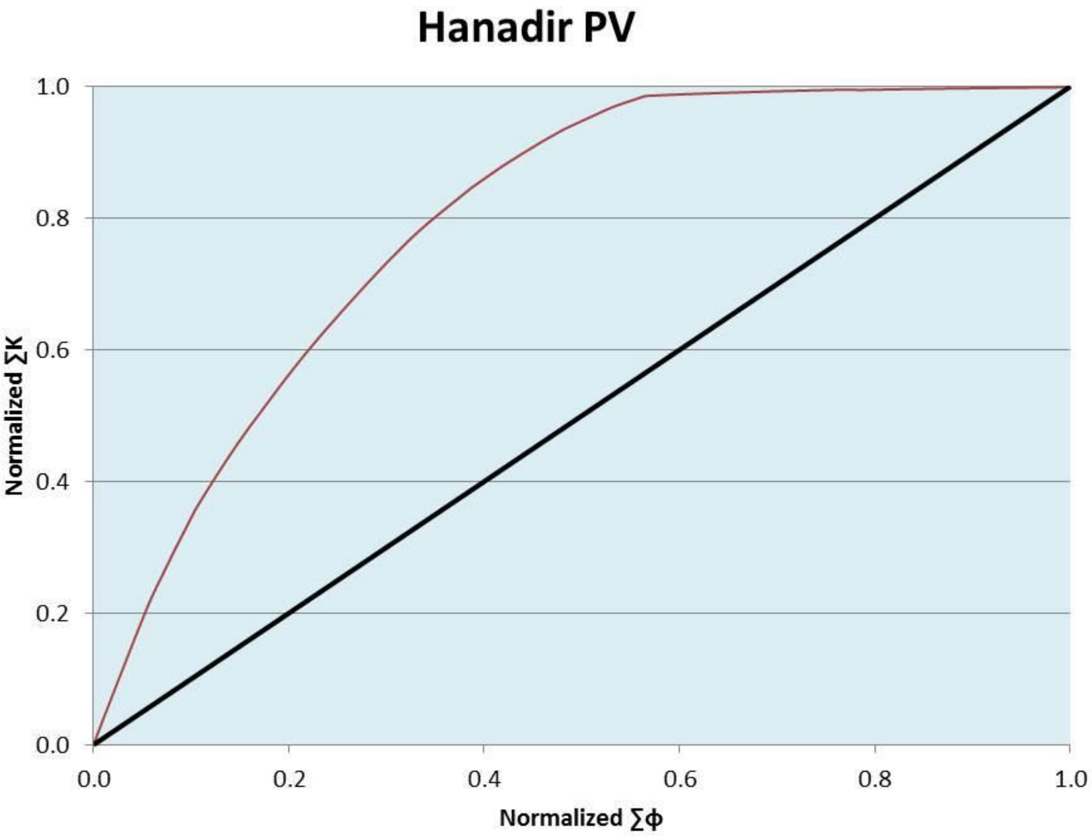

Figure 5-23: Lorenz plot for Hanadir paleovalley

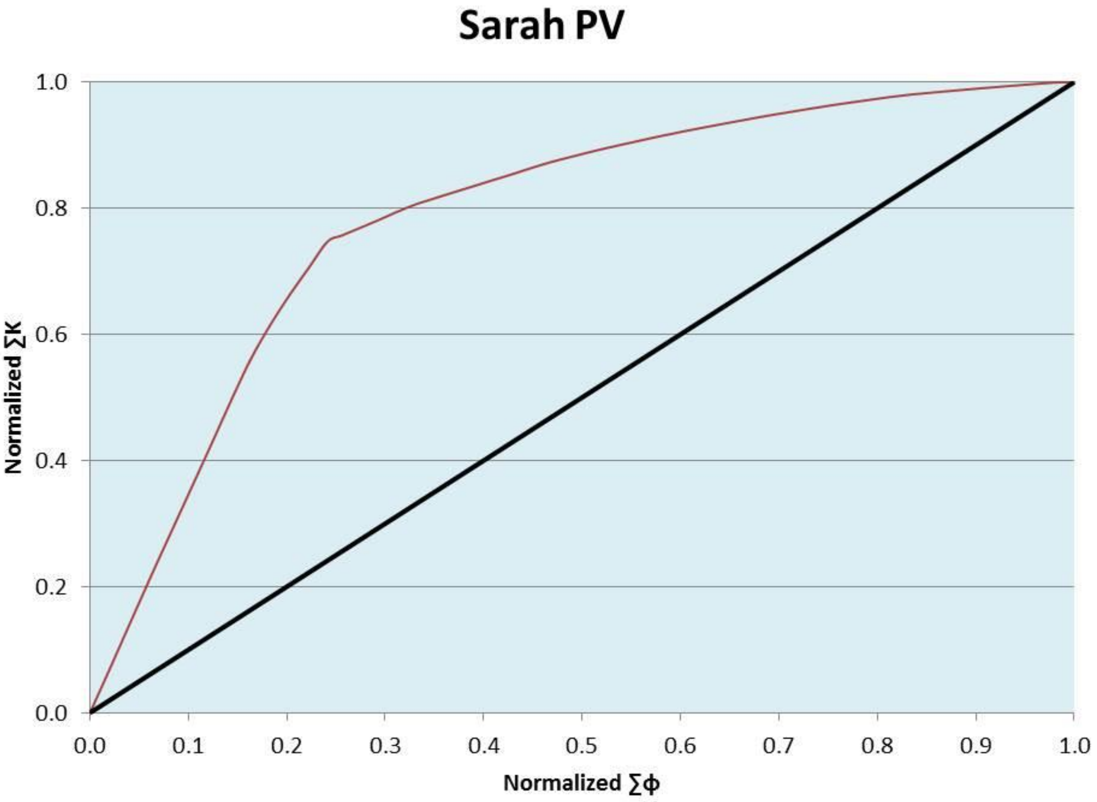

Figure 5-24: Lorenz plot for Sarah paleovalley

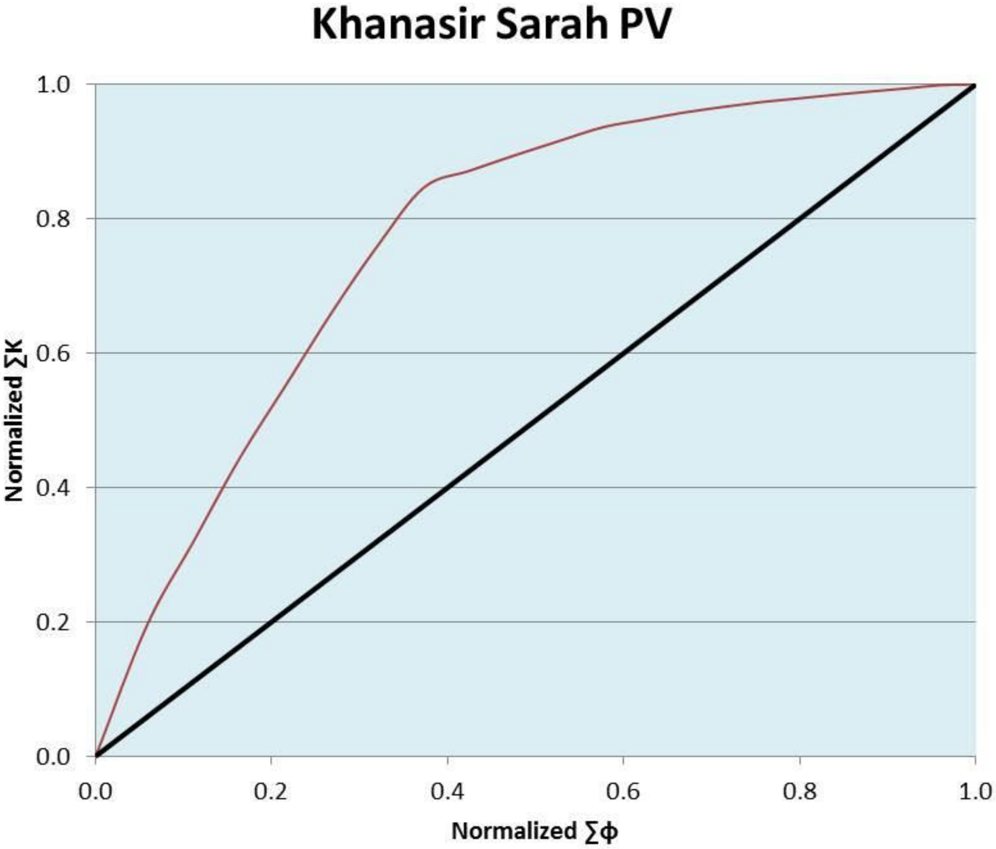

Figure 5-25: Lorenz plot for Khanasir Sarah paleovalley

The Lorenz coefficients for the studied paleovalleys indicate high variability in the distribution of porosity and permeability. The Lc for Bukayriyah, Hanadir, Sarah and Khanasir Sarah paleovalleys are 0.30, 0.59, 0.58 and 0.54, respectively.

5.7.4. Summary of Heterogeneity of Sarah Paleovalleys

Table 5-9 shows comparison of Heterogeneity parameters for Sarah paleovalleys. The coefficient of variation values range between 0.63 and 1.93, indicating extremely heterogeneous distribution. Dykstra-Parsons coefficient values range from 0.56 to 0.88 suggesting very to extremely heterogeneous reservoirs. Lorenz coefficients show good correlation with Dykstra-Parsons coefficient for Sarah paleovalleys (Figure 5-26). The studied heterogeneity parameters indicate that Sarah paleovalleys represent heterogeneous to very heterogeneous reservoirs.

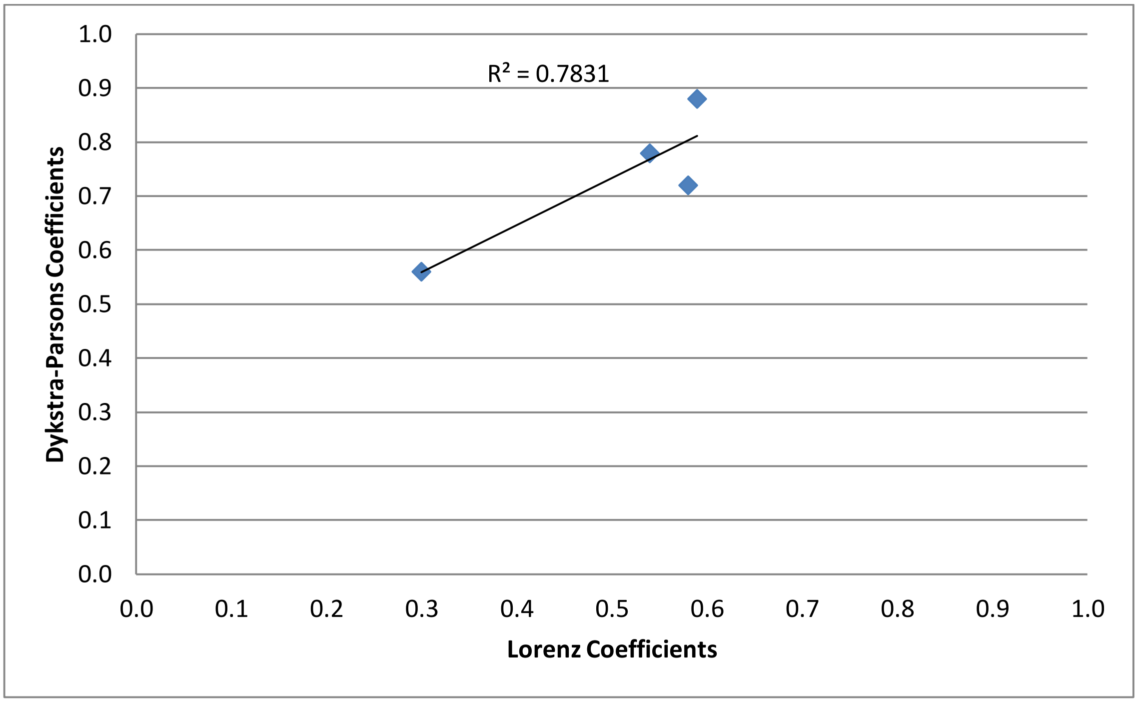

Figure 5-26: Correlation between Lorenz and Dykstra-Parsons coefficients for Sarah paleovalleys.

Table 5-9: Heterogeneity parameters for Sarah paleovalleys

Parameters	Bukayriyah	Hanadir	Sarah	Khanasir Sarah
Mean	9.66	106.88	459.89	398.45
Median	10.41	26.99	237.70	172.76
Standard Deviation	6.07	208.89	573.66	476.72
CV	0.63	1.95	1.25	1.20
V_{DP}	0.56	0.88	0.72	0.78
Lc	0.30	0.59	0.58	0.54
Heterogeneity	Heterogeneous to Very heterogeneous reservoirs			

CHAPTER SIX

CONCLUSIONS AND RECOMMENDATIONS

I conducted this study to characterize and compare different scales of depositional and post-depositional heterogeneity of the late Ordovician glacio-fluvial paleochannels. I studied several glacio-fluvial paleochannels of the Sarah Formation from a number of outcrops in central Arabia. Four paleovalleys were the target of this study, namely Bukayriyah, Hanadir, Sarah, and Khanasir Sarah (Sarah Ridge) paleovalleys. The approach in this study included sedimentological field investigations and laboratory petrological analysis. Laboratory studies included thin section petrography, XRD, SEM and MICP investigations. The porosity and permeability measurements were carried out for the core plugs to detect the micro-heterogeneity within the five paleovalleys.

6.1. Conclusions

The results of petrographical analysis indicate that the sandstones are dominantly fine to medium-grained, moderately- to well-sorted, quartz arenites. The quartz grains are generally mono-crystalline. Alkali-feldspars and plagioclase are the main components of the detrital feldspars in the samples. Lithic fragments are absent in most of the studied samples. Mica grains range from 0-5 percent. Heavy minerals were not observed in the thin sections. The grains are mainly sub-angular to sub-rounded. QFL diagram shows that the sandstones are quartz arenites (90-100 % quartz, 0-10 % feldspar, and 0-5 % lithic fragments).

Mud is the dominant matrix, generally less than 2%. The cementing materials (5-10%) include clay and iron oxides. The SEM and XRD analyses prove the dominance of kaolinite as cementing material. The abundance of kaolinite and ferruginous cement resulted in a critical reduction in permeability. However, the coating of quartz grains by kaolinites retarded the compaction and inhibited the quartz overgrowth, and hence played a significant role in preserving the initial porosity and permeability. Such preservation of porosity allowed the dissolution of feldspar grains by pore fluids, e.g., meteoric water, to create secondary porosity, and subsequently enhanced the permeability.

The petrophysical analysis was conducted by measuring porosity and permeability for the samples of Sarah paleovalleys. The measured porosity values from sample plugs range between 17 % and 56.7 % with an average value of 28 %. Both primary and secondary porosities have been registered. Leaching and dissolution created secondary intergranular porosity and intragranular microporosity. The studied samples showed a very wide range of permeability values ranging from 0.1 md to 2.27 Darcy, with an average of 0.25 Darcy. High permeability values were recorded from loosely packed, but poorly cemented samples, and low permeability from densely cemented and tight packed samples.

The integration and correlation between the results of thin section, XRD, SEM, MICP, poro-perm analyses reveal the textural, compositional, and diagenetic effects on the petrophysical parameters and reservoir quality of Sarah Formation. Grain size variation, compaction, cementation, dissolution, mineral replacement, quartz overgrowth, as well as pore size distribution and their connectivity are the main controls affecting porosity and permeability.

The reservoir heterogeneity analysis was conducted using three static measures, namely the coefficient of variation, Dykstra-Parsons, and Lorenz coefficients. The results indicate that Sarah Formation represents heterogeneous to very heterogeneous reservoir.

6.2. Recommendations

The following recommendations are suggested for future work and related research:

1. Extensive sedimentological studies including other paleovalleys of Sarah Formation may help in correlation and characterization of heterogeneity.
2. Integration of the outcrop studies with the subsurface data from the Arabian basin may help in understanding and predicting the reservoir quality of Sarah Formation in the subsurface.
3. Detailed geostatistical modeling study will help characterizing the spatial relationships among Sarah paleovalleys.

APPENDIX A

X-RAY POWDER DIFFRACTION RESULTS

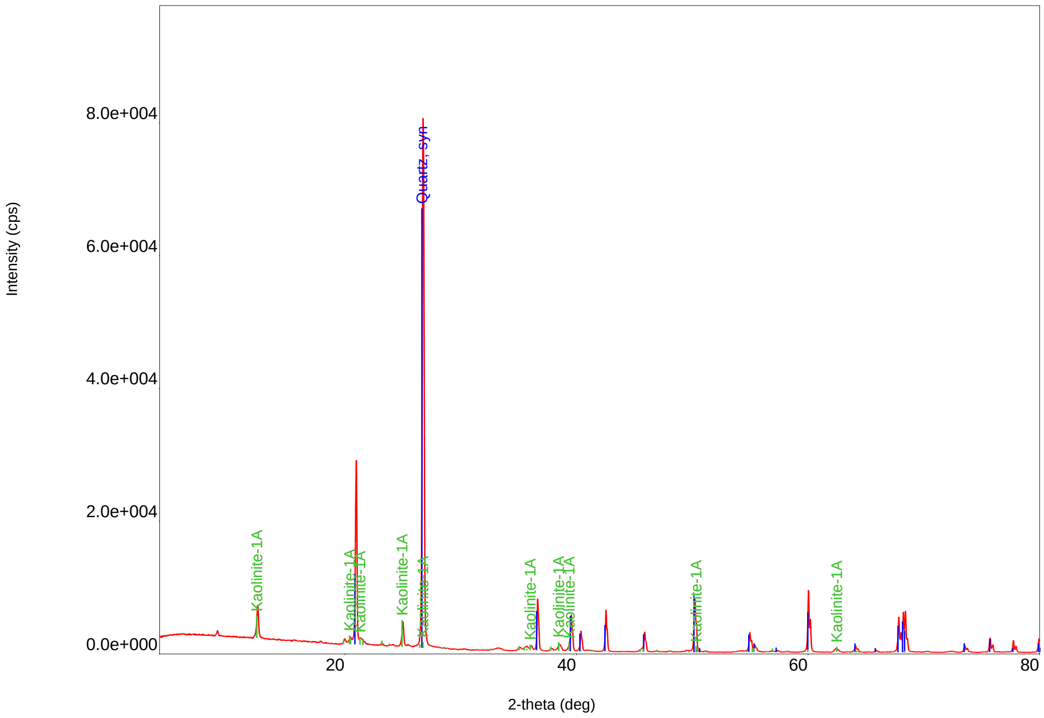

Intensity (cps)
8.0e+004
6.0e+004
4.0e+004
2.0e+004
0.0e+000
Quartz, syn
Kaolinite-1A
Kaolinite-1A
Kaolinite-1A
Kaolinite-1A
Kaolinite-1A
Kaolinite-1A
Kaolinite-1A
Kaolinite-1A
Kaolinite-1A
Kaolinite-1A
20
40
60
80
2-theta (deg)

Sample # S1H1

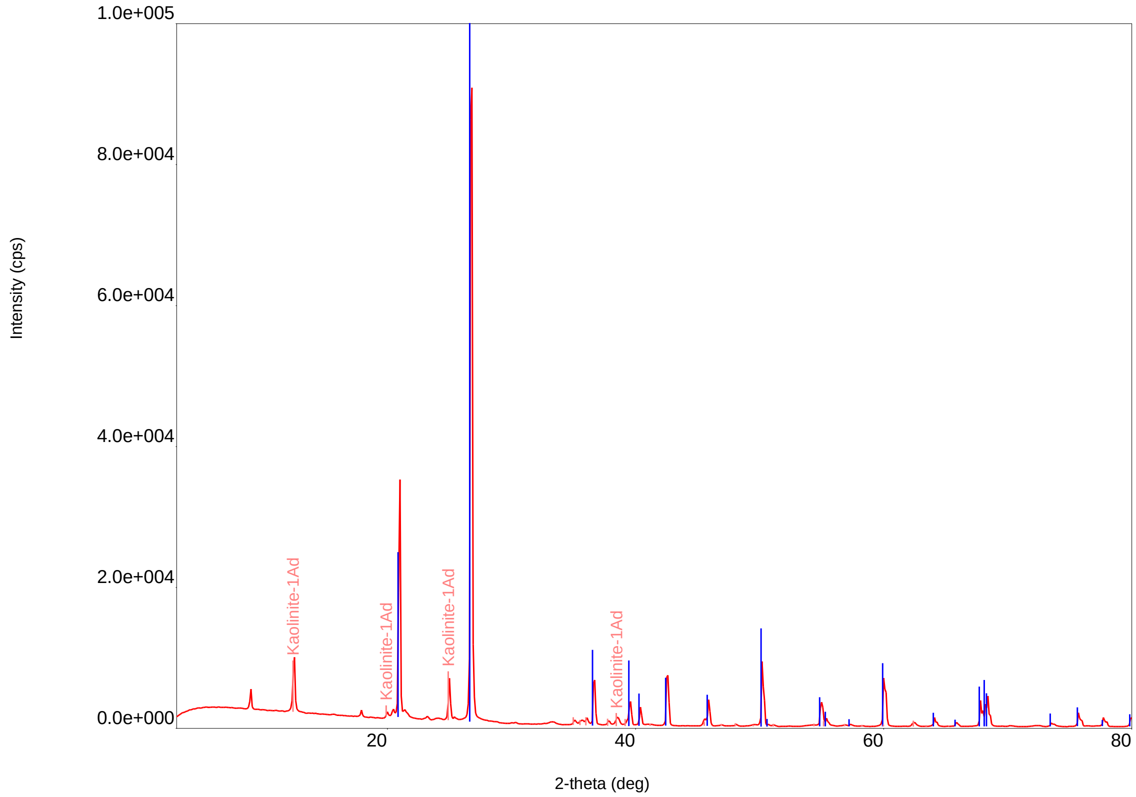
1.0e+005
8.0e+004
6.0e+004
4.0e+004
2.0e+004
0.0e+000
Intensity (cps)
Kaolinite-1Ad
Kaolinite-1Ad
Kaolinite-1Ad
Kaolinite-1Ad
20
40
60
80
2-theta (deg)

Sample # S1H6

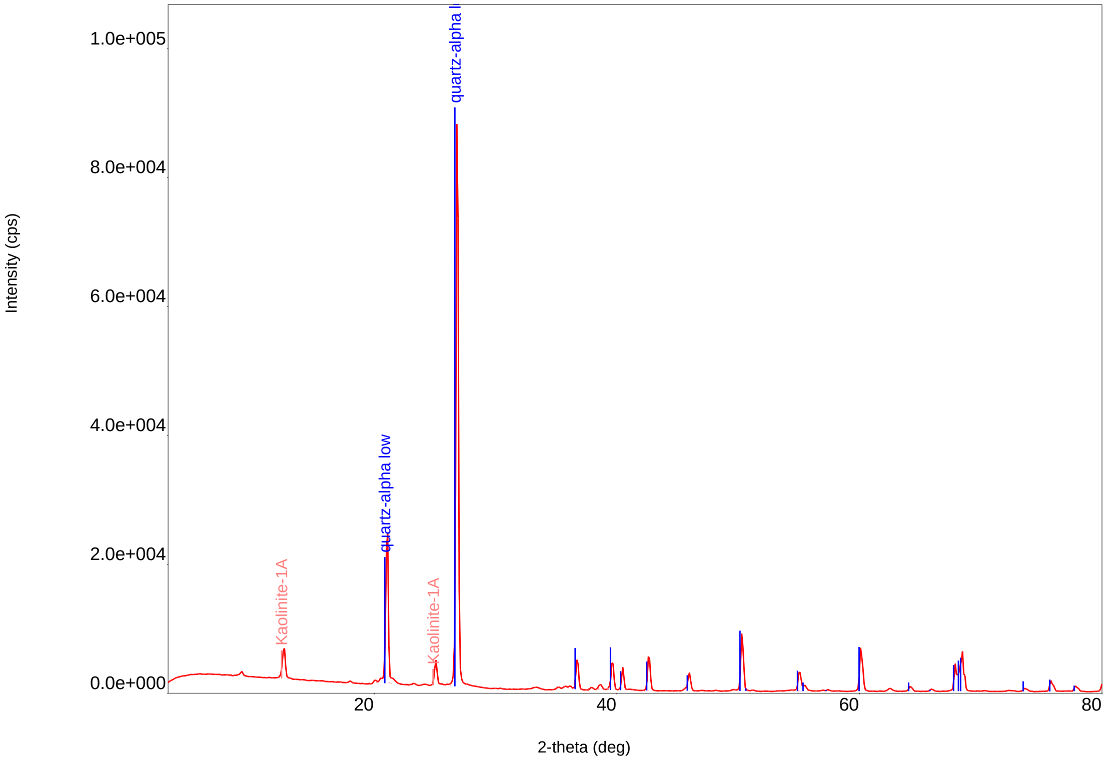
Intensity (cps)
1.0e+005
8.0e+004
6.0e+004
4.0e+004
2.0e+004
0.0e+000
quartz-alpha l
quartz-alpha low
Kaolinite-1A
Kaolinite-1A
20
40
60
80
2-theta (deg)

Sample # S1-H8

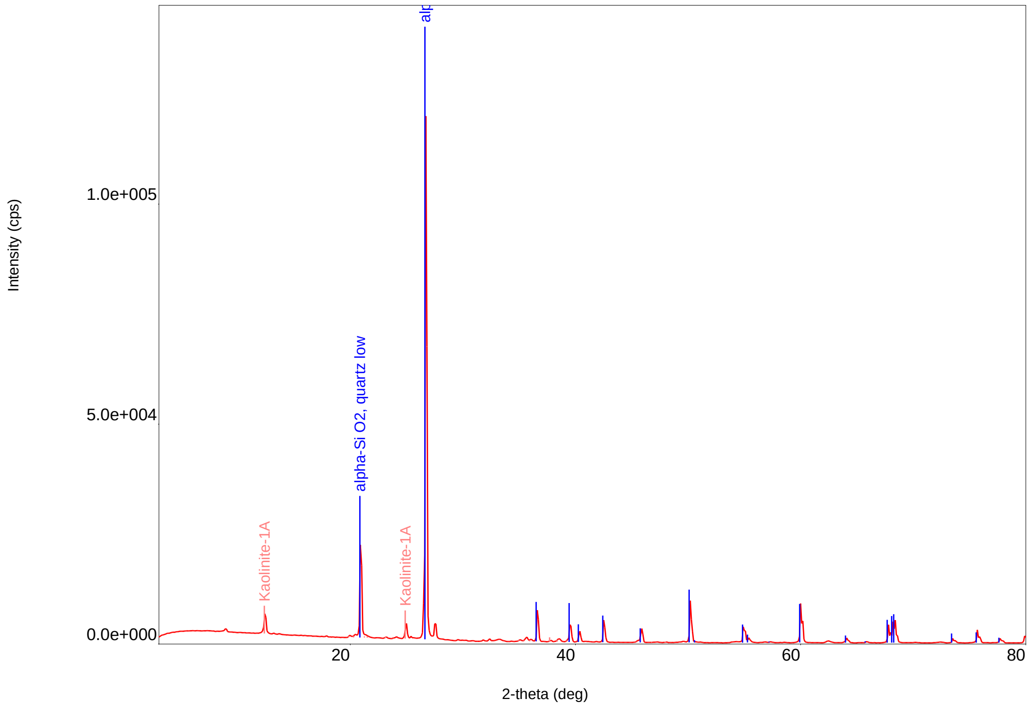
Intensity (cps)
1.0e+005
5.0e+004
0.0e+000
20
40
60
80
2-theta (deg)
Kaolinite-1A
alpha-Si O2, quartz low
Kaolinite-1A
alp

Sample # S2-H3

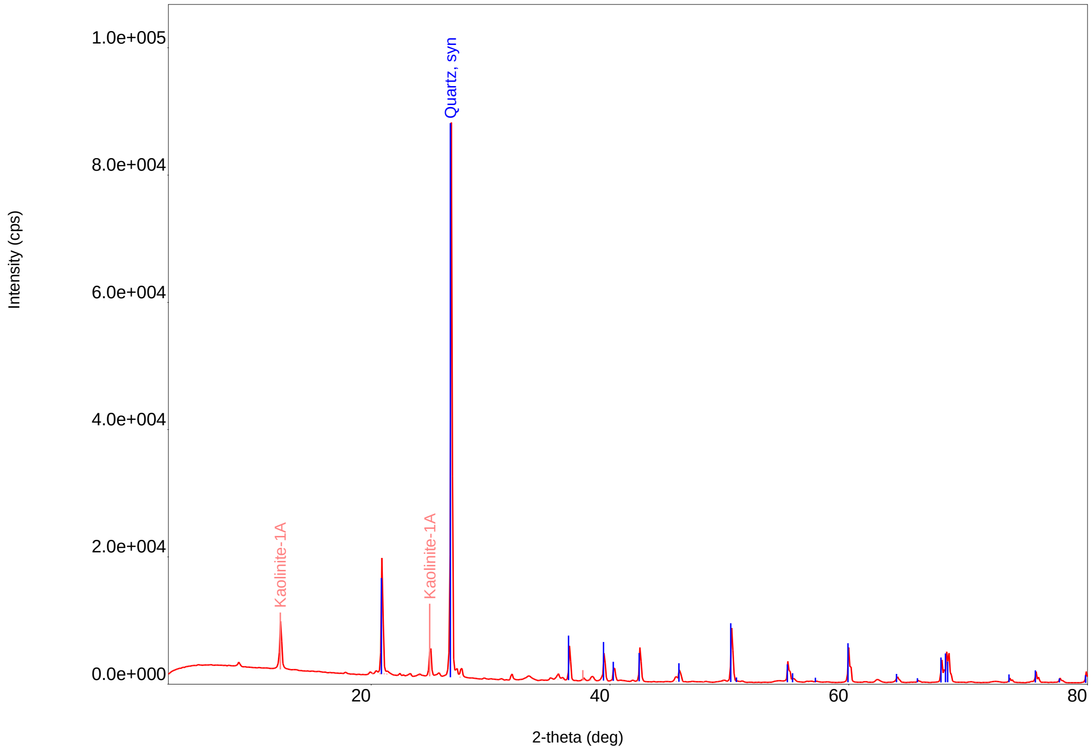
Quartz, syn
Kaolinite-1A
Kaolinite-1A
1.0e+005
8.0e+004
6.0e+004
4.0e+004
2.0e+004
0.0e+000
Intensity (cps)
20
40
60
80
2-theta (deg)

Sample # S2-H4

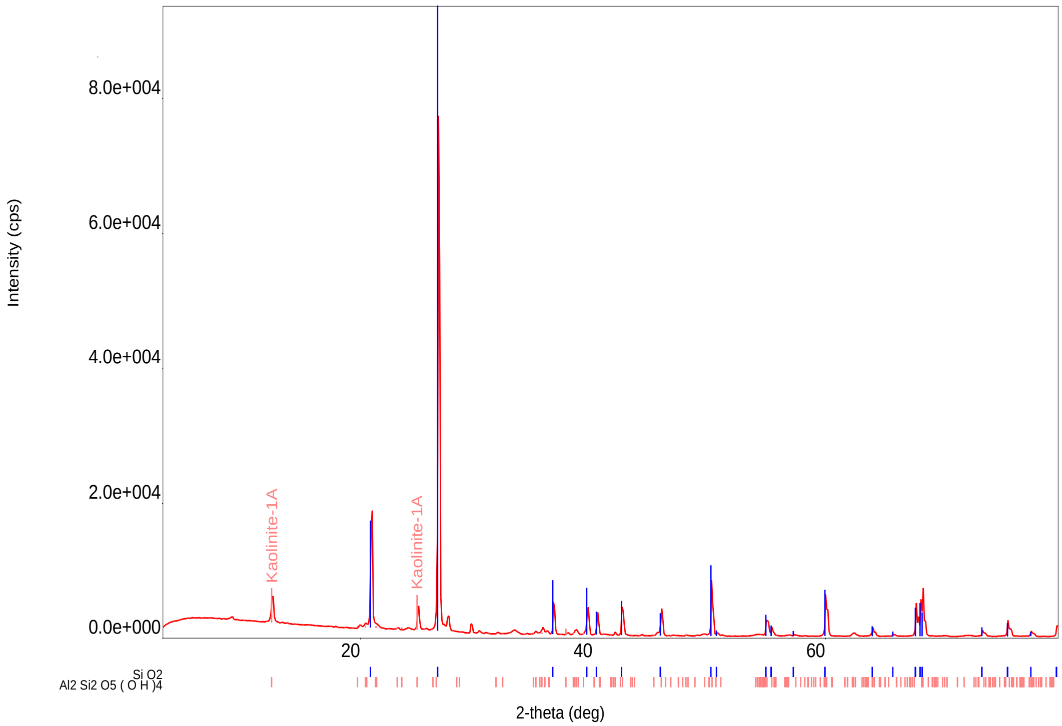
Intensity (cps)
8.0e+004
6.0e+004
4.0e+004
2.0e+004
0.0e+000
Kaolinite-1A
Kaolinite-1A
20
40
60
Si O2
Al2 Si2 O5 (O H)4
2-theta (deg)

Sample # S2-H7

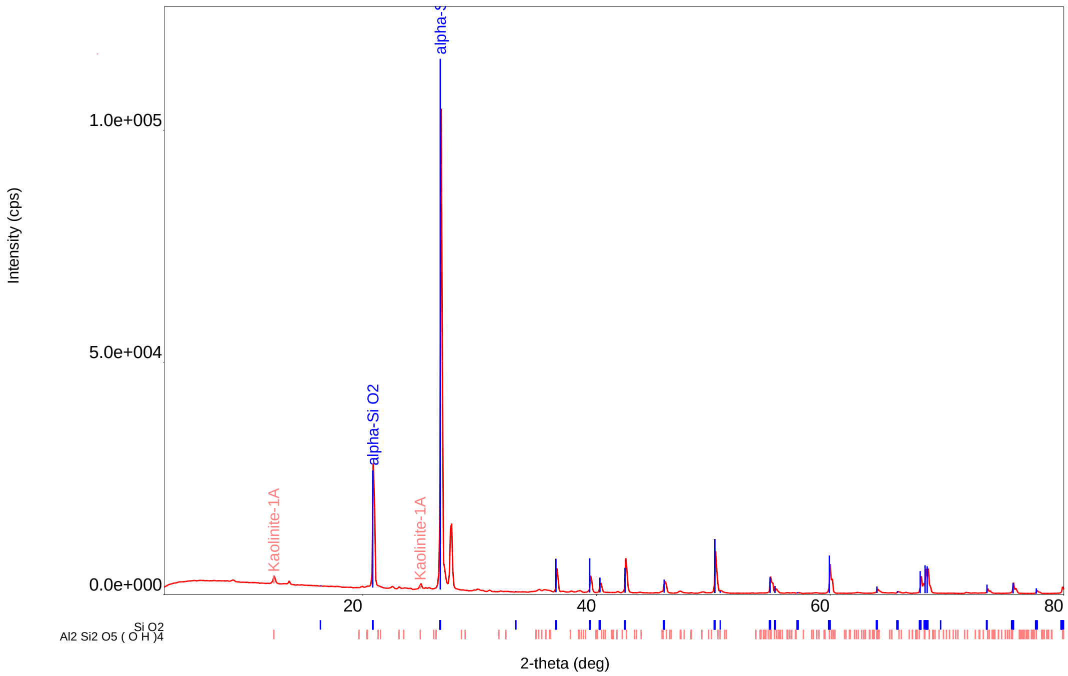
Intensity (cps)
1.0e+005
5.0e+004
0.0e+000
alpha-S
alpha-Si O2
Kaolinite-1A
Kaolinite-1A
20
40
60
80
Si O2
Al2 Si2 O5 (O H)4
2-theta (deg)

Sample # S3-H4

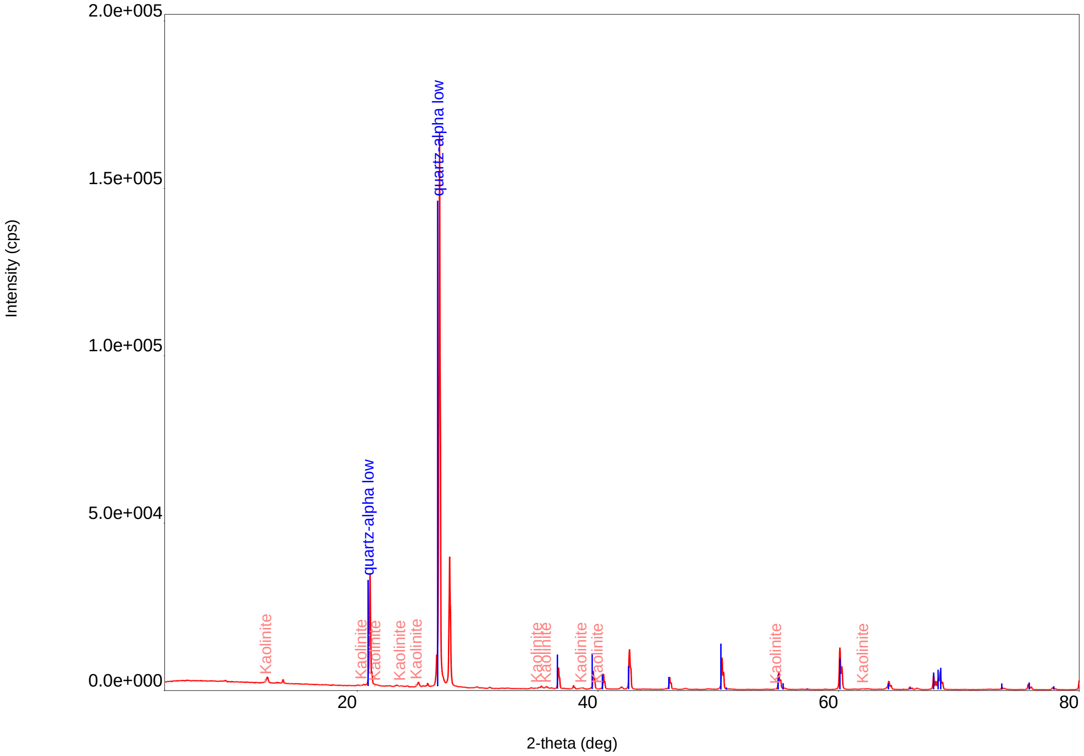
2.0e+005
1.5e+005
1.0e+005
5.0e+004
0.0e+000
Intensity (cps)
20
40
60
80
2-theta (deg)
quartz-alpha low
quartz-alpha low
Kaolinite
Kaolinite
Kaolinite
Kaolinite
Kaolinite
Kaolinite
Kaolinite
Kaolinite
Kaolinite
Kaolinite
Kaolinite

Sample # S3-H6

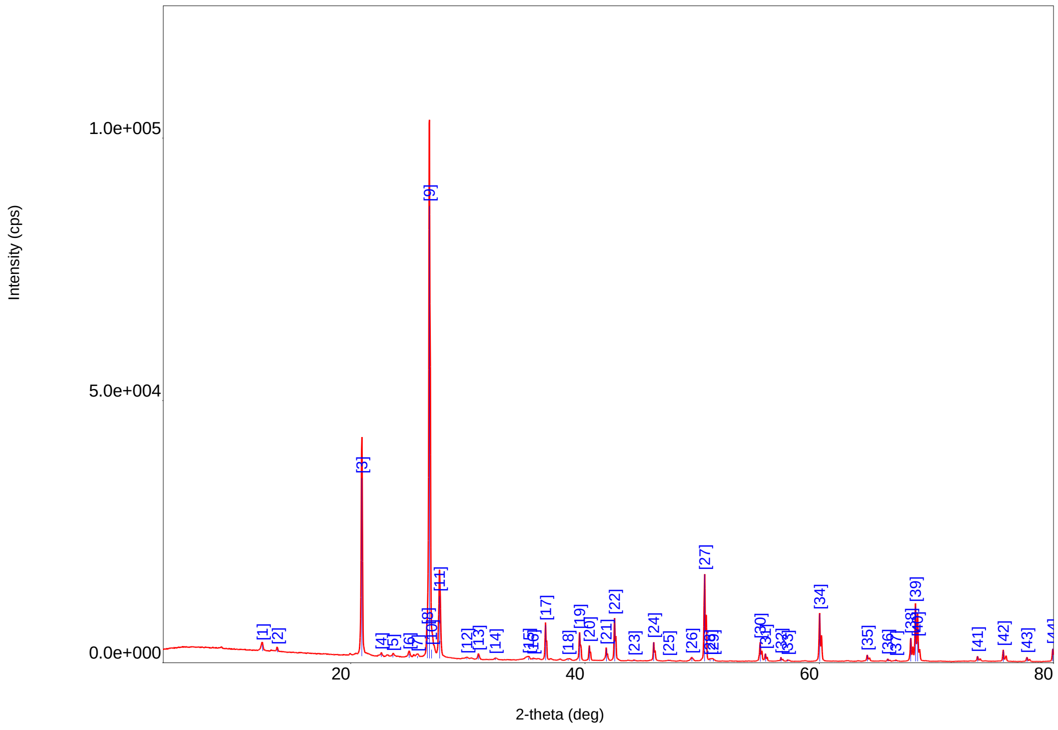
Intensity (cps)
1.0e+005
5.0e+004
0.0e+000
20
40
60
80
2-theta (deg)
[1]
[2]
[3]
[4]
[5]
[6]
[7]
[8]
[9]
[10]
[11]
[12]
[13]
[14]
[15]
[16]
[17]
[18]
[19]
[20]
[21]
[22]
[23]
[24]
[25]
[26]
[27]
[28]
[29]
[30]
[31]
[32]
[33]
[34]
[35]
[36]
[37]
[38]
[39]
[40]
[41]
[42]
[43]
[44]

Sample # S3-V8

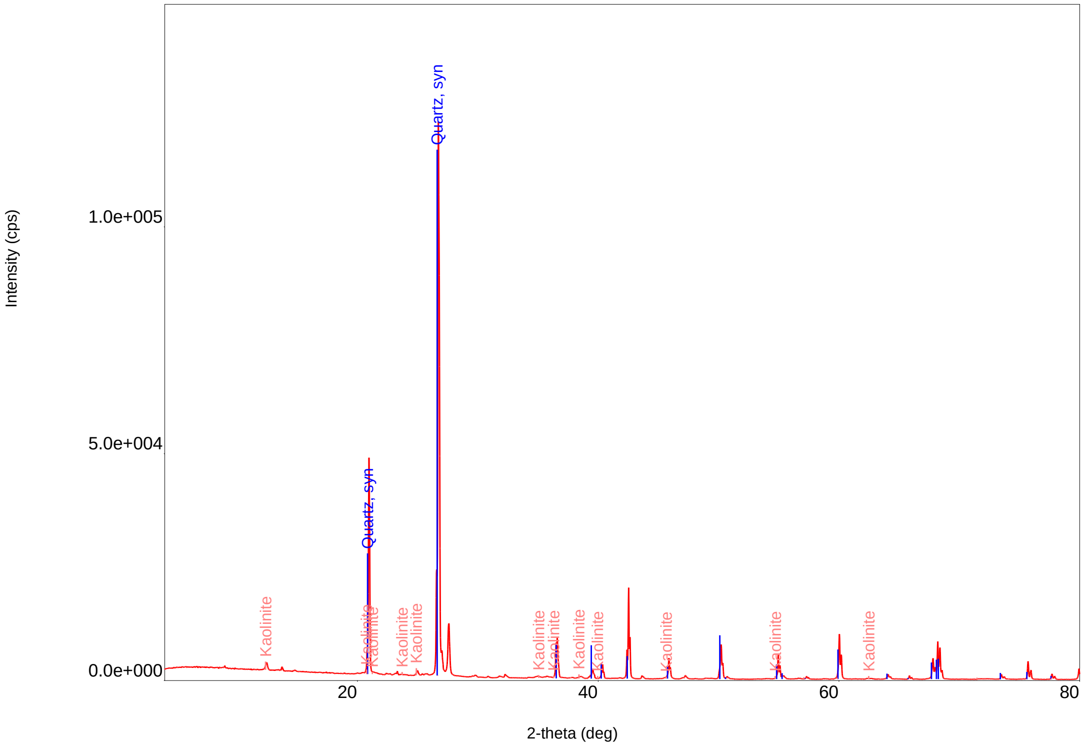
Intensity (cps)
1.0e+005
5.0e+004
0.0e+000
2-theta (deg)
20
40
60
80
Quartz, syn
Quartz, syn
Kaolinite
Kaolinite
Kaolinite
Kaolinite
Kaolinite
Kaolinite
Kaolinite
Kaolinite
Kaolinite
Kaolinite
Kaolinite
Kaolinite

Sample # S3-V9

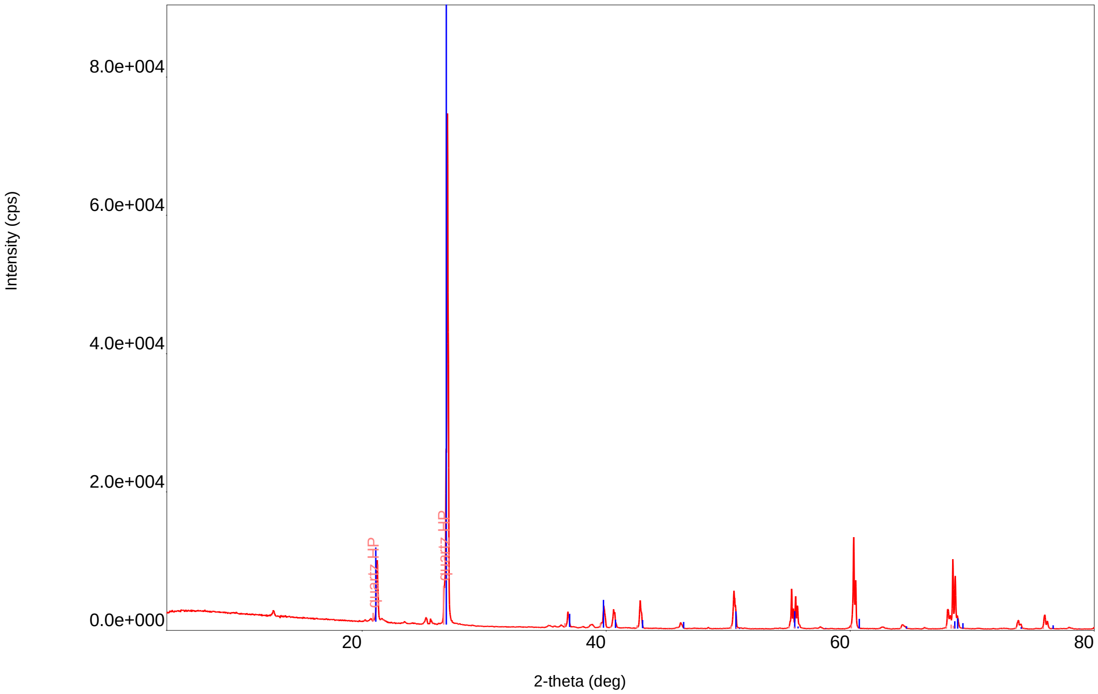

Sample # KS-3C-V3

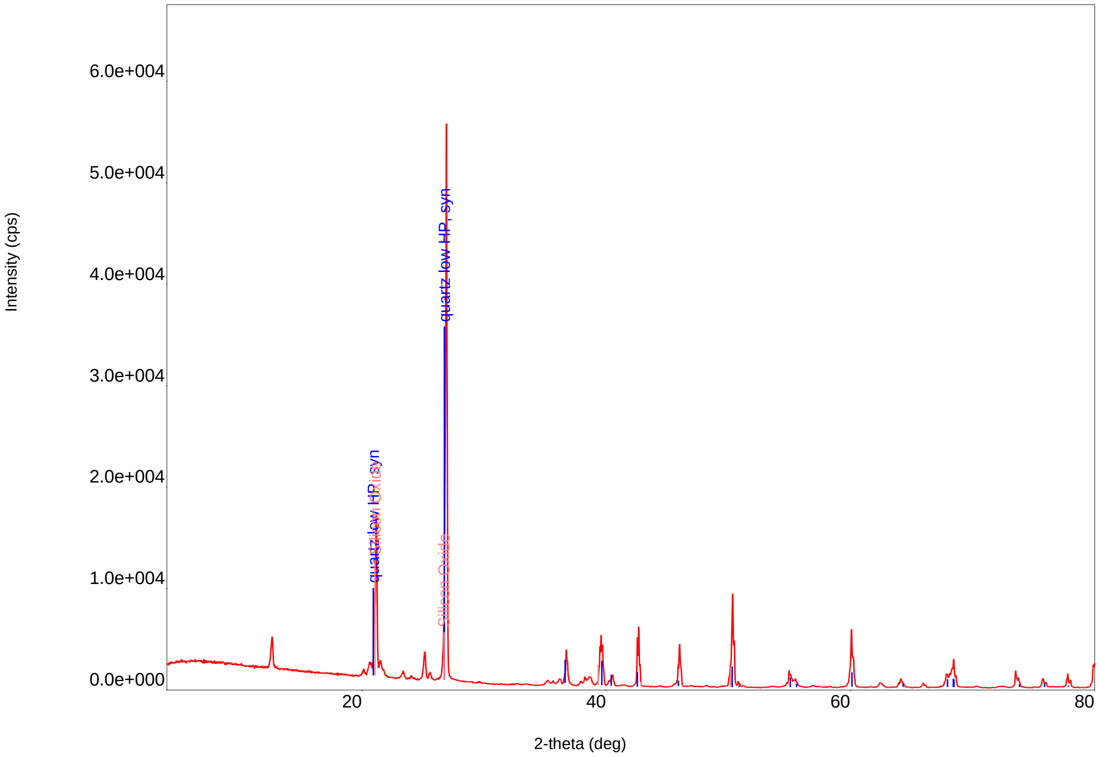

Sample # KS-9-V2

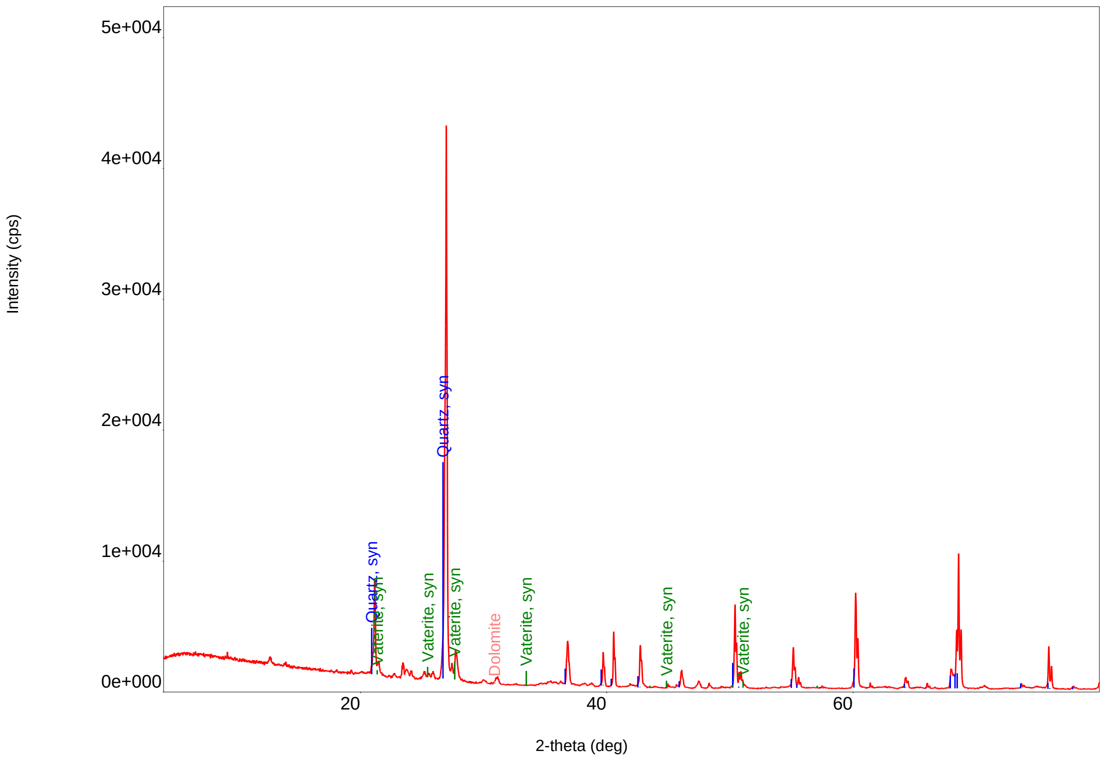

Sample # RC-1-H6

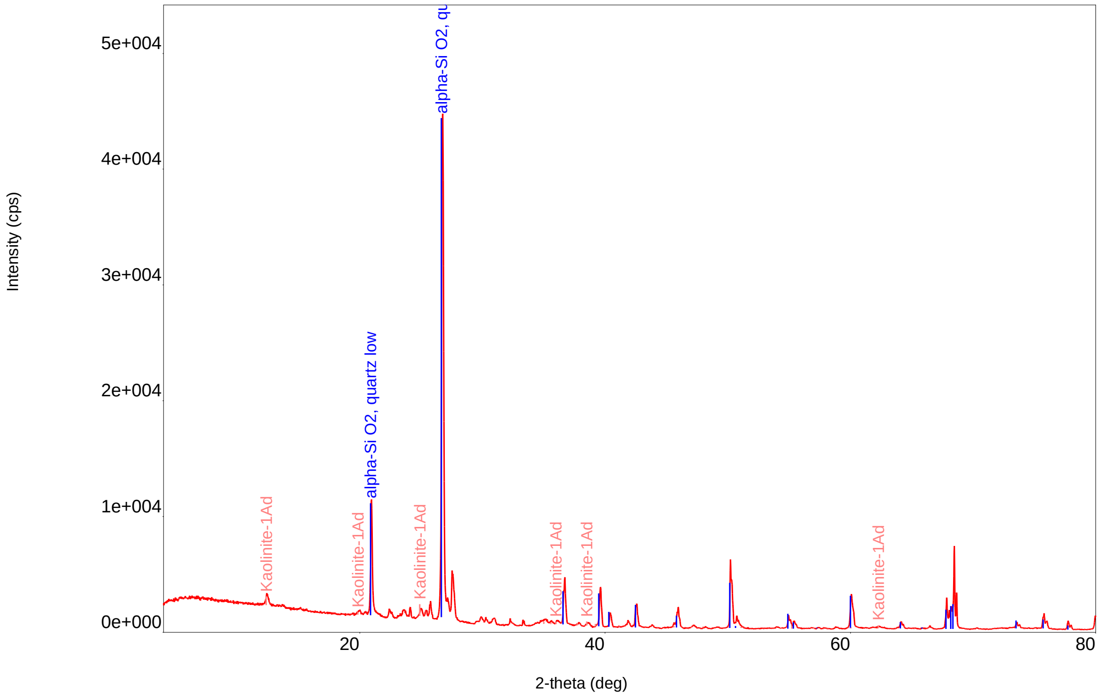

Sample # RC-3-V2

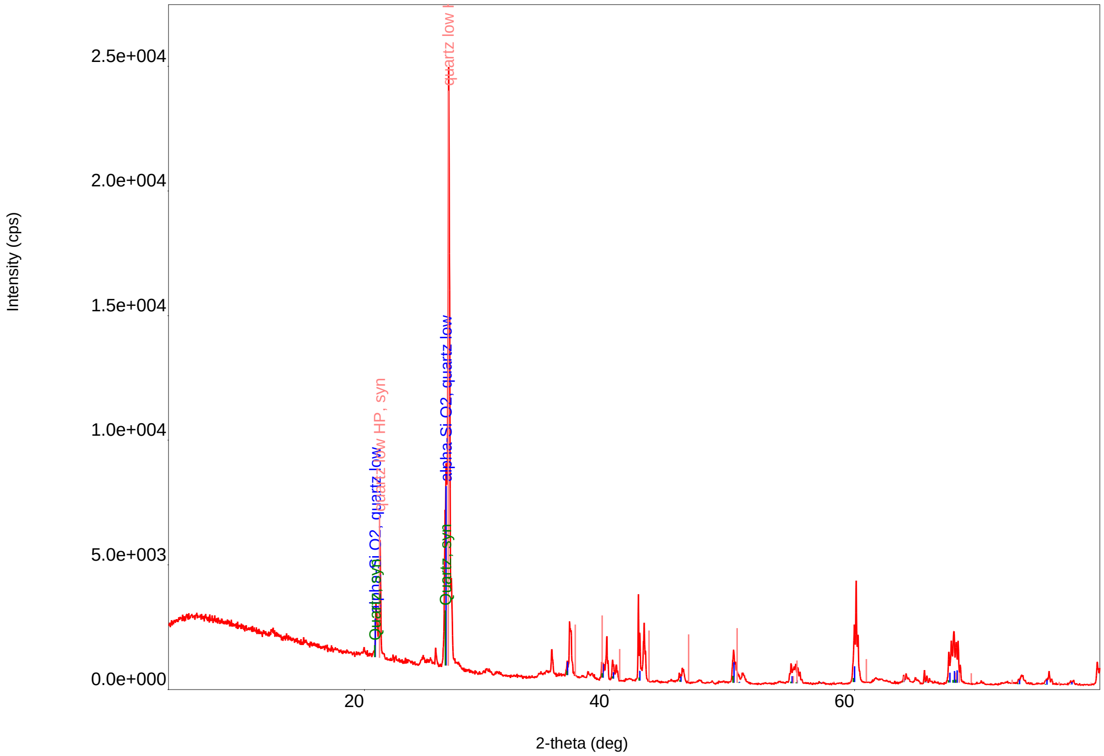

Sample # RC-4-H2

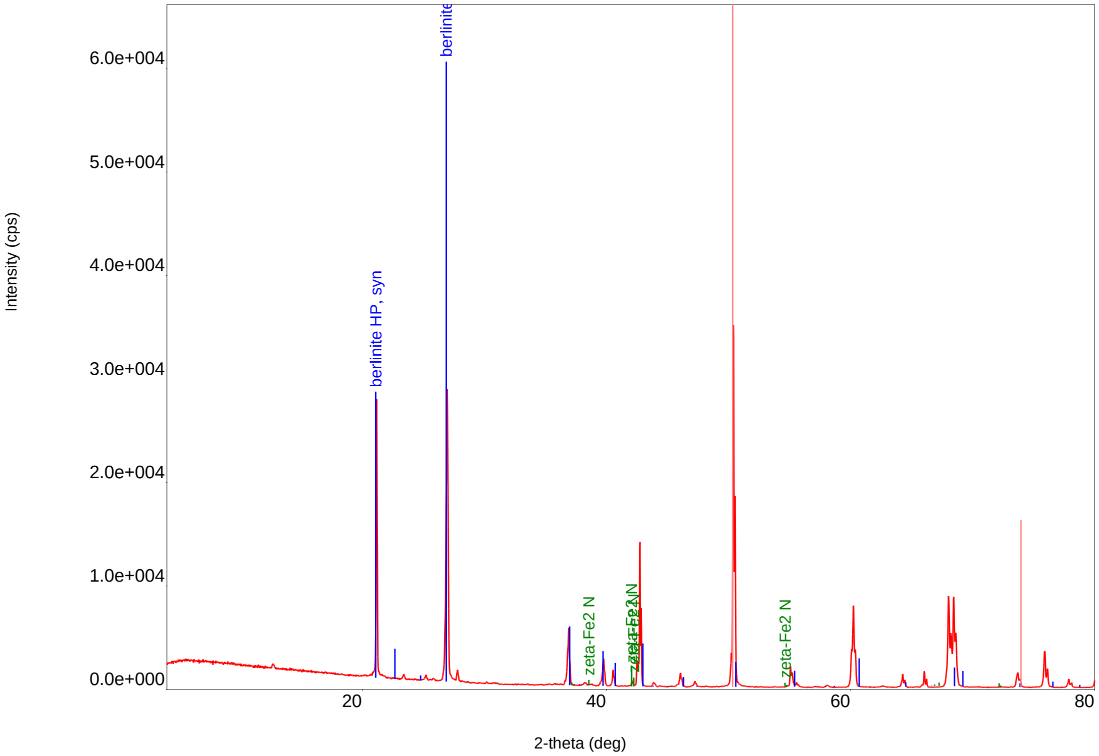

Sample # SQ-1C-H4

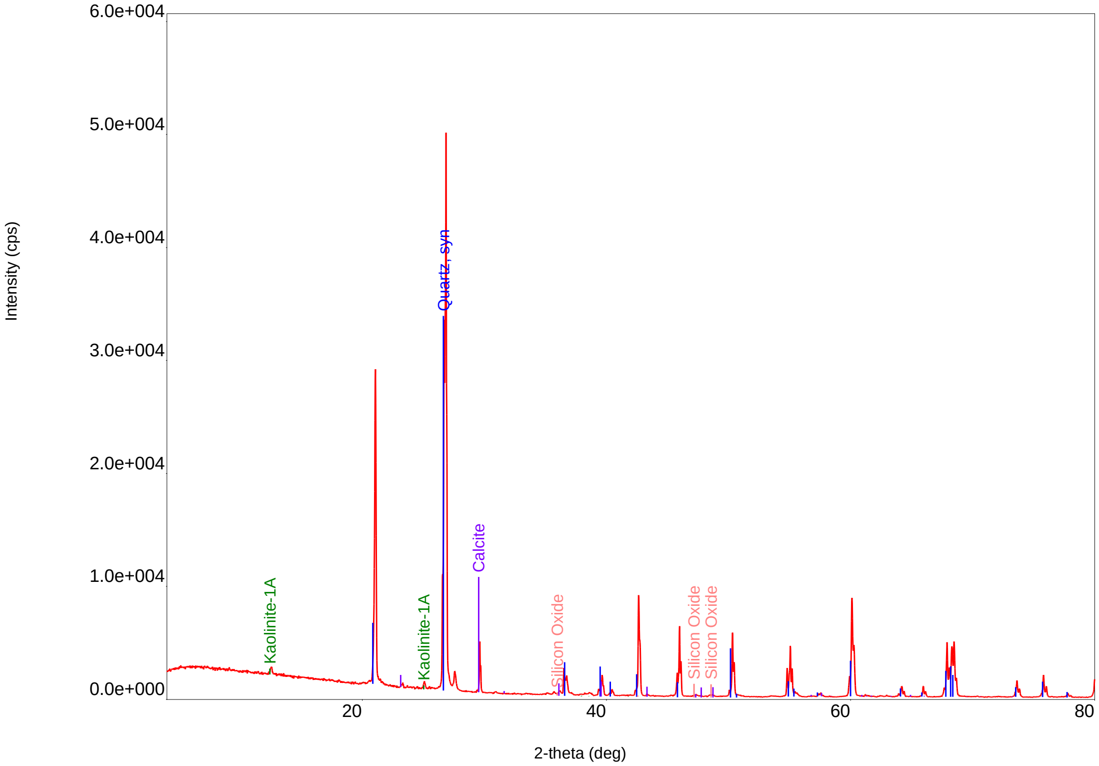

Sample # SQ-4-V3

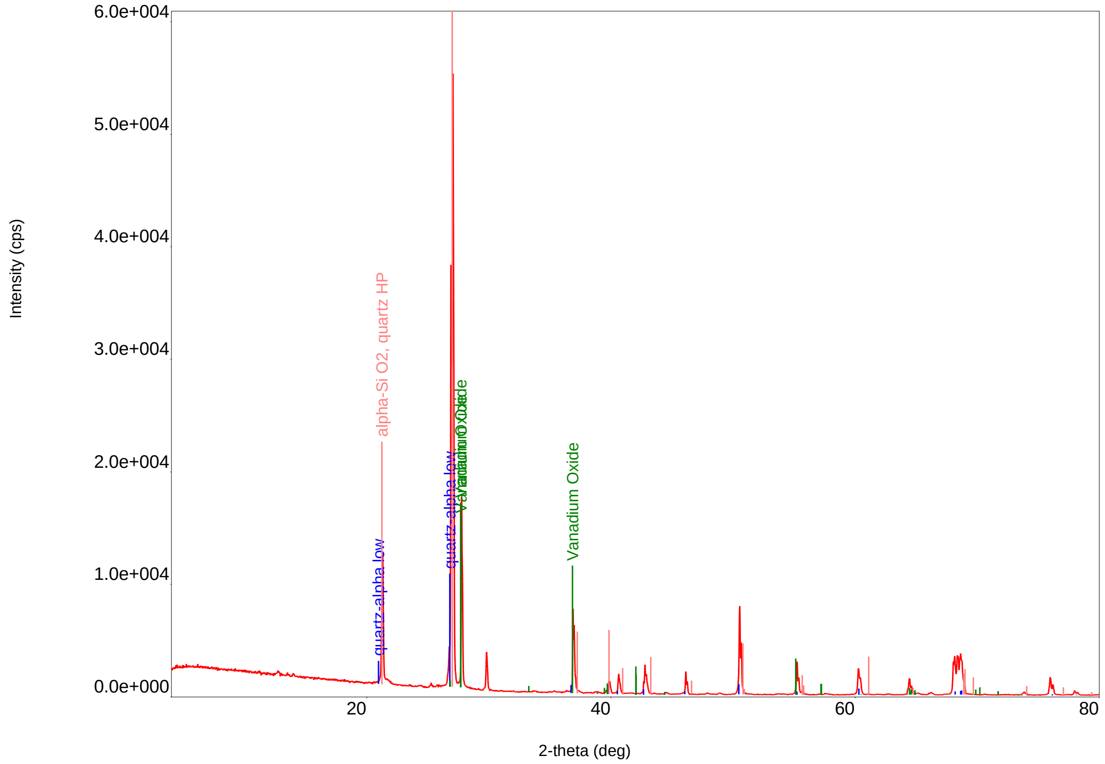

Sample # SQ-7A-H4

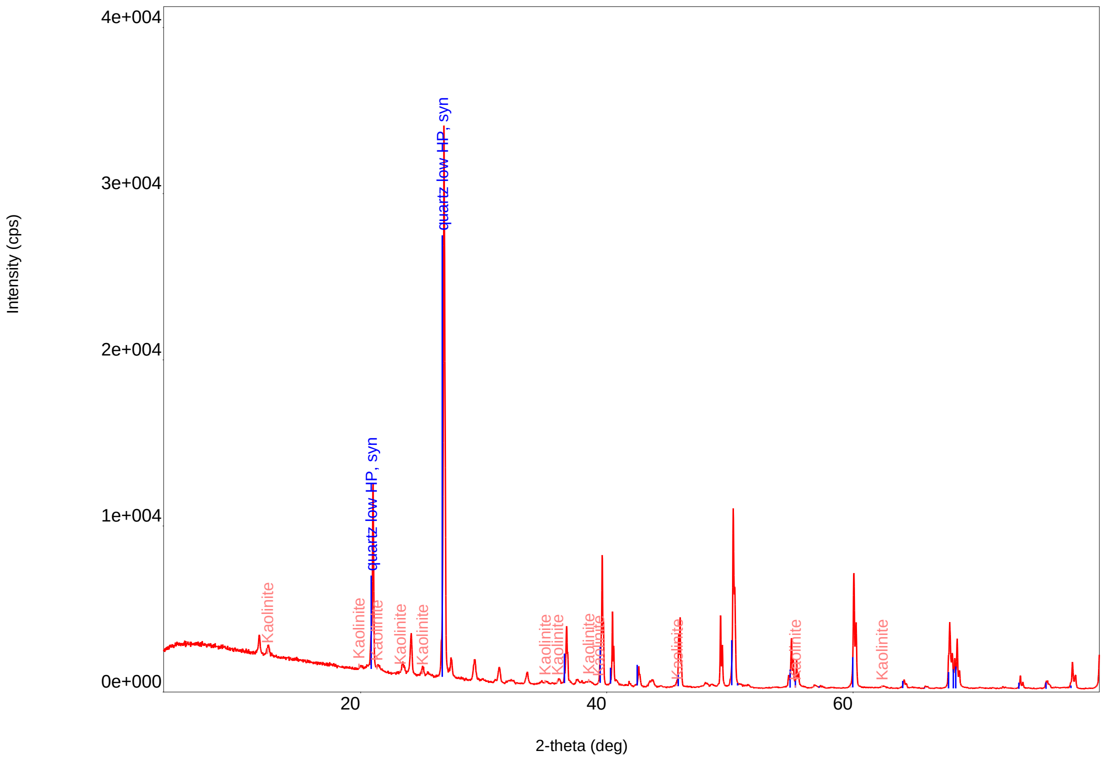

Sample # SR7A-H4

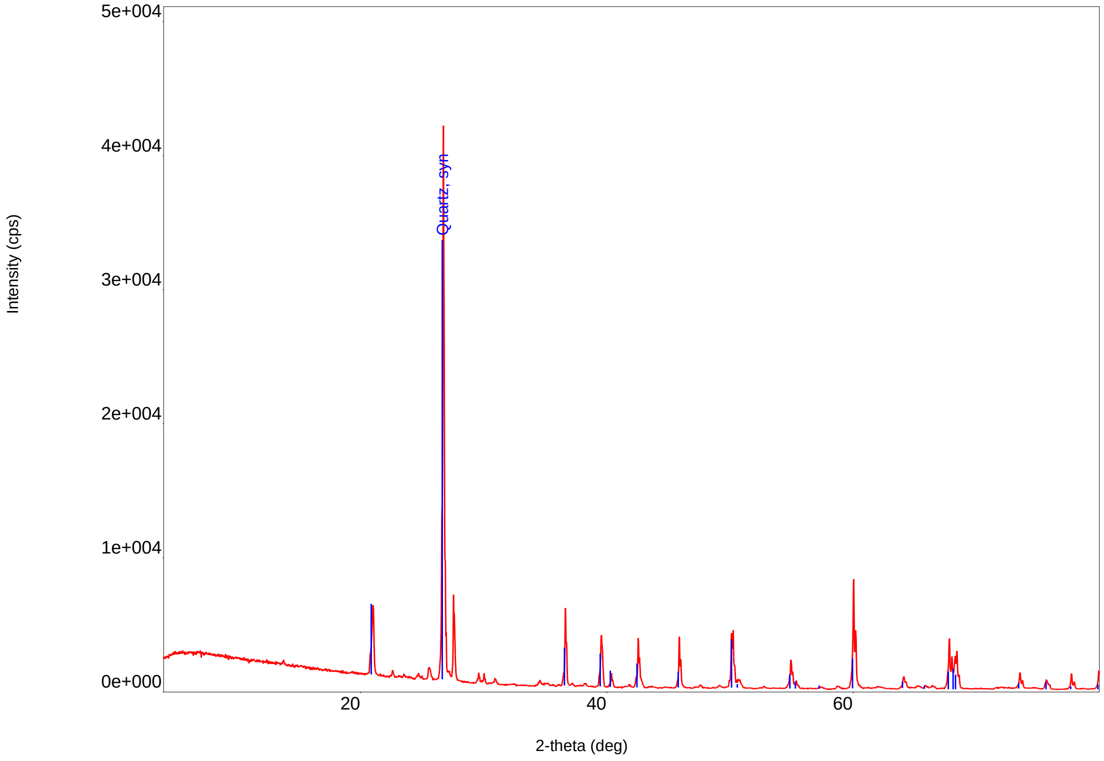

Sample # SR-9-V1

APPENDIX B

CALCULATIONS OF THE LORENZ COEFFICIENT

Table 1: Calculation of Lorenz coefficient for porosity and permeability measurements from Bukayriyah paleovalley

φ	Cumulative	% cumulative	K	Cumulative	% cumulative
34.27	0.00	0.00	27.10	0.00	0.00
29.87	34.27	0.03	23.02	27.10	0.06
29.73	64.14	0.05	18.26	50.11	0.12
29.66	93.87	0.08	17.46	68.37	0.16
29.58	123.53	0.10	16.88	85.84	0.20
29.16	153.11	0.13	15.75	102.71	0.24
28.47	182.28	0.15	15.21	118.47	0.28
28.13	210.75	0.18	14.93	133.68	0.31
28.08	238.88	0.20	13.88	148.60	0.35
27.82	266.96	0.23	13.53	162.49	0.38
27.69	294.78	0.25	13.31	176.02	0.41
27.67	322.47	0.27	13.27	189.33	0.45
27.58	350.14	0.30	12.65	202.60	0.48
27.22	377.72	0.32	12.41	215.25	0.51
27.22	404.94	0.34	11.97	227.66	0.54
27.10	432.16	0.37	11.93	239.63	0.56
27.06	459.26	0.39	11.84	251.56	0.59
26.99	486.32	0.41	11.82	263.40	0.62
26.95	513.31	0.44	11.12	275.22	0.65
26.93	540.26	0.46	11.10	286.34	0.67
26.79	567.18	0.48	10.65	297.43	0.70

Table 2: Calculation of Lorenz coefficient for porosity and permeability measurements from Bukayriyah paleovalley (Contd.)

φ	Cumulative	% cumulative	K	Cumulative	% cumulative
26.70	1.00	0.00	10.54	0.00	0.00
26.67	27.70	0.02	10.29	10.54	0.02
26.62	54.37	0.05	9.98	20.83	0.05
26.60	80.99	0.07	9.19	30.80	0.07
26.50	107.59	0.09	9.03	39.99	0.09
26.35	134.09	0.11	8.56	49.03	0.12
26.31	160.44	0.14	8.28	57.59	0.14
26.29	186.75	0.16	8.21	65.87	0.15
26.03	213.04	0.18	4.68	74.08	0.17
25.90	239.07	0.20	4.37	78.76	0.19
25.89	264.98	0.22	3.82	83.13	0.20
25.89	290.87	0.25	3.44	86.95	0.20
25.79	316.76	0.27	3.38	90.39	0.21
25.69	342.54	0.29	3.33	93.76	0.22
25.66	368.24	0.31	3.27	97.09	0.23
25.61	393.90	0.33	3.22	100.37	0.24
25.41	419.50	0.36	2.52	103.59	0.24
25.26	444.92	0.38	2.38	106.11	0.25
24.87	470.17	0.40	1.91	108.49	0.26
24.72	495.05	0.42	1.89	110.40	0.26
24.70	519.77	0.44	1.87	112.29	0.26
24.58	544.47	0.46	1.81	114.15	0.27
17.56	569.05	0.48	1.00	115.97	0.27
	586.62	0.50		116.97	0.28

Table 3: Calculation of Lorenz coefficient for porosity and permeability measurements from Hanadir paleovalley

φ	Cumulative	% cumulative	K	Cumulative	% cumulative
35.13	0.00	0.00	2252.00	0.00	0.00
34.62	36.13	0.01	2160.10	2252.00	0.05
32.84	70.75	0.03	2040.80	4412.10	0.10
32.70	103.58	0.04	2004.20	6452.90	0.14
31.74	136.28	0.05	1857.60	8457.10	0.18
31.67	168.02	0.06	1585.10	10314.70	0.22
31.67	199.69	0.07	1576.60	11899.80	0.26
31.52	231.36	0.08	1503.70	13476.40	0.29
31.37	262.88	0.09	1485.30	14980.10	0.33
31.27	294.25	0.10	1240.20	16465.40	0.36
30.98	325.53	0.12	1193.20	17705.60	0.38
30.98	356.51	0.13	1147.20	18898.80	0.41
30.83	387.48	0.14	1111.50	20046.00	0.44
30.81	418.31	0.15	1055.10	21157.50	0.46
30.81	449.13	0.16	1003.00	22212.60	0.48
30.78	479.93	0.17	1000.50	23215.60	0.50
30.74	510.71	0.18	996.48	24216.10	0.53
30.65	541.46	0.19	963.76	25212.58	0.55
30.62	572.10	0.20	939.52	26176.34	0.57
30.56	602.72	0.21	897.46	27115.86	0.59
30.45	633.28	0.23	870.87	28013.32	0.61
30.41	663.73	0.24	839.26	28884.19	0.63
30.32	694.14	0.25	832.58	29723.45	0.65
30.31	724.46	0.26	814.86	30556.03	0.66

Table 4: Calculation of Lorenz coefficient for porosity and permeability measurements from Hanadir paleovalley (Contd.)

φ	Cumulative	% cumulative	K	Cumulative	% cumulative
30.31	754.77	0.27	810.52	31370.89	0.68
30.29	785.07	0.28	787.22	32181.41	0.70
30.23	815.36	0.29	780.64	32968.63	0.72
30.21	845.59	0.30	736.70	33749.27	0.73
30.20	875.80	0.31	736.01	34485.97	0.75
30.18	906.00	0.32	689.37	35221.98	0.77
30.12	936.18	0.33	635.54	35911.35	0.78
30.02	966.30	0.34	597.56	36546.89	0.79
29.93	996.32	0.36	592.18	37144.45	0.81
29.89	1026.25	0.37	584.46	37736.63	0.82
29.86	1056.14	0.38	584.15	38321.09	0.83
29.82	1086.00	0.39	515.57	38905.24	0.85
29.77	1115.82	0.40	504.90	39420.81	0.86
29.74	1145.59	0.41	501.24	39925.71	0.87
29.70	1175.33	0.42	458.22	40426.95	0.88
29.68	1205.04	0.43	455.56	40885.17	0.89
29.67	1234.71	0.44	437.20	41340.73	0.90
29.66	1264.38	0.45	436.40	41777.93	0.91
29.54	1294.04	0.46	401.25	42214.33	0.92
29.47	1323.58	0.47	399.23	42615.58	0.93
29.37	1353.06	0.48	332.12	43014.81	0.94
29.29	1382.42	0.49	328.71	43346.93	0.94
29.20	1411.72	0.50	327.51	43675.64	0.95
29.17	1440.92	0.51	326.83	44003.15	0.96
29.13	1470.09	0.52	297.63	44329.98	0.96

Table 5: Calculation of Lorenz coefficient for porosity and permeability measurements from Hanadir paleovalley (Contd.)

φ	Cumulative	% cumulative	K	Cumulative	% cumulative
29.02	1499.23	0.53	243.33	44627.61	0.97
29.00	1528.25	0.54	232.07	44870.94	0.98
28.72	1557.25	0.56	229.69	45103.01	0.98
28.61	1585.97	0.57	40.18	45332.70	0.99
28.60	1614.59	0.58	29.91	45372.88	0.99
28.58	1643.18	0.59	28.02	45402.78	0.99
28.54	1671.76	0.60	27.68	45430.80	0.99
28.42	1700.30	0.61	26.81	45458.48	0.99
28.40	1728.72	0.62	24.73	45485.28	0.99
28.24	1757.11	0.63	23.50	45510.02	0.99
28.22	1785.35	0.64	22.28	45533.51	0.99
28.20	1813.57	0.65	21.72	45555.79	0.99
28.15	1841.77	0.66	20.76	45577.51	0.99
28.11	1869.92	0.67	20.62	45598.28	0.99
28.09	1898.02	0.68	20.52	45618.90	0.99
28.05	1926.11	0.69	19.56	45639.42	0.99
27.97	1954.16	0.70	18.87	45658.98	0.99
27.79	1982.13	0.71	17.76	45677.85	0.99
27.76	2009.92	0.72	16.76	45695.61	0.99
27.62	2037.69	0.73	16.25	45712.36	0.99
27.61	2065.31	0.74	15.40	45728.61	0.99
27.58	2092.91	0.75	14.89	45744.01	0.99
27.02	2120.50	0.76	14.60	45758.91	0.99
27.00	2147.52	0.77	14.49	45773.51	1.00
27.23	2174.52	0.78	-32.75	45787.99	1.00

Table 6: Calculation of Lorenz coefficient for porosity and permeability measurements from Hanadir paleovalley (Contd.)

φ	Cumulative	% cumulative	K	Cumulative	% cumulative
26.79	2201.75	0.78	13.04	45755.25	0.99
26.55	2228.54	0.79	11.72	45768.29	1.00
26.45	2255.09	0.80	11.44	45780.01	1.00
26.02	2281.53	0.81	10.82	45791.45	1.00
25.98	2307.55	0.82	10.35	45802.27	1.00
25.31	2333.53	0.83	10.10	45812.63	1.00
25.31	2358.84	0.84	9.49	45822.73	1.00
24.84	2384.15	0.85	8.32	45832.22	1.00
24.77	2408.98	0.86	7.73	45840.54	1.00
24.76	2433.76	0.87	7.69	45848.27	1.00
24.21	2458.51	0.88	7.54	45855.96	1.00
24.10	2482.72	0.88	7.46	45863.51	1.00
24.09	2506.83	0.89	7.34	45870.97	1.00
23.62	2530.91	0.90	7.30	45878.31	1.00
22.91	2554.53	0.91	6.92	45885.62	1.00
22.58	2577.44	0.92	6.49	45892.54	1.00
22.37	2600.02	0.93	6.04	45899.03	1.00
22.06	2622.40	0.93	5.34	45905.07	1.00
21.53	2644.46	0.94	5.12	45910.41	1.00
21.37	2665.99	0.95	4.98	45915.53	1.00
21.12	2687.36	0.96	4.91	45920.51	1.00
21.06	2708.49	0.97	4.37	45925.42	1.00
19.93	2729.55	0.97	4.12	45929.79	1.00
19.37	2749.48	0.98	3.83	45933.91	1.00
19.10	2768.85	0.99	2.81	45937.74	1.00
19.05	2787.95	0.99	2.79	45940.54	1.00
	2807.00	1.00		45943.33	1.00

Table 7: Calculation of Lorenz coefficient for porosity and permeability measurements from Sarah paleovalley

φ	Cumulative	% cumulative	K	Cumulative	% cumulative
56.71	0.00	0.00	757.48	0.00	0.00
55.74	57.71	0.02	755.60	757.48	0.07
55.70	113.45	0.04	750.41	1513.08	0.15
55.22	169.15	0.06	723.88	2263.49	0.22
55.09	224.37	0.08	721.37	2987.37	0.29
54.47	279.46	0.10	717.09	3708.74	0.36
53.68	333.93	0.12	713.88	4425.83	0.43
53.42	387.61	0.14	675.06	5139.71	0.50
53.13	441.02	0.16	559.27	5814.77	0.56
52.86	494.16	0.18	493.63	6374.04	0.61
52.39	547.02	0.20	443.12	6867.67	0.66
51.13	599.41	0.22	432.28	7310.79	0.71
38.32	650.54	0.24	99.22	7743.07	0.75
37.47	688.85	0.26	94.81	7842.29	0.76
36.88	726.32	0.27	91.93	7937.10	0.77
35.08	763.21	0.28	90.11	8029.04	0.77
33.22	798.29	0.30	90.01	8119.15	0.78
33.17	831.51	0.31	84.60	8209.16	0.79
33.10	864.68	0.32	75.92	8293.75	0.80
33.08	897.77	0.33	62.79	8369.67	0.81
32.90	930.85	0.35	62.22	8432.46	0.81
32.64	963.75	0.36	60.46	8494.68	0.82
30.45	996.39	0.37	56.64	8555.14	0.83

Table 8: Calculation of Lorenz coefficient for porosity and permeability measurements from Sarah paleovalley (Contd.)

φ	Cumulative	% cumulative	K	Cumulative	% cumulative
28.17	1026.84	0.38	52.61	8611.78	0.83
27.98	1055.01	0.39	52.58	8664.38	0.84
27.73	1082.98	0.40	52.33	8716.96	0.84
27.19	1110.71	0.41	49.33	8769.29	0.85
26.31	1137.90	0.42	49.27	8818.62	0.85
25.07	1164.21	0.43	49.20	8867.88	0.86
25.07	1189.28	0.44	48.84	8917.08	0.86
24.93	1214.34	0.45	45.60	8965.92	0.86
24.64	1239.27	0.46	44.31	9011.52	0.87
24.45	1263.91	0.47	37.84	9055.83	0.87
24.33	1288.36	0.48	37.50	9093.67	0.88
24.28	1312.68	0.49	37.36	9131.17	0.88
24.26	1336.96	0.50	36.77	9168.53	0.88
24.11	1361.22	0.51	35.98	9205.30	0.89
24.04	1385.33	0.51	33.93	9241.28	0.89
24.02	1409.37	0.52	32.75	9275.21	0.89
24.01	1433.39	0.53	32.42	9307.97	0.90
23.94	1457.40	0.54	32.04	9340.39	0.90
23.89	1481.34	0.55	31.88	9372.43	0.90
23.79	1505.23	0.56	31.45	9404.31	0.91
23.76	1529.02	0.57	30.68	9435.75	0.91
23.48	1552.78	0.58	29.79	9466.43	0.91
23.47	1576.27	0.59	29.21	9496.22	0.92
23.38	1599.74	0.59	28.91	9525.43	0.92
23.37	1623.12	0.60	27.61	9554.33	0.92

Table 9: Calculation of Lorenz coefficient for porosity and permeability measurements from Sarah paleovalley (Contd.)

φ	Cumulative	% cumulative	K	Cumulative	% cumulative
23.36	1646.49	0.61	26.99	9581.94	0.92
23.30	1669.85	0.62	26.57	9608.93	0.93
23.24	1693.15	0.63	26.15	9635.50	0.93
23.23	1716.38	0.64	26.04	9661.65	0.93
23.21	1739.62	0.65	25.82	9687.69	0.93
23.11	1762.83	0.65	25.37	9713.51	0.94
23.04	1785.93	0.66	25.28	9738.88	0.94
23.00	1808.98	0.67	25.19	9764.16	0.94
22.92	1831.98	0.68	24.56	9789.35	0.94
22.89	1854.90	0.69	22.94	9813.92	0.95
22.87	1877.79	0.70	22.78	9836.85	0.95
22.82	1900.66	0.71	22.68	9859.64	0.95
22.81	1923.48	0.71	22.67	9882.31	0.95
22.56	1946.29	0.72	22.46	9904.98	0.96
22.41	1968.85	0.73	21.59	9927.45	0.96
22.17	1991.25	0.74	20.92	9949.04	0.96
22.15	2013.42	0.75	20.32	9969.96	0.96
22.03	2035.57	0.76	20.27	9990.28	0.96
21.97	2057.60	0.76	18.86	10010.55	0.97
21.97	2079.57	0.77	18.59	10029.41	0.97
21.90	2101.54	0.78	18.47	10048.00	0.97
21.85	2123.44	0.79	18.35	10066.47	0.97
21.82	2145.30	0.80	18.09	10084.81	0.97
21.76	2167.12	0.80	17.87	10102.91	0.97
21.67	2188.88	0.81	16.10	10120.78	0.98

Table 10: Calculation of Lorenz coefficient for porosity and permeability measurements from Sarah paleovalley (Contd.)

φ	Cumulative	% cumulative	K	Cumulative	% cumulative
21.32	2210.55	0.82	14.48	10136.88	0.98
21.31	2231.88	0.83	14.40	10151.36	0.98
21.22	2253.19	0.84	11.63	10165.76	0.98
21.10	2274.40	0.84	11.53	10177.40	0.98
20.90	2295.50	0.85	11.41	10188.93	0.98
20.88	2316.40	0.86	11.17	10200.33	0.98
20.81	2337.28	0.87	11.05	10211.50	0.98
20.70	2358.09	0.88	11.03	10222.55	0.99
20.69	2378.79	0.88	11.01	10233.59	0.99
20.65	2399.48	0.89	10.89	10244.60	0.99
20.65	2420.13	0.90	10.74	10255.49	0.99
20.23	2440.79	0.91	9.98	10266.23	0.99
20.21	2461.02	0.91	9.89	10276.21	0.99
20.10	2481.23	0.92	9.62	10286.11	0.99
20.08	2501.32	0.93	9.52	10295.73	0.99
19.82	2521.41	0.94	9.45	10305.25	0.99
19.71	2541.22	0.94	9.24	10314.70	0.99
19.66	2560.93	0.95	9.08	10323.95	1.00
19.50	2580.59	0.96	8.63	10333.02	1.00
19.37	2600.09	0.97	8.60	10341.66	1.00
19.34	2619.46	0.97	8.33	10350.25	1.00
19.31	2638.80	0.98	5.07	10358.58	1.00
19.26	2658.11	0.99	2.30	10363.65	1.00
16.92	2677.37	0.99	1.26	10365.95	1.00
	2694.29	1.00		10367.22	1.00

REFERENCES

Abdullatif, O. and Makkawi, M., 2004. Geological and geostatistical modeling of Paleozoic sandstone hydrocarbon reservoir of Quwarah Member, Qasim, Saudi Arabia. ARI Grant Project. KFUPM, Dhahran, Saudi Arabia.

Abdullatif, O. and Makkawi, M., 2010. Geological and geostatistical aquifer characterization of the outcrop analog of Wajid Sandstone in South west Saudi Arabia., KACST Project # 25-65. KFUPM, Dhahran, Saudi Arabia.

Abed, A., Makhlouf, I., Amireh, B. and Khalil, B., 1993. Upper Ordovician glacial deposits in southern Jordan. Episodes, 16(1-2): 316-328.

Adams, E.W., Grélaud, C., Pal, M., Csoma, A.É., Al Ja'aidi, O.S. and Al Hinai, R., 2011. Improving reservoir models of Cretaceous carbonates with digital outcrop modelling (Jabal Madmar, Oman): static modelling and simulating clinoforms. Petroleum Geoscience, 17(3): 309-332.

Aguilera, R.F., Harding, T. and Krause, F., 2008. Natural gas production from tight gas formations: A global perspective, 19th World Petroleum Congress, Spain.

Ahmed Tarek, H., 2001. Reservoir engineering handbook. Houston, Texas: Butterworth-Heinemann.

Al-Ajmi, H., Hinderer, M., Keller, M., Rausch, R., Blum, P. and Bohnsack, D., 2011. The role of outcrop analogue studies in for the characterization of aquifer properties. Int J Water Resour Arid Environ, 1: 48-54.

Al-Harbi, O.A. and Khan, M.M., 2011. Source and origin of glacial paleovalley-fill sediments (Upper Ordovician) of Sarah Formation in central Saudi Arabia. Arabian Journal of Geosciences, 4(5-6): 825-835.

Al-Mahmoud, M.J. and Al-Ghamdi, I., 2010. Overview of Tight Gas reservoirs in Saudi Arabia, Second Middle East Tight Gas Reservoirs Workshop. EAGE, Bahrain, pp. 331-347.

Amireh, B., Schneider, W. and Abed, A., 2001. Fluvial-shallow marine-glaciofluvial depositional environments of the Ordovician System in Jordan. Journal of Asian Earth Sciences, 19(1): 45-60.

Boggs, S., 2010. Principles of sedimentology and stratigraphy. Pearson Education, Ink.

Briner, A., Hulver, M., Azzouni, A. and Harvey, C., 2010. Regional Reservoir Quality of a Tight Gas Play: the Ordovician Sarah Formation in the Rub'Al Khali Basin of Southern Saudi Arabia, Second Middle East Tight Gas Reservoirs Workshop, Bahrain.

Bukhamseen, R.H., Khakimov, A., Sierra, L., Machala, M. and Young, D., 2010. First Successful Selective Tight Gas Reservoir Completion and Fracture Stimulation in Sarah Formation, Rub Al-Khali Empty Quarter of Saudi Arabia, SPE Russian Oil and Gas Conference and Exhibition, Moscow, Russia.

Chamley, H., 1994. Clay mineral diagenesis, Quantitative diagenesis: Recent developments and applications to reservoir geology. Kluwer Academic Publishers, Netherlands, pp. 161-188.

Clarkson, C.R., Freeman, M., He, L., Agamalian, M., Melnichenko, Y.B., Mastalerz, M., Bustin, R.M., Radlinski, A.P., and Blach, T.P., 2012. Characterization of tight gas reservoir pore structure using USANS/SANS and gas adsorption analysis. Fuel, 95, pp. 371-385.

Clark-Lowes, D., 2005. Arabian glacial deposits: recognition of palaeovalleys within the Upper Ordovician Sarah Formation, Al Qasim district, Saudi Arabia. Proceedings of the Geologists' Association, 116(3): 331-347.

Comisky, J., Newsham, K., Rushing, J. and Blasingame, T., 2007. A comparative study of capillary-pressure-based empirical models for estimating absolute permeability in tight gas sands, SPE Annual Technical Conference and Exhibition.

Dogan, A.U., Al-Ramadan, K. and Senalp, M., 2012. Overview of the Sarah Formation, NW Saudi Arabia: an Example for unconventional tight gas sandstones, Geological Society of America Abstracts with Programs, New Mexico, U.S.A., pp. 92.

Dykstra, H. and Parsons, R., 1950. The prediction of oil recovery by waterflood. Secondary Recovery of Oil in the United States, 2: 160-174.

Edwards, M., 1986, Glacial environments, in Reading, H.G., ed., Sedimentary environments and facies, Blackwell Scientific Publications, Oxford, U.K., p. 445-470.

Fitch, P., Davies, S., Lovell, M. and Pritchard, T., 2013. Reservoir Quality and Reservoir Heterogeneity: Petrophysical Application of the Lorenz Coefficient. Petrophysics, 54(5): 465-474.

Folk, R., 1974. Petrography of sedimentary rocks. Univ. Texas, Hemphill, Austin, Tex.

Ghienne, J.-F., 2011. The Late Ordovician glacial record: State of the art. Ordovician of the World. Cuadernos del Museo Geominero, 14: 13-19.

Graham, D.J. and Midgley, N.G., 2000. Graphical representation of particle shape using triangular diagrams: an Excel spreadsheet method. Earth Surface Processes and Landforms, 25(13): 1473-1477.

Grammer, G.M., Harris, P.M.M. and Eberli, G.P., 2004. Integration of outcrop and modern analogs in reservoir modeling: Overview with examples from the Bahamas.

Hambrey, M., 1985. The Late Ordovician—Early Silurian glacial period. Palaeogeography, Palaeoclimatology, Palaeoecology, 51(1): 273-289.

Higley, D.K., Pantea, M.P. and Slatt, R.M., 1997. 3-D Reservoir Characterization of the House Creek Oil Field, Powder River Basin, Wyoming, V1.00, U.S. Geological Survey Digital Data Series DDS-33. Accessed online on Nov. 17, 2013 http://pubs.usgs.gov/dds/dds-033/USGS_3D/ssx_txt/heterog.htm.

Jennings, J., Ruppel, S. and Ward, W., 2007. Geostatistical analysis of permeability data and modeling of fluid-flow effects in carbonate outcrops (SPE-65370). SPE Reservoir Evaluation and Engineering.

Jensen, J.L., 2000. Statistics for petroleum engineers and geoscientists, 2. Access Online via Elsevier.

Kazemi, H., 1982. Low-permeability gas sands. Journal of Petroleum Technology: 2229-2232.

Khalil, M.H., 2012. Reservoir Sweet Spots in the Arabian Petroleum Basin; Types and Controls, GEO 2012, Bahrain.

Krumbein, W. and Monk, G., 1943. Permeability as a function of the size parameters of sedimentary particles: Am. Inst. Min. and Met. Eng. Tech. Pub, 1492: 153-163.

Laboun, A.A., 2010. Paleozoic tectono-stratigraphic framework of the Arabian Peninsula. Journal of King Saud University-Science, 22(1): 41-50.

Lake, L. and Jensen, J., 1989. A review of heterogeneity measures used in reservoir characterization (SPE-20156). Society of Petroleum Engineers.

Le Heron, D.P., Craig, J. and Etienne, J.L., 2009. Ancient glaciations and hydrocarbon accumulations in North Africa and the Middle East. Earth-Science Reviews, 93(3): 47-76.

Le Heron, D.P., Craig, J., Sutcliffe, O.E. and Whittington, R., 2006. Late Ordovician glaciogenic reservoir heterogeneity: an example from the Murzuq Basin, Libya. Marine and Petroleum Geology, 23(6): 655-677.

Lorenz, M.O., 1905. Methods of measuring the concentration of wealth. Publications of the American Statistical Association, 9(70): 209-219.

Manivit, J., Vaslet, D., Berthiaux, A., Le Start, P., & Fourniguet, J., 1986. Geologic map of the Buraydah quadrangle, sheet 26G. Kingdom of Saudi Arabia (with text): Saudi Arabian Deputy Ministry for Mineral Resources Geoscience Map GM-114A, scale, 1(250,000).

McClure, H., 1978. Early paleozoic glaciation in Arabia. Palaeogeography, Palaeoclimatology, Palaeoecology, 25(4): 315-326.

McGillivray, J.G. and Husseini, M.I., 1992. The Palaeozoic petroleum geology of central Arabia. American Association of Petroleum Geologists Bulletin, v. 76, no. 10, p. 1473-1490.

Miall, A.D., 1996. The geology of fluvial deposits: Sedimentary facies, basin analysis, and petroleum geology. Springer (Berlin and New York).

Millson, J., Mercadier, C., Livera, S. and Peters, J., 1996. The Lower Palaeozoic of Oman and its context in the evolution of a Gondwana continental margin. Journal of the Geological Society, London, 153(2): 213-230.

Moscariello, A., Spaak, P., Jourdan, A. and Azzouni, A.-H., 2009. The Ordovician Glaciation in Saudi Arabia—Exploration Challenges Part 1. Geology (Outcrop, Subsurface, Analogues). Search and Discovery

Naik, G. C., 2003. Tight Gas Reservoirs–An Unconventional Natural Energy Source for the Future. *www. sublette-se. org/files/tight_gas. pdf. Accessado em, 1*(07), 2008.

Nairn, A. and Alsharhan, A., 2003. Sedimentary basins and petroleum geology of the Middle East. Access Online via Elsevier.

Paris, F. and Robardet, M., 1990. Early Palaeozoic palaeobiogeography of the Variscan regions. Tectonophysics, 177(1): 193-213.

Peters, E.J., 2012. Advanced Petrophysics: Geology, Porosity, Absolute Permeability, Heterogeneity, and Geostatistics, 1. Greenleaf Book Group.

Pettijohn, F., Potter, P. and Siever, R., 1987. Sand and Sandstone, 2nd. Springer-Verlag, New York.

Pranter, M.J., Reza, Z.A. and Budd, D.A., 2006. Reservoir-scale characterization and multiphase fluid-flow modelling of lateral petrophysical heterogeneity within dolomite facies of the Madison Formation, Sheep Canyon and Lysite Mountain, Wyoming, USA. Petroleum Geoscience, 12(1): 29-40.

Purcell, W., 1949. Capillary pressures-their measurement using mercury and the calculation of permeability therefrom. Journal of Petroleum Technology, 1(2): 39-48.

Rogers, J.J. and Head, W.B., 1961. Relationships between porosity, median size, and sorting coefficients of synthetic sands. Journal of Sedimentary Research, 31(3): 467-470.

Schenk, C. and Pollastro, R., 2000. Assessment of undiscovered oil and gas resources of the Greater Rub ‘al Khali basin by application of the total petroleum system concept—Part II. The Qusaiba-Paleozoic petroleum system: GeoArabia, 5: 175.

Schmalz, J. and Rahme, H., 1950. The variation of waterflood performance with variation in permeability profile. Producers Monthly, 15(9): 9-12.

Selley, R.C., 1998. Elements of Petroleum Geology. Academic Press, San Diego, U.S.A.

Senalp, M. and Al-Laboun, A., 2000. New Evidence on the Late Ordovician Glaciation in Central Saudi Arabia. Saudi Aramco Journal of Technology: 11-40.

Shafer, J. and Neasham, J., 2000. Mercury Porosimetry Protocol for Rapid Determination of Petrophysical and Reservoir Quality Properties, International Symposium of the Society of Core Analysts, pp. 18-22.

Thurmond, J., Loseth, T., Rivenaes, J., Martinsen, O., Xu, X. and Aiken, C., 2005. Using outcrop data in the 21st Century–New methods and applications, with example from the Ainsa Turbidite System, Ainsa, Spain. Deep-water outcrops of the world atlas: Tulsa, Oklahoma: American Association of Petroleum Geologists Special Publication CD-ROM.

Tiab, D. and Donaldson, E.C., 2004. Petrophysics: Theory and practice of measuring reservoir rock and fluid transport properties. Elsevier, New York, 88 pp.

Tucker, M.E., 2001. Sedimentary petrology: an introduction to the origin of sedimentary rocks (3rd ed.). Blackwell Science Ltd.

Turner, B.R., Makhlouf, I.M. and Armstrong, H.A., 2005. Late Ordovician (Ashgillian) glacial deposits in southern Jordan. Sedimentary Geology, 181(1-2): 73-91.

Vaslet, D., 1987. Early Paleozoic glacial deposits in Saudi Arabia--a lithostratigraphic revision: Deputy Ministry for Mineral Resources. Kingdom of Saudi Arabia, Technical Record BRMG-TR-07-1.

Vaslet, D., 1989. Late Ordovician glacial deposits in Saudi Arabia: a lithostratigraphic revision of the Early Paleozoic succession.

Ministry of Petroleum and Mineral Resources Deputy Ministry for Mineral Resources.

Vaslet, D., 1990. Upper Ordovician Glacial Deposits in Saudi-Arabia. Episodes, 13(3): 147-161.

Washburn, E.W., 1921. Note on a method of determining the distribution of pore sizes in a porous material. Proceedings of the National Academy of Sciences of the United States of America, 7(4): 115.

Williams, H., Turner, F.J. and Gilbert, C.M., 1982. Petrography: An introduction to the study of rocks in thin section. WH Freeman and Company.

VITAE

Name : Islam Mahmoud El-Deek

Nationality : Egyptian

E-mail : isdeek@gmail.com

AREA OF INTEREST

Clastic Sedimentology, Reservoir Characterization, Petrophysics.

ACADEMIC BACKGROUND

- **Master of Science (M.Sc.),** (2014). Sedimentology and Petroleum Geology, King Fahd University of Petroleum & Minerals, Dhahran 31261, Saudi Arabia.
- **B.Sc. in Geology**, (2007). Faculty of Sciences, Zagazig University, Zagazig, Egypt

CAREER HISTORY

Feb., 2011 – Apr., 2014	Research Assistant; King Fahd University of Petroleum & Minerals
Aug., 2009 - Feb., 2011	Exploration geologist, geologic database management; Egyptian General Petroleum Corporation
Dec., 2008 - Aug., 2009	Wellsite geologist, well log interpretation, subsurface mapping; Merlon Petroleum El Fayoum Company
Jun., 2008 – Dec., 2008	Exploration geologist; Egyptian General Petroleum Corporation

PROFESSIONAL AFFILIATIONS

- *AAPG* "American Association of Petroleum Geologists",
  - ✓ Vice President of *AAPG* Student Chapter at KFUPM.
- *EAGE* "European Association of Geoscientists & Engineers".
- *SPE* "Society of Petroleum Engineers".
- *SEG* "Society of Exploration Geophysicists".
- *DGS* "Dhahran Geoscience Society".
- *ESSP* "Egyptian Syndicate of Scientific Professions".

AWARDS, CONFERENCES AND PUBLICATIONS

Awards

- Received a fully paid scholarship with stipend from KFUPM to pursue M.S.
- **1st Place Award**, Academy of Scientific Research and Technology, Paper Competition**,** Egypt, 2007.

Conference Publications

- **El-Deek**, I., Abdullatif, O., Al-Ramadan, K., & Korvin, G. (2014). Integration of Sedimentology, Petrophysics and Statistics for Characterizing the Reservoir Heterogeneity of the Late Ordovician Sarah Formation, Central Saudi Arabia. EGU General Assembly 2014: Geophysical Research Abstracts, Vol. 16, EGU2014-9871-3. Vienna, Austria.
- **El-Deek**, I., Abdullatif, O. (2014). Sedimentological and Stratigraphical Heterogeneity of the Late Ordovician Glacio-Fluvial Sarah Formation Paleovalleys in Central Saudi Arabia: An Outcrop Analog Approach. 2014 LIPE & AAPG Northern Arabia Geoscience Conference & Exhibition. Beirut, Lebanon.
- **El-Deek**, I., Abdullatif, O., Al-Ramadan, K., & Korvin, G. (2013). Reservoir heterogeneity and quality of the Late Ordovician Sarah Formation: Outcrop analog for tight gas sandstone, Saudi Arabia. 10th Meeting of the Saudi Society for Geosciences. KFUPM, Dhahran, Saudi Arabia.
- **El-Deek**, I., & Abdullatif, O. (2013). Characterization of Reservoir Quality from the Outcrop Analog for the Paleozoic Sarah Formation Glacial and Fluvial Reservoirs, Qasim Area, Saudi Arabia. Graduate Research Day, King Fahd University of Petroleum & Minerals. Dhahran, Saudi Arabia.